



Quality and Reliability of RF-MEMS Switches for Space Applications

Emilien Lemoine

► To cite this version:

Emilien Lemoine. Quality and Reliability of RF-MEMS Switches for Space Applications. Micro and nanotechnologies/Microelectronics. Université de Limoges, 2014. English. NNT : 2014LIMO0062 . tel-01161778

HAL Id: tel-01161778

<https://theses.hal.science/tel-01161778>

Submitted on 9 Jun 2015

HAL is a multi-disciplinary open access archive for the deposit and dissemination of scientific research documents, whether they are published or not. The documents may come from teaching and research institutions in France or abroad, or from public or private research centers.

L'archive ouverte pluridisciplinaire **HAL**, est destinée au dépôt et à la diffusion de documents scientifiques de niveau recherche, publiés ou non, émanant des établissements d'enseignement et de recherche français ou étrangers, des laboratoires publics ou privés.

UNIVERSITY OF LIMOGES
THEMATIC PhD SCHOOL S2IM
FACULTY OF SCIENCE AND TECHNOLOGY

Year : 2014

Thesis N° X

PhD Thesis

In Partial Fulfillment of the Requirements for the Degree of

**DOCTOR OF PHILOSOPHY IN THE UNIVERSITY OF
LIMOGES**

Mention : Science of Engineering for Information, Mathematics

presented et defended by

Émilien LEMOINE

11th December 2014

<p>Quality and Reliability of RF-MEMS Switches for Space Applications</p>
--

PhD Thesis directed by Pierre BLONDY and Aurelian CRUNTEANU

JURY :

Dominique BAILLARGEAT	Professeur, XLIM, Université de Limoges	Président
Fabio COCCETTI	Ingénieur, HDR, Fialab, Toulouse	Rapporteur
Jorge D. MARTÍNEZ PÉREZ	Professeur, Université Polytechnique de Valence, Espagne	Rapporteur
Dominique CROS	Professeur XLIM, Université de Limoges	Examineur
Laurent MARCHAND	Ingénieur, ESA-ESTEC, Noordwijk, Pays-Bas	Examineur
Olivier VENDIER	Ingénieur, Thales Alenia Space, Toulouse	Examineur
Aurelian CRUNTEANU	Chargé de Recherches CNRS, XLIM	Examineur
Pierre BLONDY	Professeur XLIM, Université de Limoges	Examineur
Romain STEFANINI	Directeur, Airmems	Invité

“Il n’y a pas de génie sans un grain de folie.”

“Rien dans notre intelligence qui ne soit passé par nos sens.”

Aristote

“С любимыми не расставайтесь ! С любимыми не расставайтесь ! С любимыми не расставайтесь ! Всей кровью прорастайте в них, И каждый раз навек прощайтесь ! И каждый раз навек прощайтесь ! И каждый раз навек прощайтесь ! Когда уходите на миг !”

Александр Сергеевич Кочетков

“Where there’s a will there’s a way.”

Proverb

à Grég & Marco,

Remerciements

Les travaux présentés dans ce manuscrit ont été effectués au sein du département MINACOM (Micro et NANotechnologies pour Composants Optoélectroniques et Micro-ondes) de l'institut de recherche XLIM, UMR CNRS 7252, à l'Université de Limoges. Je remercie dans un premier temps Monsieur Dominique CROS, précédent directeur du laboratoire et Professeur à l'Université de Limoges, pour m'avoir permis de commencer ces travaux et pour les avoir examiner à la toute fin.

J'adresse mes profonds remerciements à Monsieur Dominique BAILLARGEAT, Professeur à l'Université de Limoges et actuel directeur du laboratoire pour m'avoir permis de conclure ces travaux et pour avoir accepté de présider le jury de ma soutenance de thèse.

Je remercie sincèrement Messieurs Fabio COCCETTI, Ingénieur Habilité à Diriger les Recherches, à Fialab, Toulouse et Jorge Daniel MARTÍNEZ PÉREZ, Professeur à l'Université Polytechnique de Valence, Espagne, d'avoir accepté d'être les rapporteurs de mes travaux de recherche.

Je remercie également Messieurs Laurent MARCHAND et Nicolas SAILLEN Ingénieurs à l'ESA-ESTEC (European Space Agency - European Space Research and Technology Centre), Pays-Bas, ainsi que Monsieur Olivier VENDIER, Ingénieur à Thales Alenia Space, Toulouse, pour avoir examiner mes travaux et pour avoir soutenu et financé ce projet le cadre du programme NPI de l'ESA, en collaboration avec Thales Alenia Space (Fr) et l'Université de Limoges.

Je remercie également Monsieur Romain STEFANINI, Directeur d'Airmems, Limoges, pour avoir accepté l'invitation à la soutenance de mes travaux de recherche.

Je souhaite également adresser mes remerciements à Monsieur Aurelian CRUNTEANU, Chargé de recherche CNRS, co-encadrant de ma thèse, pour ses idées et ses conseils.

Je remercie finalement Pierre BLONDY, Professeur à l'Université de Limoges, pour m'avoir fait confiance et pour m'avoir encadré dans de véritables conditions de travail.

Sur le plan personnel et affectif, je remercie en premier lieu mon rival Romain (plus sympathiquement connu sous le pseudonyme Père Dodu, et oui les escalopes, elles sont toujours sautées !!), Elena, Ricky, Jofroid, Stefano, mon Filou et Panda.

Les Anciens, Johnny, Tatabinou, Marmotte, Ludo, Dr. Kiounel, Lisette, Mansoib, Aurélie, Cheikh, Ling Yan, Katell de Luna, Denis, Jonathan, Nico le carveur forever tout schuss dans les ruisseaux... (assis trampo!!)

Les Prochains, à qui j'envoie mes encouragements, Cyrielle, Mélanie, Mathieu, Maryna, Johann, Fabien, Chloë, Yoann et son humour noir, Paulo le p'tit coquinou, Nico Jyn le sarcastique et Karthik.

Je remercie également Kevin, Marie-Laure, Damien, Cyril et Mathilde pour leur efficacité et l'aide qu'ils m'ont apportée dans les moments cruciaux.

Les amis et collègues d'Estec, Pedro, Stéphan, Benoit, Lise, Rafouf, Antoine, Marina, Martin, Aleix, Robert, Jacopo, Chrystel, Marie-Geneviève, Kenneth, Nikolai, Kristien et tous les collègues du couloir Ef.

At last but not least, je remercie ma grande et belle famille pour leur soutien inconditionnel, intemporel, peu importe la distance.

Table of Contents

List of Figures	5
List of Tables	11
General Introduction	13
Chapter 1 : Presentation of MEMS Technology	17
1.1 MEMS technology	18
1.1.1 Actuators and sensors	19
1.1.2 Fabrication process	21
1.2 Radio-Frequency (RF) MEMS for space and telecommunications	22
1.2.1 Definition	22
1.2.2 Main parameters and variables of switches	27
1.2.3 Failure mechanisms	30
1.2.4 Focus on main failures mechanisms	34
1.3 Conclusion	35
Chapter 2 : Creep in RF-MEMS Switches	37
2.1 Creep in MEMS	38
2.1.1 Definition of creep	40
2.1.2 Different regimes of creep	40
2.1.3 State of the art of creep measurement techniques	43
2.2 Short introduction on the need of creep measurement	44
2.3 First measurement technique: Assessment of creep using constant constraint based on partially biasing the switch	47
2.3.1 Introduction	47
2.3.2 Presentation of the test bench	48
2.3.3 Precautions and approximations	49
2.3.3.1 Drift of constant constraint	50
2.3.4 Creep measurements at room temperature, varying bias voltage	52
2.3.4.1 Measurement results on S5-switch	53
2.3.4.2 Measurement results on SYM-switch	54
2.3.4.3 Measurement results on ASYM-switch	55
2.3.4.4 Measurement results on Omron switch	56
2.3.4.5 Discussion	58
2.3.5 Creep measurements at constant bias voltage ($80\%V_p$) varying temperature	59
2.3.5.1 Measurement results on SYM-switch	59
2.3.5.2 Measurement results on ASYM-switch	60
2.3.6 Discussion	61
2.4 Second measurement technique: Assessment of creep using constant contact force based on the servo controlling of the contact resistance	62
2.4.1 Introduction	62
2.4.2 Elements on the theory of electrical contact	63
2.4.2.1 Constriction resistance	63
2.4.2.2 Contact mechanics	64
2.4.2.3 Supertemperature and the Wiedemann-Franz law	65
2.4.2.4 Softening, melting	65

2.4.2.5	Contact resistance as a function of bias voltage	66
2.4.3	Presentation of the test bench	68
2.4.4	Results on S5-switches	70
2.4.5	Results on SYM- and ASYM-switches	72
2.4.6	Results on Omron RF-MEMS switch	74
2.4.7	Discussion	75
2.5	Further testing conducted on Omron MEMS switch	76
2.6	Conclusion	80
Chapter 3 : Reliability Assessment Methodologies .		81
3.1	Introduction to reliability	82
3.1.1	General definition	82
3.1.2	The Weibull distribution	84
3.1.2.1	Theoretical elements	85
3.1.2.2	Acceleration factors	88
3.1.2.3	Practical examples	88
3.2	Initial reliability testing on Xlim micro-switches	92
3.3	Parallel test bench	95
3.3.1	Introduction	96
3.3.2	Design of PCB (Printed Circuit Boards)	97
3.3.3	Test with micro-controller	100
3.3.3.1	Presentation of test bench	102
3.3.3.2	Increasing accuracy of measurements with help coming from Atmel	102
3.4	Initial sorting of switches on wafer	104
3.5	Presentation of hot and cold switching	104
3.6	Conclusion	105
Chapter 4 : Possible Improvements for Reliability of RF-MEMS		107
4.1	Bouncing suppression using asymmetrical design	108
4.1.1	Principle	108
4.1.2	Design	110
4.1.3	Measurements	111
4.1.3.1	S-parameters	111
4.1.3.2	Dynamic behaviour	111
4.1.4	Conclusion	112
4.2	Recommendations for improving reliability of RF-MEMS switches	114
4.3	Three recommended testings for reliability assessment of RF-MEMS	118
4.4	Conclusion	120
General Conclusion		123
Annex A		127
Annex B		129
Bibliography		133

List of Figures

1.1	Geometry and circuit connections of the Resonant Gate Transistor [1]. . . .	18
1.2	(a) Micro-shutters, courtesy of NASA - (b) Gaia flow sensor, courtesy of ESA.	19
1.3	Simplified view of smart-phone board of today , MEMS are in red, courtesy of Yole Développement.	20
1.4	Simplified view of smart-phone board of tomorrow , MEMS are in red, courtesy of Yole Développement.	20
1.5	Expected market estimated by Yole développement from 2012 to 2018 [2]. .	21
1.6	The main steps of the fabrication process of a MEMS switch.	22
1.7	(a) S-parameters of an ohmic contact micro-switches in OFF- and ON-states. (b) S-parameters of a capacitive micro-switch in OFF- and ON-states. .	24
1.8	Pictures of the RF-MEMS switches (ohmic and capacitive) main actors. . .	26
1.9	Typical curve of a switch with transmission as a function of bias voltage $T(V)$	28
1.10	Operating principle of a switch biased by a bi-polar triangle waveform. . .	29
1.11	Stages of creep from the time when the load is applied on the shelf until the load is removed. Rupture will occur if the load stays on the shelf. This phenomenon is accelerated with temperature.	31
1.12	Transmission as a function of bias voltage when creep is occurring.	31
1.13	Transmission as a function of bias voltage when stiction is occurring. . . .	32
1.14	Destruction of an RF-MEMS during testing because of high voltage applied on dielectric layer [3].	33
1.15	Charge trapping in micro-switches when a bias is applied on the movable structure [4].	34
1.16	Transmission as a function of bias voltage when dielectric charging is occurring.	34
2.1	The stages occurring in RF-MEMS with shifting of C_{off} and deformation of contact because of mechanical creep.	39
2.2	The typical curve of strain versus time to represent creep behavior at constant constraint and temperature. Creep is divided in three regimes. . . .	41
2.3	Testing set up to assess the evolution of pull-down and release voltages of capacitive RF-MEMS switches.	45
2.4	(a) 50 V bipolar bias voltage, 50% duty cycle - (b) 50 V unipolar bias voltage. .	45
2.5	Comparison between unipolar and bipolar bias to see charging or not in dielectric layers.	46
2.6	Capacitive switch pulled 3 weeks in down state with bipolar bias.	46
2.7	The two (up and down) states of S_{21} parameter of an ohmic switch as a function of frequency.	48
2.8	Cross-section of the switch and the different bias voltages applied on the structure to study the effect of creep.	49
2.9	Test bench to assess creep consisting in partially biasing the switch and get the S-parameters via a Vector Network Analyzer (VNA) and save data with Labview.	49
2.10	(a) and (b) The 5-anchors circular structure, S5-switch from Xlim (c) and (d) The 2-anchors symmetrical cantilever, SYM-switch from Xlim (e) and (f) The Omron RF-MEMS.	52

2.11	Measurement results of the transmission parameter shifting over time for three S5-switches biased at 70%, 80% and 90% of their pull-down voltage. .	53
2.12	Measurement results of the transmission parameter shifting over time for two SYM-switches biased at 70% and 80% of their pull-down voltage. . . .	54
2.13	Measurement results of the transmission parameter shifting over time for two ASYM-switches biased at 70% and 80% of their pull-down voltage. . .	56
2.14	Photograph of PCB mounted Omron switch with connectors.	57
2.15	Photograph of PCB mounted Omron switch with connectors.	57
2.16	Measurement result of the transmission parameter shifting over time for the Omron RF-MEMS switch 2SMES-01 biased at 80% of its pull-down voltage.	58
2.17	Photograph of PCB mounted Omron switch with connectors.	59
2.18	Evolution of the transmission parameter shifting over time for the SYM-switch at different temperatures. The bias voltage is 80% of the pull-down voltage.	60
2.19	Evolution of the transmission parameter shifting over time for the ASYM-switch at different temperatures. The bias voltage is 80% of the pull-down voltage.	61
2.20	Schematic of two rough metallic surfaces in contact crossed by a current. .	63
2.21	Deformation of hemispherical contact asperity [5].	64
2.22	Contact resistance versus bias voltage for 3 switches that get different metallic contacts, evidence of hysteresis of switches and hardness of metals.	67
2.23	Principle of assessment of creep servo controlling the contact resistance. .	69
2.24	Test bench to assess creep consisting in servo controlling the contact resistance of switch with bias voltage.	70
2.25	The shift of bias voltage at different temperatures for a constant contact resistance demonstrating the behavior of creep on S5-switches.	70
2.26	Evidence of creep accelerated by temperature given by an Arrhenius' plot.	72
2.27	Evolution of the bias voltage to maintain the SYM-switch at a constant contact resistance over time at 25°C and 40°C to observe creep phenomenon.	73
2.28	Evolution of the bias voltage to maintain the ASYM-switch at a constant contact resistance over time at 25°C and 40°C to observe creep phenomenon.	74
2.29	Evolution of the bias voltage to maintain the Omron switch at a constant contact resistance over time demonstrating the insensitivity of the switch on creep phenomenon for more than 55 hours.	75
2.30	Complete test bench with lumped elements to assess the reliability of the Omron with DC testing at 25°C and 70°C.	76
2.31	Waveform of the bias voltage applied on the Omron switch to follow the evolution of its parameters during a test held in down state.	77
2.32	Transmission versus bias voltage $T(V)$ for the Omron switch at room temperature in the beginning of the test and after 14 hours in down state. . . .	78
2.33	Evolution of actuation voltages versus time of the Omron switch held in down state at room temperature.	78
2.34	Transmission versus bias voltage $T(V)$ for the Omron switch at 70°C in the beginning of the test and after 62 hours in down state.	79
2.35	Evolution of actuation voltages versus time of the Omron switch held in down state at 70°C.	79

3.1	The bathtub curve describes the failure rate as a function of time, divided in three regimes, infant mortality, normal life and end of life.	83
3.2	Example of lifetime of tyres plotted in a log-log graph with β and α representing the Weibull distribution parameters.	84
3.3	Two examples of reliability assessment of fabrication process plotted in a Weibull graph.	85
3.4	Main functions of the Weibull distribution [6].	86
3.5	Example of acceleration factor extracted from the Weibull distribution. . .	88
3.6	Weibull curves for a fabrication process improved, Radant RF-MEMS [7]. .	89
3.7	Weibull curves for a switch with different contact materials, Sandia National Laboratories, Argonne National Laboratory, USA [8].	90
3.8	Weibull curves to assess the evolution of the fabrication process, Memtronics, LeHigh University, USA [9].	91
3.9	Schematic of the reliability bench to assess the lifetime of S5 RF-MEMS switches. R_1 is 10 k Ω and R_2 is 40 k Ω . The current in the switch is always less than 500 μ A.	93
3.10	Recording of an S5 ohmic contact RF-MEMS switch during cold switching under 5V.	93
3.11	Cumulative failures versus number of cycles for 20 S5-type RF-MEMS switches.	94
3.12	Recording of an S5-type ohmic contact RF-MEMS switch during cold switching under 28 dBm.	96
3.13	Elementary pattern of the 8 channels PCB design for parallel testing. R_1 is 10 k Ω and R_2 is 40 k Ω . R_{Bias} is large enough to prevent current in the bias line.	98
3.14	Surface Mounted Devices (SMD) resistance.	99
3.15	Photograph of the duroid board mounted with switches and resistances exhibiting 8 parallel channels.	99
3.16	Photograph of the parallel test bench running with Arduino board getting output voltages from the duroid PCB where are mounted the switches. . .	100
3.17	Design of elementary pattern to test 48 switches in parallel on a 2 inches PCB.	100
3.18	Design of the next duroid board to test 48 switches in parallel.	101
3.19	Photograph of the Arduino Mega2560 board based on an Atmel AT-MEGA2560 micro-controller showing all the different inputs and outputs. .	102
3.20	Flowchart of Arduino code that allow to count the number of switching done by micro-switches.	103
3.21	(a) Voltage generators waveforms for hot switching, (b) Voltage generators waveforms for cold switching.	105
4.1	Beam height versus time for a step bias voltage, generating multiple bounces before final contact closure.	109
4.2	Front view of a symmetrical device contact closure (top) and asymmetrical device (bottom).	109
4.3	Design of switches.	110
4.4	Isolation of the two switches with 100V bias voltage applied.	111
4.5	Insertion losses of the two switches with 100V bias voltage applied. . . .	112
4.6	Test bench for the dynamic behaviour of the switch.	112

4.7	Measured responses for various bias voltages of the symmetric (top) and asymmetric (bottom) switches.	113
4.8	Example of curves for switches assessing the mechanical behaviour.	119
4.9	Example of curves for which the switches are partially biased and transmission parameter is monitored to know if the switch pulls in down state or not.	119
4.10	Example of curves for which the switches that are subjected to contamination. In the left case the contact resistance does not change over time, in the right case the contact resistance varies a lot meaning that contamination occurs and species are introduced in the contact.	120
4.11	Example of curves for which the switches shows sensitivity to mechanical creep or not. The technique used is the monitoring of contact resistance servo controlling the bias voltage.	121

List of Tables

1.1	OFF and ON states of capacitive and ohmic switches with equivalent electrical circuits.	23
1.2	Comparison of 3 technologies of RF switches.	25
1.3	Cavendish Kinetics, Digital Variable Capacitors.	27
1.4	Main parameters of RF-MEMS switches.	28
1.5	Failure mechanisms sorted by weight of importance.	35
2.1	Summary of the different regimes of mechanical creep.	42
2.2	Summary of the slopes measured on several switches at several constant constraints.	58
2.3	Summary of slopes and lifetimes measured on SYM- and ASYM-switches at different temperatures.	61
2.4	Softening and melting voltages and temperatures of some common metals [10].	66
2.5	Comparison of pull-down and release voltages for 3 switches giving the ratio V_p/V_r	67
3.1	Summary of measurement testing and computed parameters.	94

General Introduction

Man has always needed to communicate, as well as learning something or transmitting something. Faster and further, thus are born telecommunications. The telecommunications regard all systems that can send and receive a signal from a wide range of frequencies to share information. The direction taken by telecommunications deals with miniaturization of components since compactness and lightweight are essential criteria, especially for space and mobile applications. Indeed, not so many people enjoy carrying a 500 gr mobile phone in his pocket. Moreover, since cost of a satellite is directly proportional to its weight, much money can be saved from payload miniaturization.

RF-MEMS stands for Radio-Frequency Micro-Electro-Mechanical-Systems. Those are tiny components operating using static bias voltage at Radio-Frequencies. They provide functions like switches, varactors for a wide range of telecommunications applications. Compared to the current technologies of RF-switches, i.e. electromechanical relays (Reed relays), PIN diode and Field Effect Transistors, the RF-MEMS have many assets like compactness, lightweight, performances, low power consumption and low fabrication process cost that can provide a better solution for mobile and space applications.

However one important step is full understanding of reliability. Understanding the failure mechanisms of RF-MEMS is a key to make them reliable and this thesis takes place in this frame. Based on previous works, the reliability of RF-MEMS is studied through various measurements. Comparisons between several technologies will be done and the pros and the cons for each of them will be highlighted. This is such a vast domain involving multidisciplinary fields that not only one PhD thesis can answer itself.

This manuscript is divided in three chapters. In the first chapter, a global introduction to MEMS and RF-MEMS is presented. An overview of the current technologies is given with some examples. The main steps of a basic fabrication process are detailed. Then, the thesis focuses on RF-MEMS, reminding some definitions. An overview of commercially available RF-MEMS switches is presented. The vocabulary related with the thesis and the main parameters of RF-MEMS are presented. Finally, the last part of this first chapter presents the failure mechanisms and the priority in solving them.

The chapter two is dedicated to the assessment of mechanical creep. Indeed, creep is one of the major failure mechanism involved in reducing the lifetime of RF-switches. As a consequence, a short introduction on the theory of creep is given to understand its origin and its parameters. Then, two innovative test benches dedicated to the assessment of mechanical creep are presented, each having pros and cons. The measurement results will follow presentation of benches and conclusions will be discussed.

In the third chapter, the lifetime of RF-MEMS switches will be studied through various operation conditions. The first section is dedicated to theory of reliability with a general definition. A detailed definition of the Weibull distribution follows with an introduction to acceleration factors and practical examples. The second section presents the results

of reliability testing using a simple test bench with various operation conditions. From these results a Weibull plot will be extracted showing the dependence of switch lifetime on bias voltage and input-to-output voltage. The third section presents a parallel test bench for RF-MEMS switches from 8 parallel channels up to 48 channels. The fast acquisition system with Arduino boards allows 1kHz switching rate for DC voltages.

The fourth chapter gives guidelines for reliability of RF-MEMS. An innovative asymmetrical design that prevent bounces in micro-switches will be presented. Information to improve reliability of RF-MEMS are given in the following. And finally three recommended test benches are presented to assess the global behaviour of a switch.

The general conclusion summarises the main results of each chapter and will discuss about future works.

Chapter 1 :

Presentation of MEMS Technology

In this first chapter a general state of the art on MEMS-based technology is presented. The first section of this chapter gives general information about MEMS technology through a bit of history, the main devices and the most popular applications of these devices. Then, the second section focuses on presentation of these devices and their principle of operation. Some theoretical models will be introduced to understand the failure mechanisms and the main steps of the work to do.

1.1 MEMS technology

In 1967, Nathanson et al. reported for the first time an original use of the semi-conductors fabrication process to create a device with a suspended silicon beam at the micrometer scale called The Resonant Gate Transistor [1]. This device was originally made to reduce parasitic capacitance of MOS transistors. A sketch of the device is visible in figure 1.1 and detailed below.

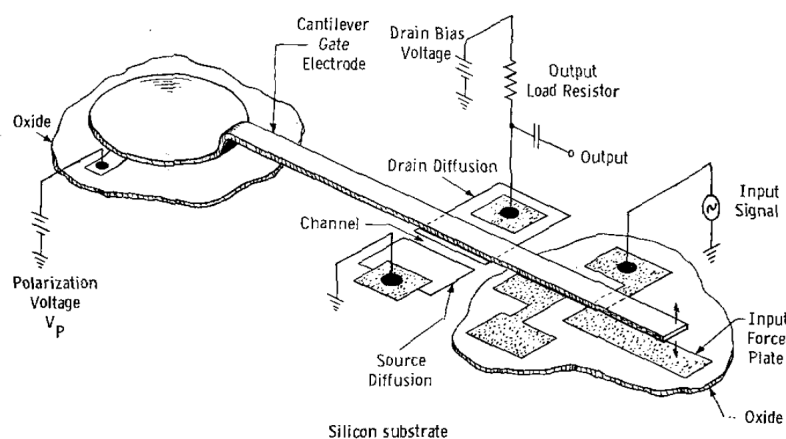


Figure 1.1: Geometry and circuit connections of the Resonant Gate Transistor [1].

Vibration of a metal beam generated by an oscillating input signal on the cantilever gate electrode creates variation of charges induced by field-effect in the channel and are detected from the drain. The gain of the detector is controlled by the bias voltage applied on the beam. If the input signal is not running at the frequency of the beam, the current is strongly attenuated when it reaches the drain. This device actually works like a mechanical filter, maximizing signal transfer around its resonance frequency.

Several years after this demonstration MEMS have found numerous applications, and surface micro-machining has opened new opportunities. Few of them related to space borne payloads will be presented, together with actuators and sensors that have been integrated into consumer electronics, as well as satellite payloads. Then a simple explanation of fabrication process is done so as to get an idea of how it is built.

1.1.1 Actuators and sensors

In space applications, the James Webb Space Telescope (JWST) that will replace Hubble Space Telescope, is equipped with MEMS micro-shutter arrays (figure 1.2 (a)) whose function is to open and close allowing for sequential observation of several stellar objects at the same time. The JWST is going to analyse 100 objects at the same time and they have to be clearly distinguishable among all different light sources. It is assembled on the Multi-image Near Infra-Red Spectrometer (NIR-Spec) which main mission is to go back in time observing the first galaxies that will provide information on the early ages of the universe. This application is also for next generation of screens, in smart-phones and tablets, with a component called the Interferometric Modulator Display (IMoD).

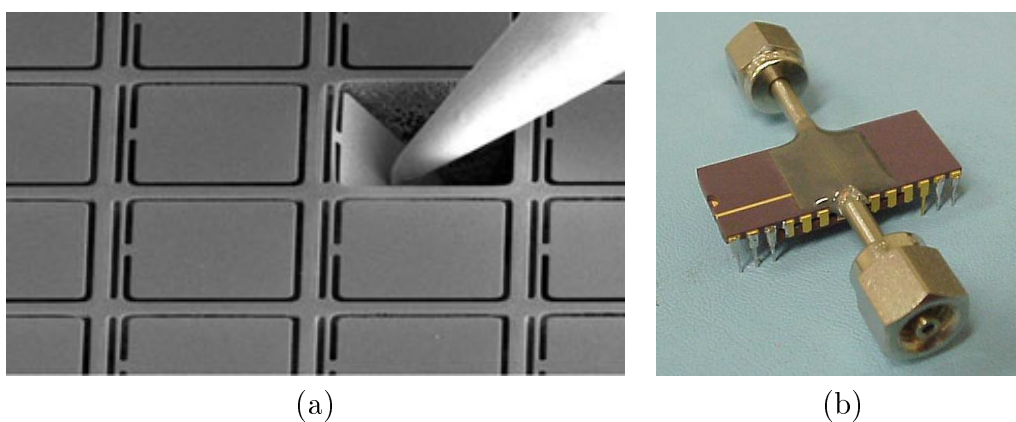


Figure 1.2: (a) Micro-shutters, courtesy of NASA - (b) Gaia flow sensor, courtesy of ESA.

Still related with space, GAIA, the billion stars surveyor satellite needs an extreme output thrust accuracy because of the astrometric accuracy (around 20 μ arcs) required to watch on billions stars with precision never reached before. Thus, a μ N thrust is needed to get the correct orientation of the satellite and the only option to do that is using a MEMS flow sensor (figure 1.2 (b)) [11].

Related to consumer electronics, mobile phones contain a wide range of MEMS technologies (figure 1.3). For instance, a microgyroscope lets the smart-phone display a landscape or portrait photo on its screen. Combined with an accelerometer, it enhances the precision of the GPS positioning system or increases the gaming interactivity. This is also applicable to the remote controls of video games. All information regarding positioning, displacement and rotation is usually integrated into one single chip called an Inertial Measurement Unit (IMU). Other MEMS embedded in smart-phones are magnetometers, microphones, pressure sensors, humidity and temperature sensors, as well as Bulk Acoustic Waves (BAW) filters and duplexers and antenna tuners.

As reported by Yole [2], the market of MEMS in smart-phone is expected to be \$6.4B by 2018 from \$2.2B in 2012. For these achievements, more MEMS components are ex-

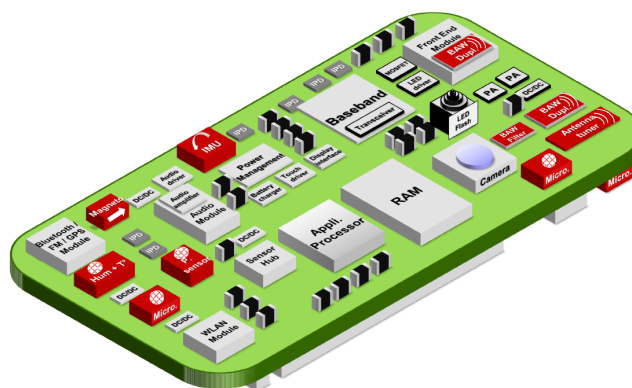


Figure 1.3: Simplified view of smart-phone board of **today**, MEMS are in red, courtesy of Yole Développement.

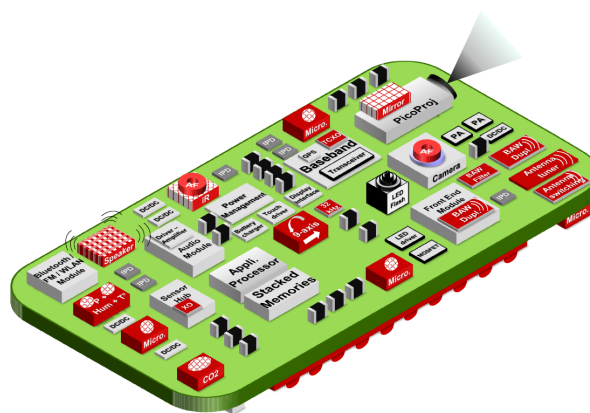


Figure 1.4: Simplified view of smart-phone board of **tomorrow**, MEMS are in red, courtesy of Yole Développement.

pected to be integrated in future smart-phones like 9-axis sensor and a combination of pressure, humidity and temperature sensor in one single chip (figure 1.4). Moreover, there could be mirrors for pico-projectors, auto-focus MEMS for camera. Finally, there may be other fields to explore like gas/biochemical sensors as well as infra-red and ultra-violet sensors for security matters and energy harvesting according to future environmental considerations.

The market for MEMS technologies is expected to grow up to 20 billions USD by 2018 (figure 1.5) where the biggest growth areas should be micro-fluidics, MEMS for videos and projections, Inertial Movement Units (INU), microphones, pressure sensors and ink-jet heads. Regarding our study, the RF MEMS market follows the trend meaning that this technology is very promising for the future.

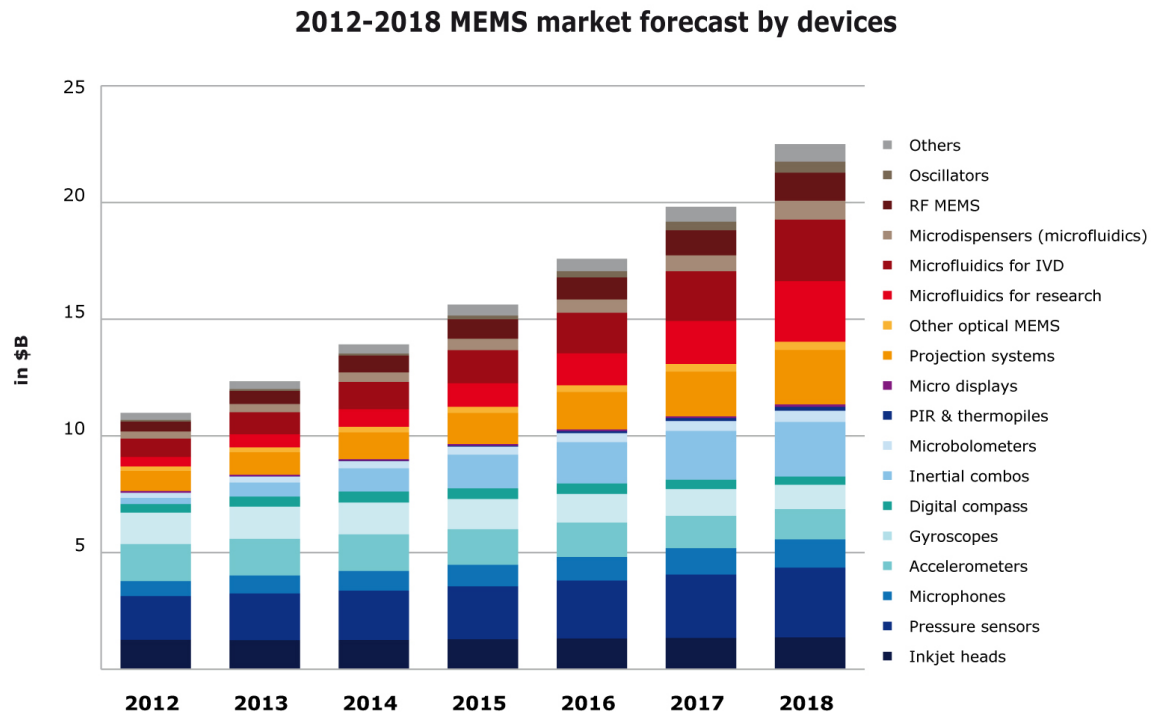


Figure 1.5: Expected market estimated by Yole développement from 2012 to 2018 [2].

1.1.2 Fabrication process

A MEMS fabrication process is derived from integrated circuit manufacturing. MEMS are made in a clean-room environment and like CMOS, fabrication is a succession of deposition - lithography sequences on several thin layers that can be metal, dielectric (passive) or sacrificial layers. The layers are deposited on top of silicon wafers, using various deposition methods like thermal evaporation, reactive sputtering. The final chips are obtained after several tens of deposition - lithography sequences and a final release step, where sacrificial layers are removed to suspend mechanical layers. An example of fabrication process of a RF-MEMS switch is given in figure 1.6.

The different steps of the fabrication are listed below according to figure 1.6.

- A. The first metal layer is deposited all over the surface of wafer.
- B. Photoresist is deposited on the first metallisation.
- C. The photoresist is exposed to UV rays through a mask according to the shape of the design and developed.
- D. The metal layer is etched where it is not protected by the resin.

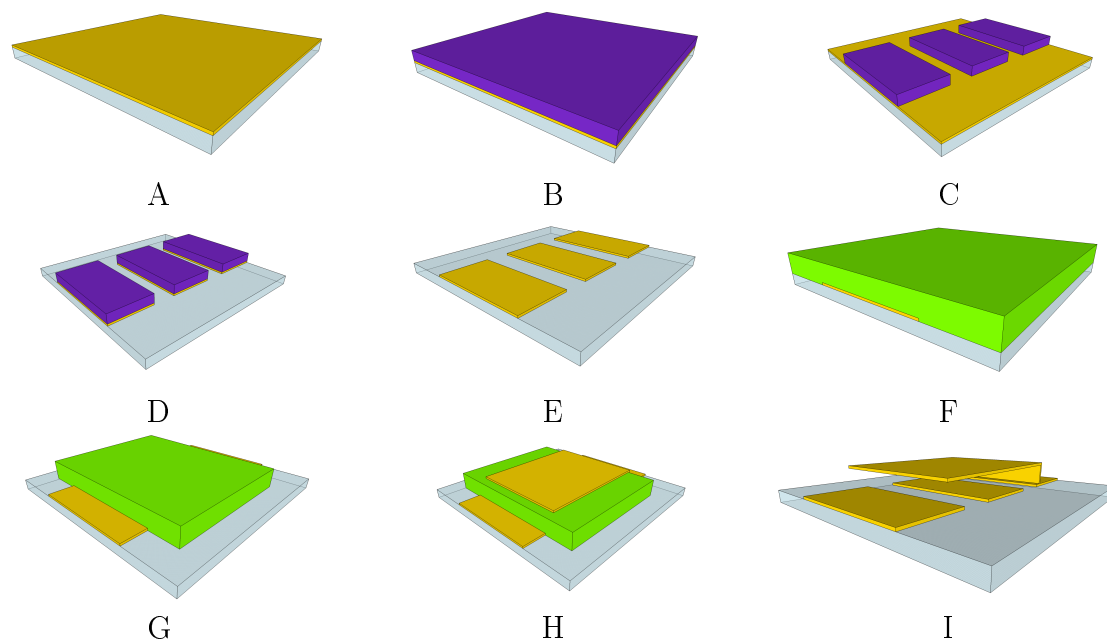


Figure 1.6: The main steps of the fabrication process of a MEMS switch.

- E.** The photoresist is fully exposed to UV rays and totally removed.
- F.** The sacrificial layer is deposited on the first metal.
- G.** The sacrificial layer is etched according to C and D.
- H.** The second metal layer is deposited and etched.
- I.** The suspended beam is released after the removal of the sacrificial layer.

1.2 Radio-Frequency (RF) MEMS for space and telecommunications

1.2.1 Definition

An RF-MEMS switch is an electronic component that allows or stops an RF-signal propagating through wave-guides. The switch is operated by an electrostatic voltage applied on a bias pad. There are two types of switches, the ohmic contact switch and the capacitive switch (see for example figure 1.1).

The switch operation is described by two states which are the ON-state and the OFF-state. When the switch is ON, it allows the RF-signal through the wave-guide and the switch is equivalent to a series resistance (in case of ohmic contact switch) or an ON-state

capacitance (in case of capacitive switch). When the switch is OFF, it stops the RF-signal, driving it to the ground and the switch is equivalent to an OFF-state capacitance. The ON-state capacitance is larger than the OFF-state capacitance by a factor named the capacitance ratio. The two states of capacitive and ohmic switches are summarized in table 1.1 with the equivalent electrical circuits.

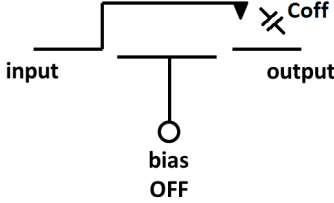
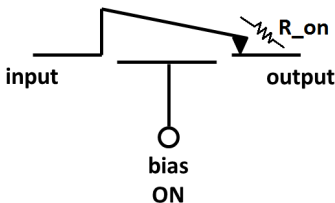
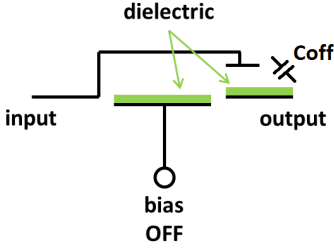
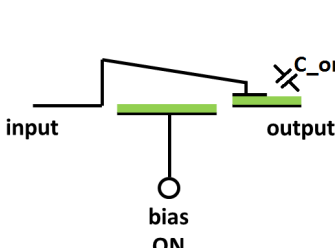
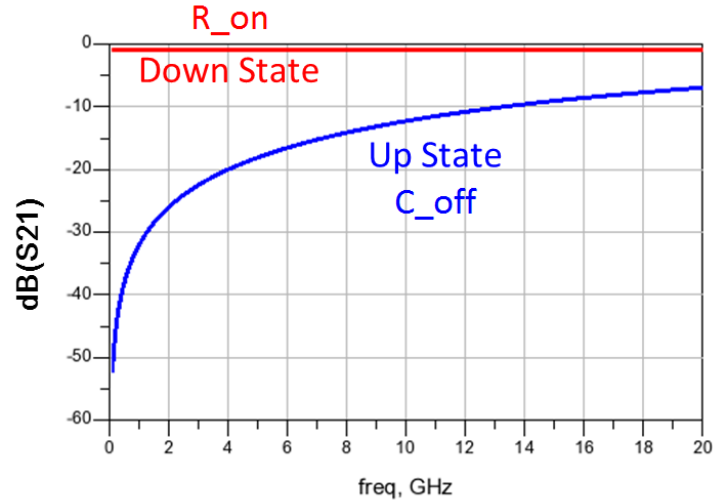
		State	
		OFF	ON
Ohmic	Cross section		
	Equivalent circuit	Low series capacitance C_{off}	Series resistance R_{on}
Capacitive	Cross section		
	Equivalent circuit	Low series capacitance C_{off}	Large series capacitance C_{on}

Table 1.1: OFF and ON states of capacitive and ohmic switches with equivalent electrical circuits.

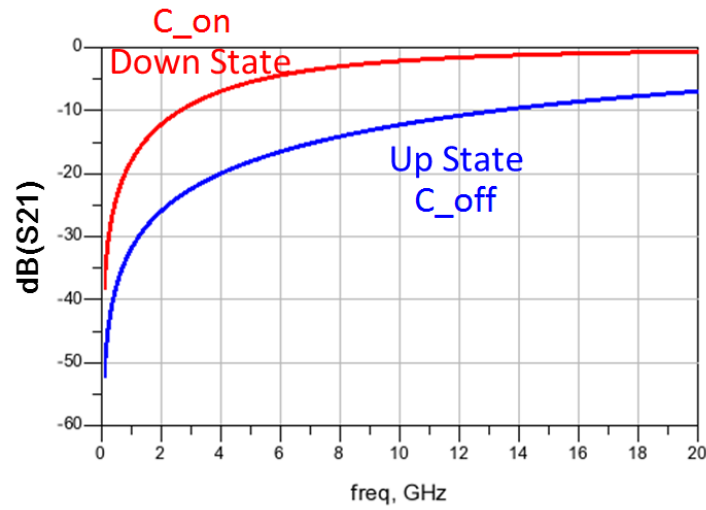
Performances of RF-switches are assessed using S-parameters measurement. S-parameters are measured values ratios of power waves (incident, transmitted and reflected) in frequency domain that depend on characteristics of the switch. The measurement results are plotted in Decibels (dB) versus frequency according to figure 1.7. The frequency range used in this work starts from DC up to 20 GHz.

A series resistance is plotted with a straight line, independent on frequency. A large resistance value has large insertion losses, the dB value is low. Whereas the dB value of a low resistance is close to 0 dB.

A series capacitance is represented by a curve that increases over frequency. At fixed frequency, a large capacitance (milliFarad) has a high dB value, whereas a lower capacitance (femtoFarad) has a low dB value.



(a)



(b)

Figure 1.7: (a) S-parameters of an ohmic contact micro-switches in OFF- and ON-states. (b) S-parameters of a capacitive micro-switch in OFF- and ON-states.

RF-MEMS switch has many advantages over semi conductors switches, since it combines the advantages of mechanical relays and the compactness, the mass fabrication process of microelectronics. Losses, linearity and power consumption are greatly reduced compared to semi conductor counterparts.

A brief comparison is given on table 1.2 between three RF switches technologies, which are an electromechanical relay, a solid state switch based on PIN diode and an RF-MEMS.

RF-MEMS are undoubtedly unique in terms of size, cost and power consumption that makes them very suitable for space applications and mobile telecommunications [12].

The main economic actors/companies in this area are shown below, with their main



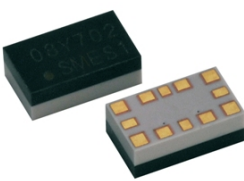
	Electromechanical	Solid-state (PIN)	RF-MEMS
Designation	Agilent 8762B	Agilent P9402C	Omron 2SMES-01
Size (mm)	70.1 * 53.3 * 14.1	52.1 * 40.8 * 14.1	5.2 * 3 * 1.8
Frequency range	DC - 18 GHz	100 MHz - 18 GHz	DC - 10 GHz
Isolation	90 dB at 18 GHz	80 dB at 18 GHz	30 dB at 10 GHz
Insertion loss	0.5 dB at 18 GHz	4 dB at 18 GHz	1 dB at 10 GHz
Number of cycles	10^6	∞	10^8
Switching speed	30 ms	380 ns	100 μ s
Power consumption	3 W	300 mW	10 μ W
Cost	€600	€750	€120
Picture			

Table 1.2: Comparison of 3 technologies of RF switches.

products. Some companies have fabricated RF-MEMS switches and most of them are presented to state global performances of such devices. They are presented in figure 1.8.

The first RF-MEMS company cited here is Radant (USA), that provides ohmic contact switches working from DC to 40 GHz [7]. The switch is created with a metal cantilever and is hermetically packaged. The switch can exceed 100 billion cycles in cold switching (a definition of cold switching is given in section 3.5 page 104), it has a 1 Ω contact resistance and a power consumption about 5 μ W at 1 kHz switching rate.

Another ohmic contact switches has been developed by Omron, a Japanese company who has manufactured RF relays hermetically packaged, working from DC to 10 GHz achieving 100 million operations [13]. The switch gets a 1 Ω contact resistance and has a power consumption about 10 μ W. At the time this thesis is written, Omron has just stopped the manufacturing of the switch due to low customer demand.

In 2006, Teravicta Technologies (USA) presented its RF-MEMS switch working from DC to 20 GHz achieving 50 million life cycle reliability with insertion loss less than 0.5 dB and a power consumption less than 10 μ W [14]. The company went bankrupt in 2008.

Airmems (France) is a company developing RF-MEMS switches targeting defense and space applications. Their switch is derived from XLIM technology developments, that have led to the success test of RF-MEMS technology in orbit, on the Athena Fidus GEO satellite in february 2014.

Delfmems (France) is a "fabless" company created in 2006 working with semiconductor foundries to provide solutions with RF-MEMS for mobile applications. They developed a switch with 0.2 dB insertion loss up to 2 GHz and 45 dB of isolation at 2 GHz [15].

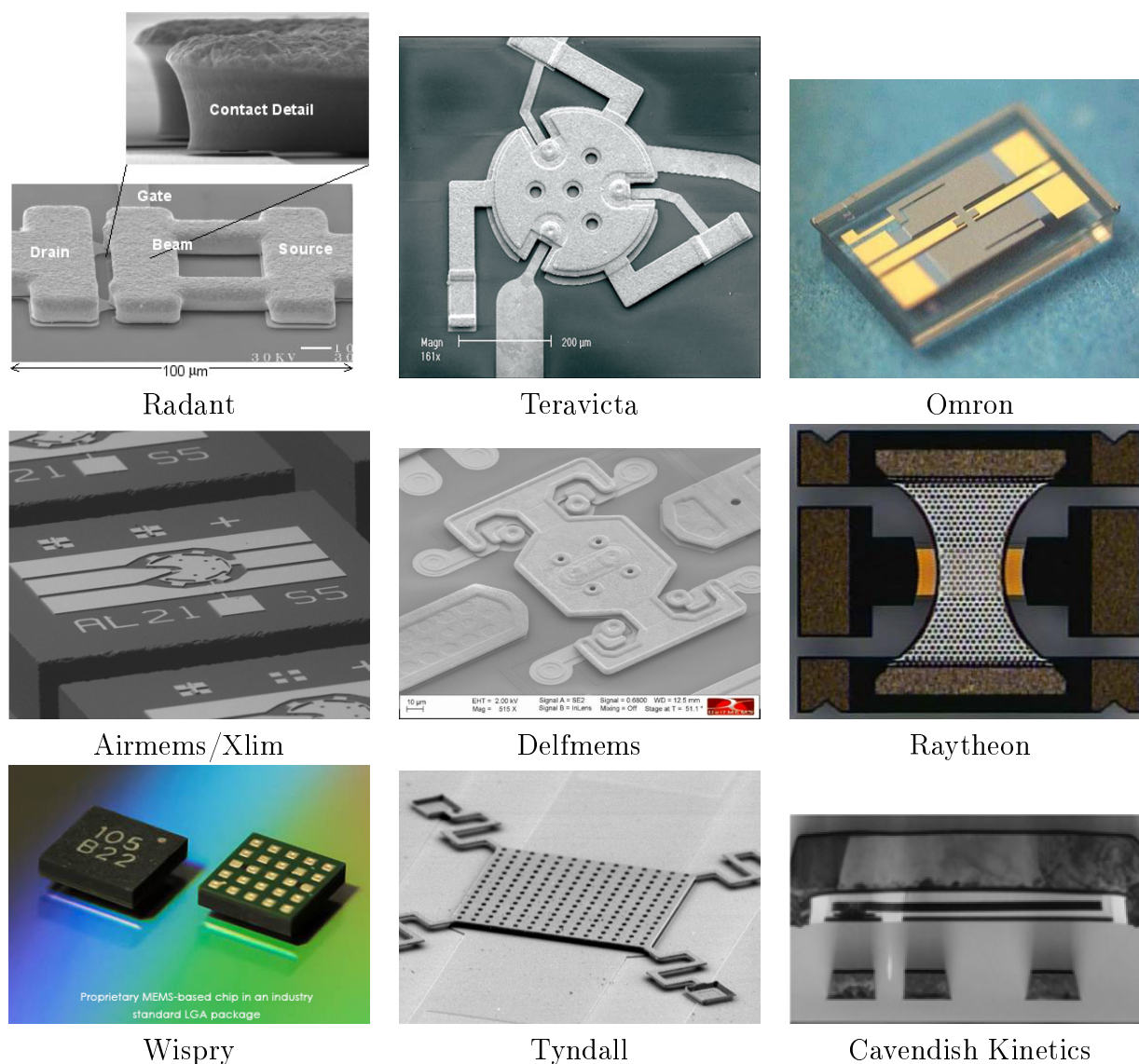


Figure 1.8: Pictures of the RF-MEMS switches (ohmic and capacitive) main actors.

Capacitive switches are a second family of RF-MEMS devices, taking advantages of large ON/OFF ratios between up and down states of bridge.

WiSpry (USA) was the first company developing capacitive RF-MEMS entering consumer electronics market inside Smart-phone Samsung Focus Flash [16] [17]. The single-chip provided by WiSpry permits antenna tuning so that the smart-phone has more flexibility and lower power consumption according to LTE telecommunication standards (4G/Long-Term Evolution).

The defence and aerospace systems company Raytheon (USA) also developed a capacitive RF-MEMS switch that also led to the founding of Memtronics. The capacitive switch can achieve 100 billion cycles of lifetime with a capacitance ratio more than 10:1. The switch is packaged with a low cost encapsulation process [18].

The National Institute Tyndall (Ireland) has developed a RF-MEMS capacitive switch

that achieves 5 billion switching cycles. The fabrication process is compatible with CMOS, the switch has insertion loss about 0.2 dB and an isolation about 19.3 dB at 30 GHz [19]. An important fact is that the switch operates between 10 and 15 V, that is low compare to other actors in the domain.

Another company, Cavendish Kinetics, provides digital variable capacitor based on capacitive RF-MEMS for precise tuning applications [20]. Their products are presented in table 1.3 offering capacitive ratios from 2.5 to 4.7 around 1 pF with step-sizes from 19 fF to 132 fF respectively. The company has recently announced reliability testings above 50 billion cycles.

Device Name	C_{min} (pF)	C_{max} (pF)	Stepsize (fF)
32CK301	0.40	1.00	19
32CK402	0.60	2.00	45
32CK503	0.65	3.10	79
32CK505	1.10	5.20	132

Table 1.3: Cavendish Kinetics, Digital Variable Capacitors.

Besides the companies presented above, there are not so many actors in the field of RF-MEMS, especially in Europe, and this technology has difficulties to break through the market and find its place. Most companies are focusing on more specific applications such as Automatic Test Equipment (ATE), mobile phones, instrumentation and RF switching.

1.2.2 Main parameters and variables of switches

RF-MEMS switches are defined and compared according to several parameters. Besides the difference in operation between ohmic and capacitive switches, all devices have similar characteristics summarised in table 1.4.

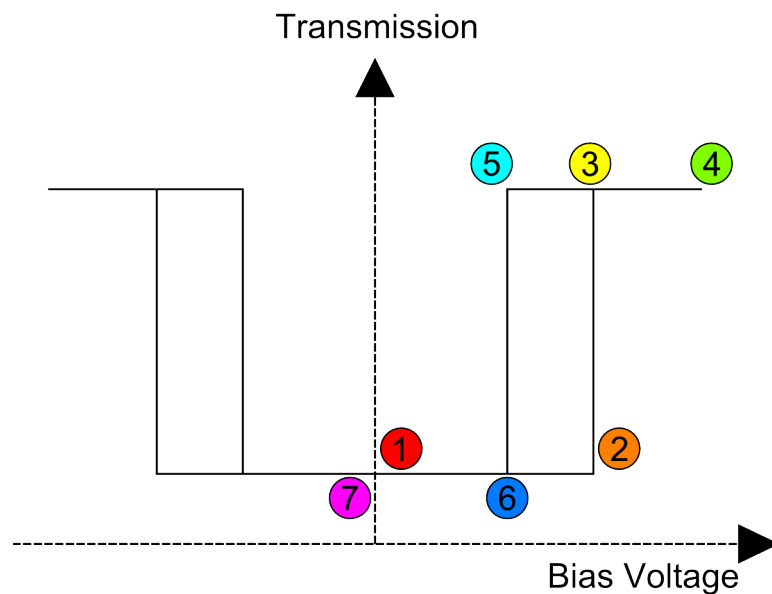
Series or shunt implementation may be considered depending on the given application. Furthermore a switch may be integrated with other switches to create a more complex circuit according to the number of pole and throw (SPST, SPDT, DPDT, SP3T, etc).

The static characteristic of RF-MEMS switches can be plotted on a Transmission versus Bias Voltage curve in figure 1.9. This is an example given for a series configuration.

The center of the curve corresponds to a low transmission (up state) of the switch at point number 1 without any applied bias. When one increases the bias voltage the switch closes itself (point number 2) and this voltage is called the pull-down voltage. Thus the switch changes its state from high transmission to point number 3 (down state). If the bias voltage is further increased, up to point number 4 one reaches the critical bias voltage for the switch (point number 4). When the bias voltage is decreased, to the point number 5 the switch is released in the up state. Indeed, the switch changes its state from high transmission (down state) to a low transmission (up state) on point number 6. Back to 0

Parameter	Abbr.	Definition
Pull-down voltage	V_p	the minimum bias voltage required to switch the RF-MEMS from OFF-state to ON-state
Release voltage	V_r	the maximum bias voltage required to switch the RF-MEMS from ON-state to OFF-state
Spring constant	k	of the movable part which depends on the design and the material
Contact force	F_c	for a given bias voltage, from tens of μN to tens of mN , depending on the design and the bias voltage
Switching times (ON and OFF)	$T_{\text{on}}, T_{\text{off}}$	with several definitions, mostly this is time between the command and the effective state changing of the switch
OFF-state capacitance	C_{off}	which is defined for rest state of the switch as two metals layers facing each other and separated by a dielectric layer
ON-state capacitance (capacitive switch)	C_{on}	which is defined between bottom electrode and top (movable) electrode separated by thin dielectric layer
Contact resistance (ohmic switch)	R_{on}	defined as the series resistance between input and output

Table 1.4: Main parameters of RF-MEMS switches.

Figure 1.9: Typical curve of a switch with transmission as a function of bias voltage $T(V)$.

V bias voltage on point number 7, the switch comes back to its initial state. The switch operates symmetrically for negative and positive bias voltage.

The transmission versus bias voltage curve $T(V)$ is also called the hysteresis curve of

the switch and gives qualitative information about the switch like hardness of materials, contact resistance/ON-state capacitance, OFF-state capacitance, pull-down and release voltages. Later in the thesis, it will be shown that the transmission versus bias voltage curve $T(V)$ will change over time because of failure mechanisms. And from the shift of curve one can deduce the phenomenon that occurs.

One simple way to get a transmission versus bias voltage curve is to bias the switch with low slopes, that can be done with a triangle waveform voltage. The transmission of a switch and the bias voltage are plotted over time in figure 1.10.

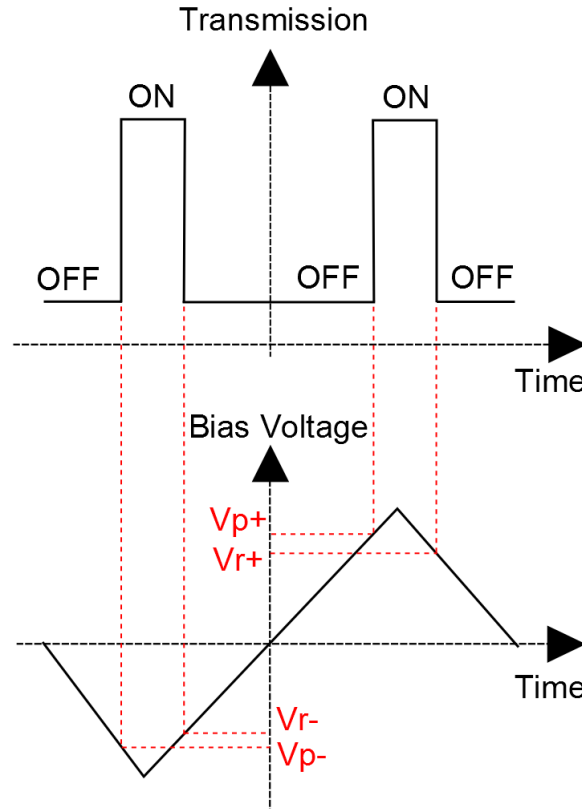


Figure 1.10: Operating principle of a switch biased by a bi-polar triangle waveform.

From these plots, the pull-down and release voltages are extracted for positive and negative bias voltages. Since the electrostatic force is proportional to the square voltage of bias, the pull-down and release voltages must be symmetrical in positive and negative ranges, i.e. $V_{p+} \approx -V_{p-}$ and $V_{r+} \approx -V_{r-}$. To get the transmission value there are two options. The first is to get the voltage across a series resistance in output of the switch as a voltage divider (DC measurements). The second is to get a voltage by a detection diode that converts the output power into a voltage (RF measurements).

1.2.3 Failure mechanisms

The failure mechanisms found in RF-MEMS take their origin in the constitutive part of the component i.e. electronics and mechanical phenomena. An exhaustive overview of phenomena involved in the failure of RF-MEMS are listed in [21] and are given here. The origin of some phenomena is discussed below.

Mechanical

As the operating elements of RF-MEMS are subjected to movement, mechanical deformation occurring over time or during fabrication may have an impact on the operation.

- Fracture

The fracture of structure may appear because of an overload of constraint in a position outside of the specifications or because of a non-proper use and in this case it would appear over time. The fatigue of material may also result in fracture when the structure is submitted to the same movement many times. This type of mechanical failure is rarely present in MEMS.

- Creep

Creep is a mechanical deformation occurring at macro-scale when for example, a shelf is loaded with a paint pot. At the beginning of the experience nothing happens if the weight of paint pot is below the requirements of shelf builder. But, from the beginning until a long time (months, years) the shelf continuously bends slowly to the ground. If the paint pot is removed, the shelf recovers a bit, and slowly tends to its original position, without reaching it. If the paint pot is kept forever on the shelf, after a while, the deformation will accelerate and result in fracture of the shelf. The mechanical creep is the plastic deformation that remains after the elastic deformation when the load is removed from the suspended structure. The evolution of creep is shown in figure 1.11.

Regarding this work, it is assumed that this phenomenon will occur in micro-structures as well. Under constant constraint and temperature, even below softening point or without reaching the yield strength, a cantilever-type or fixed-fixed beam-type mechanical structures will deform according three stages that are presented later. The structure has a semi-permanent deformation and resulting in slow shifting of parameters of the device with different characteristics. In case of video beam micro mirrors for instance, the displayed picture will be deteriorated because the deformation of mirrors will superpose the pixels and decrease the resolution.

From a measurement viewpoint, creep is visible in $T(V)$ curve (figure 1.12) where the curve narrows to the center of characteristics. This phenomenon is accelerated with temperature.

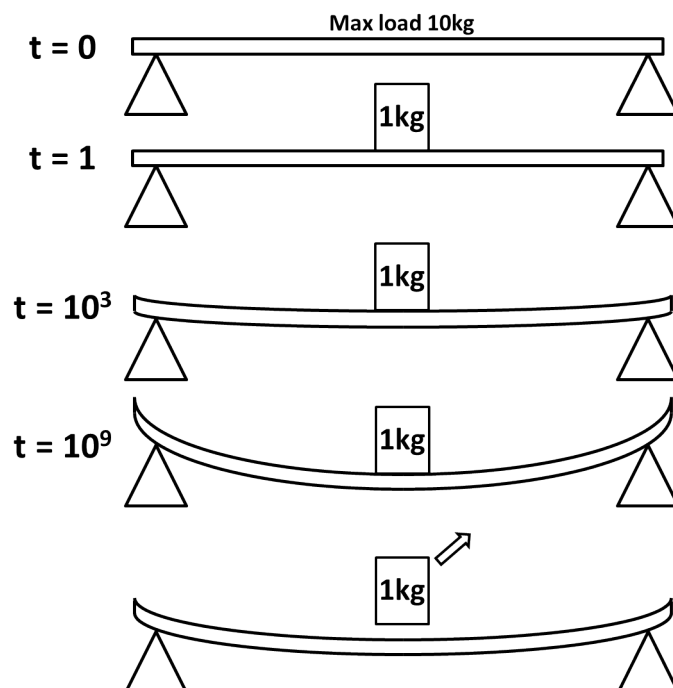


Figure 1.11: Stages of creep from the time when the load is applied on the shelf until the load is removed. Rupture will occur if the load stays on the shelf. This phenomenon is accelerated with temperature.

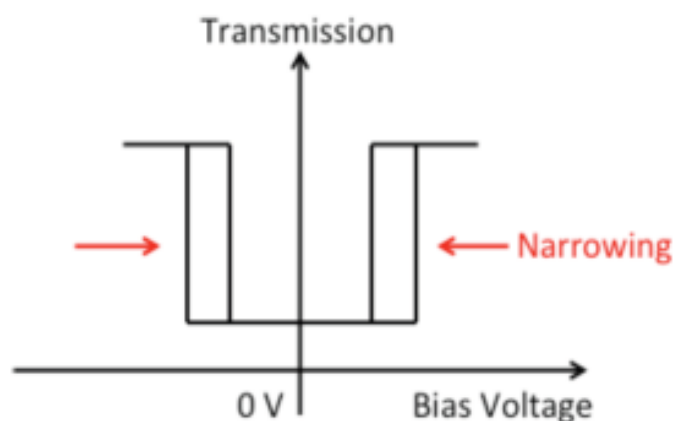


Figure 1.12: Transmission as a function of bias voltage when creep is occurring.

- Pitting of contacting surfaces

At a lower scale the roughness of the material cannot be neglected because the apparent contact surface is much less than the real contact surface. This is because of asperities of top material contacting asperities of bottom material. Upon repeated contact, the asperities can become smaller. Residual particles are pulled out from the bulk material, staying in the region of contact and preventing an efficient transmission from the top electrode to the bottom electrode. This may lead to local resistances at nano-meter scale that may impact the overall operation.

- Wear

When two different metals are touching each other the one with hard rough surface may slide on the other which is rough also but softer. This creates particles that could roll and take part in the wear. Furthermore, because of the pressure applied on the contact, the asperities due to roughness will deform plastically and since the contact may slide, then there will be welding on the asperities and finally grabbing. In case of unpropitious materials, only due to chemicals incompatibility, two materials in contact may suffer dramatically when touching and acting together.

Electrical

Failure mechanisms of RF-MEMS switches can take their origin from an electrical point of view.

- Stiction

Stiction is known as a major failure mechanism in MEMS switches especially in ohmic contact switches. Due to the high ratio between surface and thickness, MEMS structures are essentially driven by surface forces like capillary forces, Van der Waals molecular forces, electrostatic forces and solid bridging. Stiction occurring on a switch is visible on the $T(V)$ curve (figure 1.13) where the release voltage tends to zero, whereas the pull-down voltage stays stable.

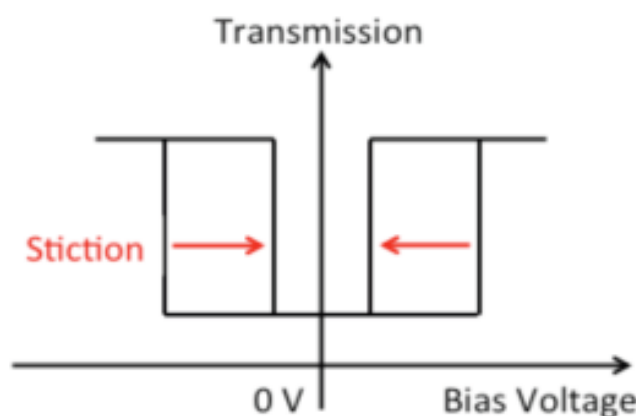


Figure 1.13: Transmission as a function of bias voltage when stiction is occurring.

- Electro-migration

Electro-migration of atoms will happen in conductors where high current densities are observed. This is the case in ohmic switches where top and bottom metals are in contact and because of roughness, the current can flow only in asperities.

- Electro-Static Discharge (ESD)

An electrostatic discharge may occur between two objects without the same potential resulting in electron transfer that may dramatically damage electronics. Proper biasing networks and handling can mitigate these effects.

- Dielectric layers

Thin dielectric layers are an important building element of capacitive switches and their quality depends on deposition conditions and materials. Designed and deposited above bias electrodes, dielectric layers allow to prevent short circuit between bias and RF-signal. Because of their thickness, thin dielectric layers are sensitive to high voltage fields required for MEMS actuation. If the bias voltage exceeds the voltage breakdown of dielectric layer, the MEMS will be strongly deteriorated or even destroyed. For example in figure 1.14 the dielectric layer was destroyed during testing because of high bias voltage.

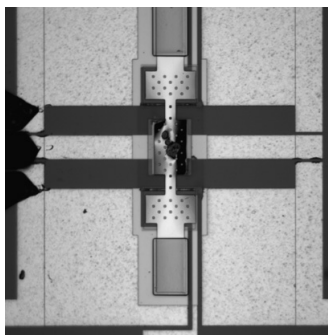


Figure 1.14: Destruction of an RF-MEMS during testing because of high voltage applied on dielectric layer [3].

Another fact that makes dielectric layers sensitive in micro-switches is the charge trapping, caused by defects and impurities in the structure. These traps will catch an electron or an hole close to bias electrode resulting in a voltage shift in the micro-switch operation. The charge trapping is represented in figure 1.15 where the charges are accumulating in the region of dielectric layer close to the movable electrode.

Dielectrics do not conduct current but there are always electrons that can cross the electronic barrier by tunnel effect for instance, and results in current leakage.

These phenomena have been studied in details and a common approach is simply to remove dielectric layers [4] [22]. The charging effect is visible on the $T(V)$ curve where the whole curve (figure 1.16) shifts to positive or negative direction.

- Contamination

Contamination arises when the component is not hermetically packaged and during operation carbonates and oxidation occur and particles come in the region of the contact and disrupt the well operation leading in an accelerated failure of the device.

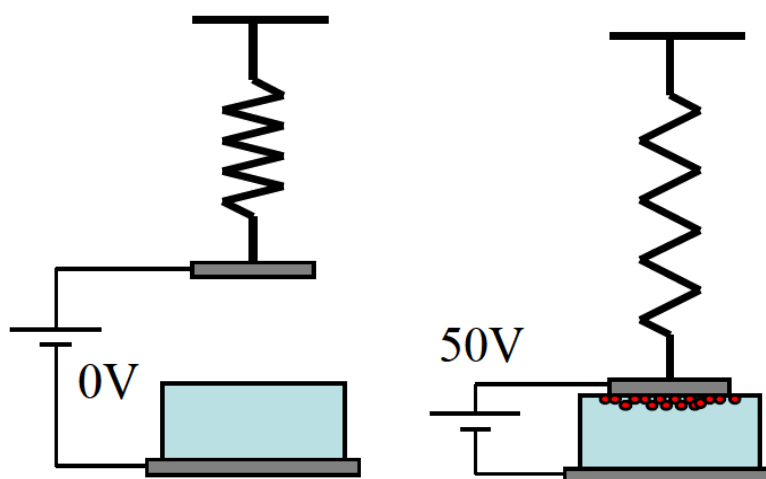


Figure 1.15: Charge trapping in micro-switches when a bias is applied on the movable structure [4].

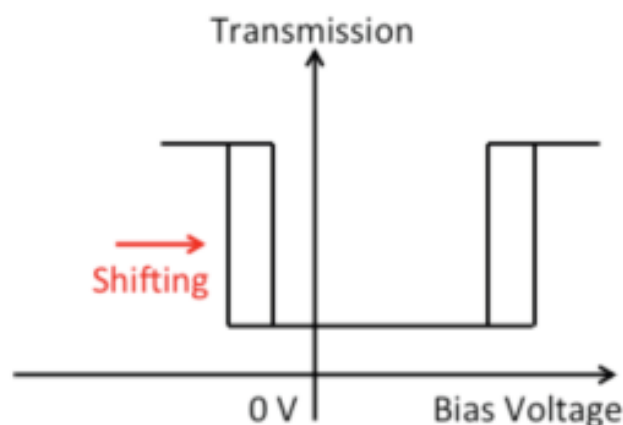


Figure 1.16: Transmission as a function of bias voltage when dielectric charging is occurring.

1.2.4 Focus on main failures mechanisms

The main failure mechanisms are summarized in table 1.5 indicating priority order to understand/solve them. High priority significance means that it is a major failure mechanism.

Stiction, creep and contamination are the most critical failure mechanisms for the reliability of RF-MEMS switches. Stiction and creep will be studied in the two next chapters.

Contamination of the contact area produces unexpected effects. As reported before [23], the environmental conditions take an important part in the lifetime of the switch. It is clear that testing measurements in a non-controlled environment for switches without protection lead to contact failure faster than in a vacuum probe station or in a hermeti-

Identification	Priority Significance	Solution
Stiction	High	Topic of this thesis, see in next chapters
Creep		Topic of this thesis, see in next chapters
Contamination		Hermetic packaging with MEMS in controlled or low pressure atmosphere
ESD	Medium	Taking care on the design to avoid floating pad and procurement of antistatic wrist strap for measurement
Wear		Inherent problem in the operation, choosing suitable materials
Delamination		A perfect understanding of deposition equipment and on the layers deposited
Electro-migration		Reducing current, choosing suitable materials
Dielectric	Low	Most problems solved without using dielectric layers
Pitting		Inherent problem in the operation, choosing suitable materials
Fracture		Precautions taken during design shall avoid fracture

Table 1.5: Failure mechanisms sorted by weight of importance.

cally package. Because of humidity, temperature, oxidation of materials, the contact will degrade faster. One way to avoid that is to hermetically package the movable part of the MEMS using an expensive technique, since price of the package may take up to 80% of the total price of the switch [24]. Among the companies presented previously, Omron and Radant succeeded in developing a package for their switches : Omron uses a glass cap to cover the MEMS and they seal the cap with glass frit bonding technique and Radant uses a similar technique.

1.3 Conclusion

The first chapter presented a global overview of MEMS technology giving some examples and the important aspects related with telecommunications and space applications. Fabrication process was introduced, to give an overview of surface micro-machining. Then, the second part of the chapter focused on RF-MEMS switches where ohmic contact and capacitive micro-switches were detailed. The current RF-MEMS companies were presented

with a short introduction to their components. Moreover, the main parameters of micro-switches were given and a technique was explained to measure them. Finally, mechanical and electrical failure mechanisms were introduced with a short definition. The most critical failure mechanisms were highlighted, which are stiction, creep and contamination. These three failure mechanisms will be studied in the next chapters.

The next chapter will focus on mechanical creep in RF micro-structures, through the development of innovative test benches.

Chapter 2 :

Creep in RF-MEMS Switches

This chapter is related to creep in Radio-Frequencies (RF) MEMS switches. The chapter is divided as follows: the first section is dedicated to theory of creep making an analogy between micro and macro-scales. The different regimes of creep will be presented and the common techniques to assess creep will be explained.

In a second section, the work done on dielectric charge trapping will be reported. The test bench will be presented, as well as measurement parameters and results. From this work, a potential presence of creep is expected to be identified.

In a third section, given the conclusion done in the previous section, an innovative assessment technique for creep based on partially biasing the switch will be presented. The results and conclusions of this technique will be discussed. At the same time, all switches used for testing will be presented.

In the last section, a second innovative assessment technique for creep will be presented. It consists in pulling down the beam of the switch controlling the applied force by servo-monitoring the contact resistance. The technique will give a better accuracy than the previous one. The results will be discussed and compared to theoretical effects.

2.1 Creep in MEMS

Creep is known as a failure mechanism in macroscopic mechanical structures, with more impact on flat and thin surfaces. This section is dedicated to the study of creep at microscopic scale. The idea is to make an analogy between macro and micro scales and infer if there is a good agreement that can be used to predict lifetime of micro-switches.

Let us consider a suspended metallic beam above a substrate. The beam is facing the output electrode as two parallel plates. The circuit is equivalent to a series capacitance with a C_{off} value. A voltage is applied on the bias pad that generates an electrostatic force between the beam and the output electrode. See for demonstration the theory of parallel plates. The force generated by the voltage pulls down the beam and allows an ohmic contact at the output. The circuit is equivalent to a series resistance R_{on} .

Due to operating conditions, the beam may remain in down state a long time. Once the beam is released to up state, it will not reach the initial position, depending on how long the beam stayed in down state. Thus, the capacitance value C_{off} will be modified. In case of antenna phase shifters, where the phase is controlled by capacitance value of RF-MEMS, creep is dramatic.

While the beam remains in down state, the spring constant decreases gradually because of creep. Once the release force, generated by the spring constant, equals the adhesion force of the contact, the beam remains stuck in down state. In case of RF switching applications, the switch will remain stuck on output electrode with no chance to open the circuit again. The circuit becomes failed.

All the steps are represented in figure 2.1.

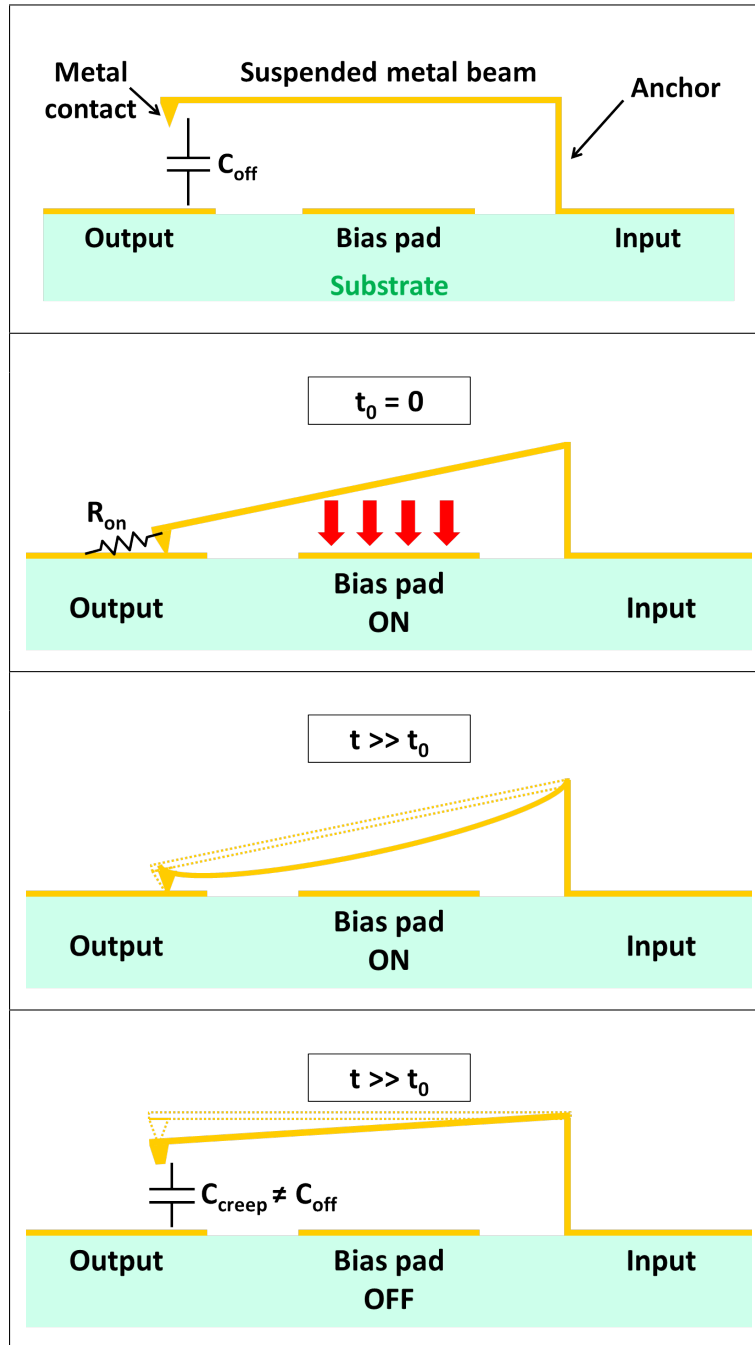


Figure 2.1: The stages occurring in RF-MEMS with shifting of C_{off} and deformation of contact because of mechanical creep.

Temperature is an important matter regarding the impact of creep. Basically, creep is accelerated with temperature. Every material that has a large thermal expansion coefficient or a low melting point will not be suitable candidates for RF-MEMS. To reach the requirements of electronic circuits that must handle a temperature about 85°C , materials have to be carefully selected. Moreover, even without being under stress, the switch may have an OFF-state capacitance that varies just because of temperature.

2.1.1 Definition of creep

Compared to macroscopic mechanical devices, MEMS are less sensitive to fatigue phenomena but more sensitive to mechanical creep [25]. Creep occurs in MEMS because of the large ratio between surface and thickness, whereas fatigue occurs for thicker structures where the cyclic stresses create fatigue cracks on the surface and then propagate inside the structure. In normal operation, MEMS bend when a constraint is applied on the structure. Locally, atoms move according different mechanisms of creep that depend on constraint, temperature and time. The mechanical creep mechanisms are discussed in next section.

It is important to notice that creep is accelerated with temperature but it is generally not considered for temperatures below 0.3 time the melting temperature of the material (in Kelvin). Despite the fact that the structure recovers a bit once the load is removed (because of the viscoelastic behaviour of materials), the deformation of the structure is irreversible even if the yield strength is not reached. Under constant constraint and temperature the deformation of a beam is divided into three modes. The primary mode occurs directly once a load ϵ_0 is applied at time $t = t_0$, it is the transient deformation usually described by a power law, which begins fast and then slows down until the secondary mode. The secondary is the steady state mode known as the linear part of creep strain versus time. During this mode the deformation is, for a part, compensated by recovery mechanisms. This information explains the slowness of the deformation. Most of the models developed in literature are expressed in this region because of the long-term use in commercial applications. To reach this mode the factories generally do a burn-in so as to control the ageing of their products. And finally, the tertiary mode leads to the rupture of the structure and its mechanisms may be numerous and complicated. The typically curve of deformation of a micro-structure under constant constraint and temperature over time is given in figure 2.2.

2.1.2 Different regimes of creep

Creep phenomenon is associated with some types of mechanism involved at grains, molecular and atomic scales. Depending on temperature and stress, these reactions are preponderant or not. The secondary mode has the longest duration (not truly representative in figure 2.2) and is usually described by the general equation (2.1).

$$\dot{\epsilon} = A. (\sigma - \sigma_0)^n \left(\frac{1}{d}\right)^p \exp^{-\frac{\Delta F}{kT}} \quad (2.1)$$

Where $\dot{\epsilon}$ is the speed of the deformation during stage 2, A is a constant, $(\sigma - \sigma_0)$ is the relative applied constraint, n is the constraint exponent, d is the grains size, p is the

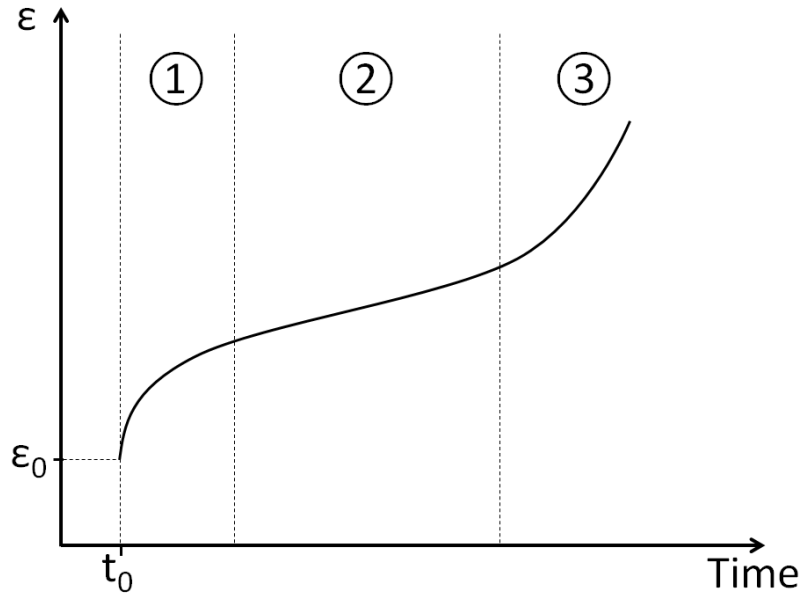


Figure 2.2: The typical curve of strain versus time to represent creep behavior at constant constraint and temperature. Creep is divided in three regimes.

size exponent, ΔF is the activation energy of the material, k is the Boltzmann's constant and T is the absolute temperature. The important parameter for us is ΔF the activation energy because it shows the dependency of a material or a structure on temperature variations and this is one of the most important requirements in space applications. Less the activation energy is and more the structure will be susceptible to temperature, leading to big deformations [26].

In macroscopic structures, creep is divided in two families, one is related with dislocation glide and the other is related with diffusion of defects.

Dislocation glides

For a wide range of temperatures, i.e. from 0.3 time the melting temperature of the material¹, and for high stresses (compared to the shear modulus) the preponderant mechanism is dislocation creep that is caused by a defect in the material that will propagate along a glide plane step by step. It is very common in monocristalline metals especially due to the symmetry of their structure (typically face-centered cubic). For polycrystalline metals, the grains act as an obstacle for the dislocation glide and so the mechanism is reduced. For dislocation glide, the typical values of n and p of equation (2.1) are $n \geq 3$ and $p \approx 0$.

¹It is generally admitted that creep has an insignificant influence for temperatures below 0.3 time the melting temperature of the material.

Diffusion of defects

For polycrystalline metals, that are mainly composed of grains, the mechanism encountered is diffusion creep. In the case of Coble diffusion creep, the crystalline defects will propagate along the grain boundaries at a lower temperature. For higher temperature than Coble, i.e. Nabarro-Herring diffusion creep, the crystalline defects will propagate through the crystal grains. Diffusion creep is known to appear rather for high temperatures i.e. 0.5 time the melting temperature of the material and above. For Nabarro-Herring diffusion creep, the typical values are $n = 1$ and $p \approx 2$. For Coble diffusion creep the typical values are $n = 1$ and $p \approx 3$.

Given these elements of theory, such a model is expected to be applicable in microstructures. Gold will be the main structural material in our switches and the maximum temperature that will be settled is 120°C. Since the melting temperature of gold is 1,064°C, the testing temperature will always remain below 0.3 time the melting temperature. So, creep mechanisms should not be observed in our switches. Otherwise, it would be expected dislocation glide rather than the diffusion creep, because of high stresses applied on the beam of switches and because of low temperature.

The following table 2.1 summarizes elements seen above.

Creep regime	Dislocation glides	Diffusion of defects	
		Coble	Nabarro-Herring
Stress level	High	Medium and below	Medium and below
Temperature range	$> 0.3 T_m$	$> 0.3 T_m$ and $< 0.5 T_m$	$> 0.5 T_m$
Formula indexes	$n \geq 3$ $p \approx 0$	$n = 1$ $p \approx 3$	$n = 1$ $p \approx 2$
Figure			
Source	[27]	[28]	[29]

Table 2.1: Summary of the different regimes of mechanical creep.

2.1.3 State of the art of creep measurement techniques

Because creep has not been widely studied in RF-MEMS, there is not much literature dealing with. However, this section is dedicated to the works what was done previously. In fact, creep is a well-known mechanism but its description is not fully understood. This is due to the complexity of the structure at atoms scale and the lack of tools to assess that. Normally, the mechanical deformations are studied according to few techniques which are introduced in the following.

Wafer curvature

The wafer curvature technique consists in measuring the deflection or the deformation of a substrate constrained by a thin (e.g. metal) layer deposited on it. This stack is supposed not to match perfectly in terms atomic compatibility, so submitting the wafer to different temperatures and measuring the bending thus induced, allow us to deduce the stress σ between the two layers thanks to the Stoney's equation (2.2) [30].

$$\sigma = \frac{E_s}{6(1 - \nu_s)} \frac{t_s^2}{t_f} \left(\frac{1}{R_2} - \frac{1}{R_1} \right) \quad (2.2)$$

Where E_s and ν_s are the Young's modulus and the Poisson's ratio of the substrate, t_s and t_f are respectively the substrate thickness and the film thickness, R_2 is the radius of the wafer curvature after deposition of the film and R_1 is the initial radius. Knowing the stress between the thin film and the substrate, it is possible to calculate the activation energy using equation (2.1). The wafer curvature technique is easy and quick to use but there is none guarantee that suspended structures will behave the same as a deposited film. Moreover the stress and the temperature are linked so that studying them separately is not possible. Whereas in the thesis, two new methods have been developed that allow to study stress and temperature separately.

Nano indentation

The nano indentation consists in applying a tiny diamond tip on a structure under test [23] [31]. It allows to know the force versus displacement curve. Together with a suited finite elements model, this technique allows to know the mechanical properties of the structure. Even if the results of this technique are very accurate, this experiment is quite expensive and long in duration.

Dedicated test structures

The use of dedicated structures [32] based on the ultimate version has the advantage to make us confident in what is measured but the accuracy of the measurement is conse-

quently, worse. Choosing this way, in the next sections, new ways to assess creep in ohmic RF-MEMS switches are investigated. Developing two methods, the results corroborate the theory of creep.

2.2 Short introduction on the need of creep measurement

A part from the main subject of the thesis, this section is presented to understand the need in studying creep in RF-MEMS. A short introduction on outlines of the charge trapping project is presented. Then, the test set up and the results are presented and discussed.

The first results presented in this thesis are the continuity of a previous thesis conducted in the lab [4] where the reliability of dielectric RF-MEMS switches was studied. The purpose of this previous thesis was to study charge trapping in thin dielectric layers to assess the reliability of capacitive switches. Some models were found to predict the lifetime of switches and solutions were given to avoid this failure mechanism. One first solution is simply to remove the dielectric layer (and get air gap instead) from the switch to avoid charging effects and to add stoppers to prevent short-circuits. A second solution is to minimize the contact area between the movable part and the dielectric layer, that can be done with stoppers. A new design has been developed and together with the test bench to assess the dielectric charging, are presented in figure 2.3. The bench is composed by an RF-source at 10 GHz and 0 dBm output power. Bias tees are on both sides of switch and the output RF-power is detected by a diode that converts the RF-signal into a voltage. The switch uses two pads. First, one applies the bias voltage V_{bias} on the bias pad to pull-down the beam. The beam is stopped by the stoppers. Then, one applies a DC-voltage on the charging pad to press the beam on dielectric layer and accelerate dielectric charging. In the down state, the switch allows the RF-signal to go from input to output.

The charging occurs when a voltage is applied between two electrodes separated by a dielectric layer, in our case this is Aluminum Nitride (AlN). Dielectric layers contain traps and can store a charge that disturbs the operation of the device, shifting pull-down and release voltages for example. One testing technique to avoid charging is to provide a symmetrical bipolar bias voltage waveform on the dielectric layer (figure 2.4 (a)). The symmetry in biasing is supposed to [33] [34] inject as many positive as negative charges in the layer, cancelling the charging effect. In the worst case of biasing (figure 2.4 (b)), the waveform would be unipolar generating only positive or negative charging accumulation.

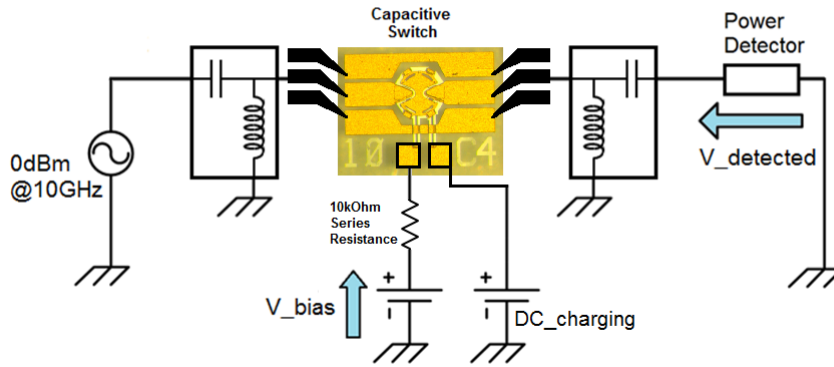


Figure 2.3: Testing set up to assess the evolution of pull-down and release voltages of capacitive RF-MEMS switches.

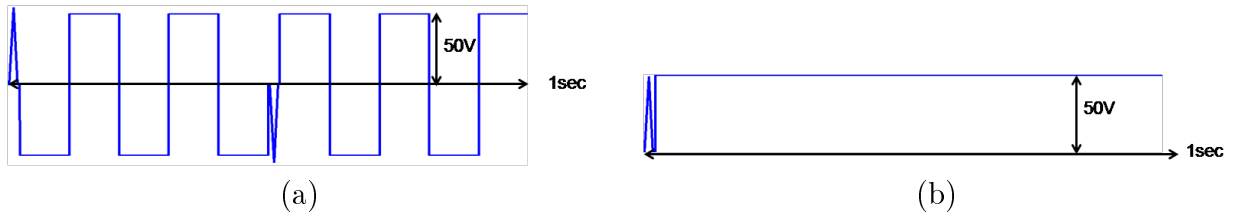


Figure 2.4: (a) 50 V bipolar bias voltage, 50% duty cycle - (b) 50 V unipolar bias voltage.

Based on the principle presented in figure 1.10, short triangles are introduced in the waveforms to monitor pull-down and release voltages over time. The pull-down voltage (V_p) is obtained on the positive slope of the triangle. The release voltage (V_r) is obtained on the negative slope of the triangle. Then V_p and V_r are plotted on the same graph versus time. The time spent in monitoring represents 2% of the total period of the stress waveform which is assumed to be low enough not to disturb the test. The switches (made on the same wafer) should have different behaviours between unipolar and bipolar waveforms if charging happens. The results are presented in figure 2.5.

Clearly, the evolution of actuation voltages is almost the same between both bias voltages. One can say that the dielectric charging is avoided with these new devices or that charging is not the most important factor of degradation. To go further we benefited from Christmas holidays to run a 3 weeks test with a switch held in down state with bipolar biasing and the result is presented in figure 2.6. The trend of actuation voltages is similar to the previous testing confirming the absence of dielectric charging and on the occurrence of other(s) failure mechanism(s).

Based on these observations, it is clear that some degradation occurs in this test and phenomena have to be decorrelated to study them separately. According to the T(V) curve (figure 1.16) presented in Chapter 1 page 33, one can say that dielectric charging is drastically reduced in these switches. But mechanical creep cannot be put aside because

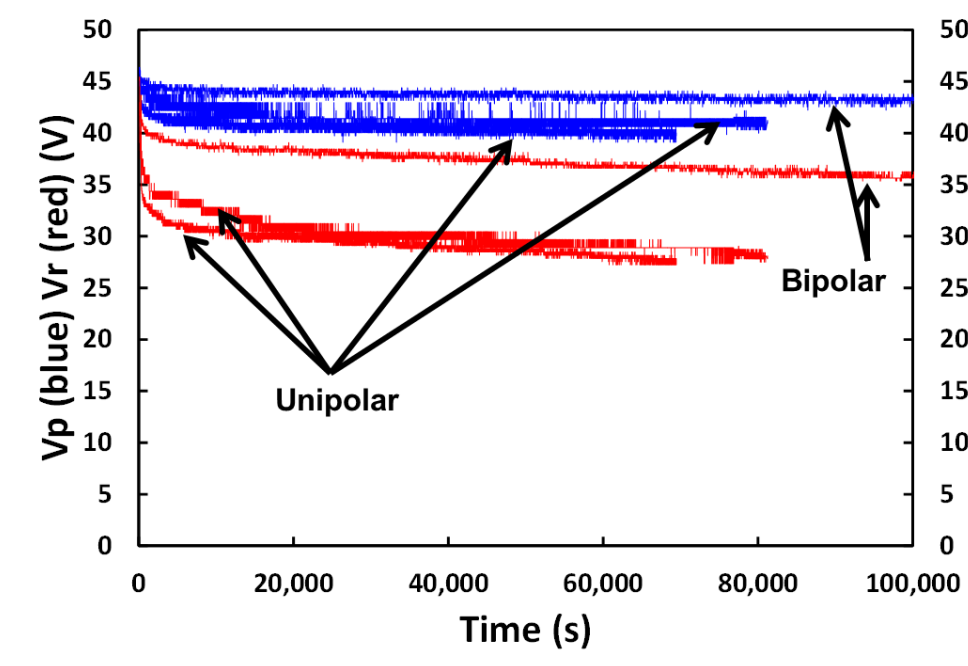


Figure 2.5: Comparison between unipolar and bipolar bias to see charging or not in dielectric layers.

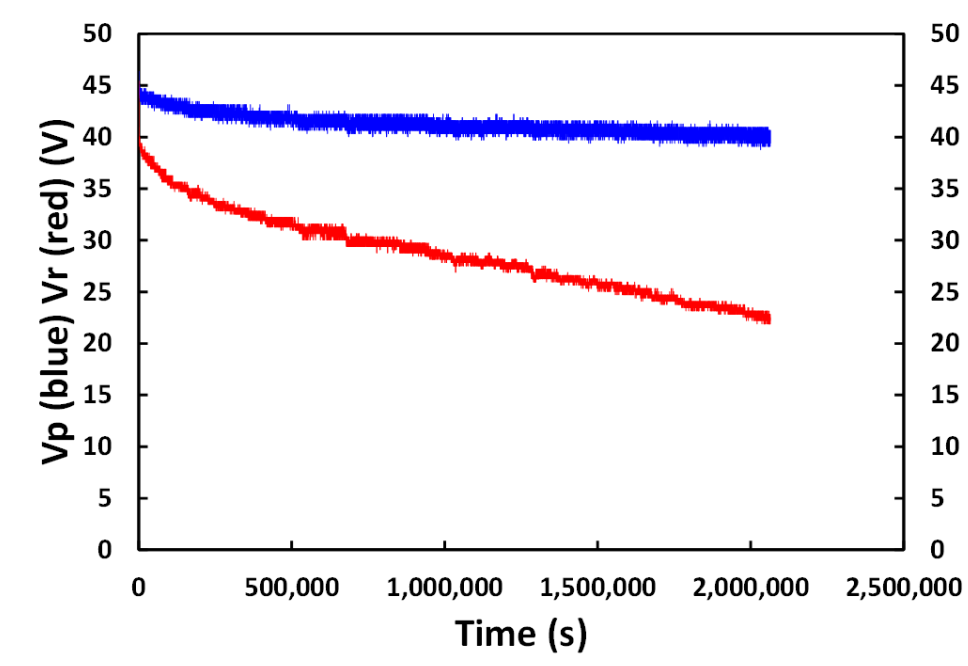


Figure 2.6: Capacitive switch pulled 3 weeks in down state with bipolar bias.

both pull-down and release voltages decrease over time. Moreover stiction must be an issue since the release voltage is decreasing more than the pull-down voltage over time. Mechanical effects are likely to be responsible for the measured shifts and the metal beams can be subjected to mechanical creep. The negative pull-down and release voltages are

important to have more information on the mechanisms occurring here.

Most of the studies on $T(V)$ shifting have been conducted on capacitive RF-MEMS switches [35] [36] [32] [37]. In this case the problem encountered is the charging of the dielectric layer what induces a shift in pull-down voltage as seen before. This shift will be superposed with the effect of creep what will be difficult to distinguish. In other words it is better using switches without dielectric layers to assess creep.

2.3 First measurement technique: Assessment of creep using constant constraint based on partially biasing the switch

Creep is a phenomenon particularly slow in duration with a very low drift, which makes it very difficult to detect and measure. The main effects of creep are structure deformation and decrease of spring constant. In this section, a first innovative test bench is presented to assess creep. In the next section will be presented a second one.

2.3.1 Introduction

As seen before, the technique commonly used to assess mechanical behaviour of thin layers may be very long and complicated requiring a lot of time and cost. The first method developed here has been proposed as an easy and quick way to assess creep in MEMS switches. The equipment used for the test bench was already available in the lab. The idea is to apply a constant force on the beam (the same as a nano-indenter) by an electrostatic force generated by a bias voltage delivered on a bias pad. Thus the bias voltage shall remain constant. Getting S-parameters from a Vector Network Analyser (VNA) allows measurements of transmission (S_{21}) or reflection (S_{11}) parameter at a certain frequency about every 6 seconds. Then, these values are recorded throughout the duration of the test. Afterwards, the equivalent capacitance of the open switch is computed for every points recorded and knowing the dimensions of the switch it allows to calculate the equivalent height of the beam compared to the substrate i.e. its deflection. The bias voltage has to be below the pull-down voltage V_p otherwise the switch pulls down and the measurement of S-parameters will not reveal information on the height of the beam.

To have an analogy in mind, the idea is very close to reproduce the set up presented in figure 1.11 in chapter 1 where a paint pot was put in a shelf. The difference is that the measurement of the deflection of beam will be done using S-parameters.

In brief, a constant mechanical constraint over time will be applied and the deflection of the beam will be measured at the same time. Mechanical creep will be investigated over

time from S-parameters measurement (S_{21}) of switches. An example of S_{21} parameter for an ohmic RF-MEMS switch is shown in figure 2.7. The down state is modelled by a series contact resistance about 0.1 dB of loss and the up state is modelled by a capacitance value of two parallel plates (tens of fF) for which the S_{21} parameter increases over frequency. The switches (in up state) are submitted to a bias voltage less than the pull-down voltage (generally 80% of V_p).

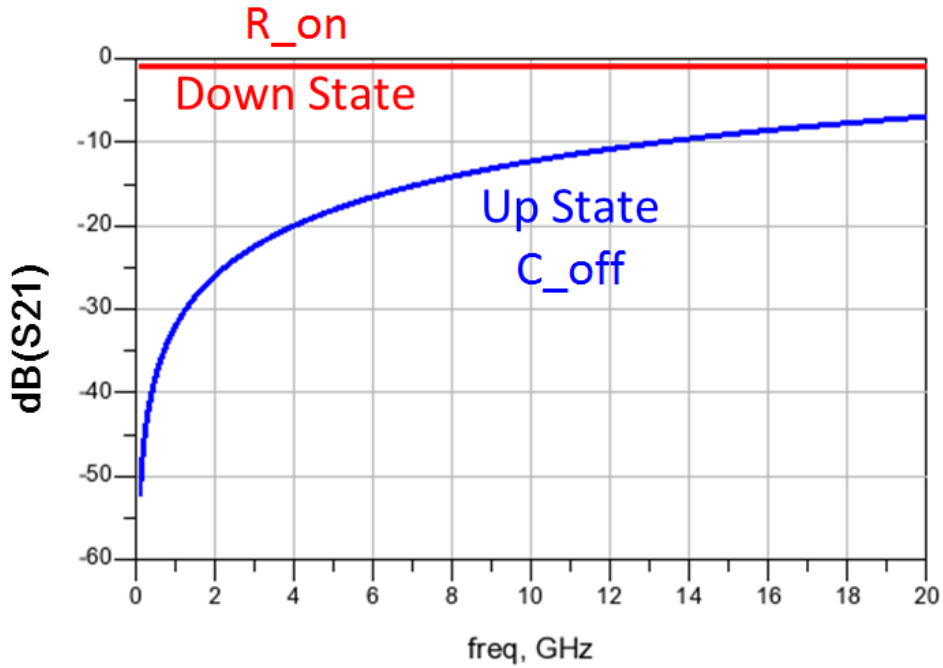


Figure 2.7: The two (up and down) states of S_{21} parameter of an ohmic switch as a function of frequency.

2.3.2 Presentation of the test bench

Previously mentioned, the test bench is quite simple consisting in a probe station connected to a VNA. The VNA is driven by a computer to get the measurement values (S_{21} , S_{11}) at 2 GHz and 12 GHz. So this is 4 measured values taken every about 6 seconds that are saved in a file. Taking 4 points instead of one allow us to have more flexibility in case of noise and series or parallel configuration, avoiding changes in the test bench. The components are usually designed in series configuration in a Coplanar Wave-guide (CPW) associated with a bias pad decoupled from CPW lines. All of them are ohmic contact switches without any dielectric layer. The bias generator is controlled manually since the voltage value is unique for one single testing. The measurement is held until the switching down or is stopped when the measurement exceeds a long time (typically more

than 12 hours). A schematic representation of the measurement technique is shown in figure 2.8 and the test bench is presented in figure 2.9.

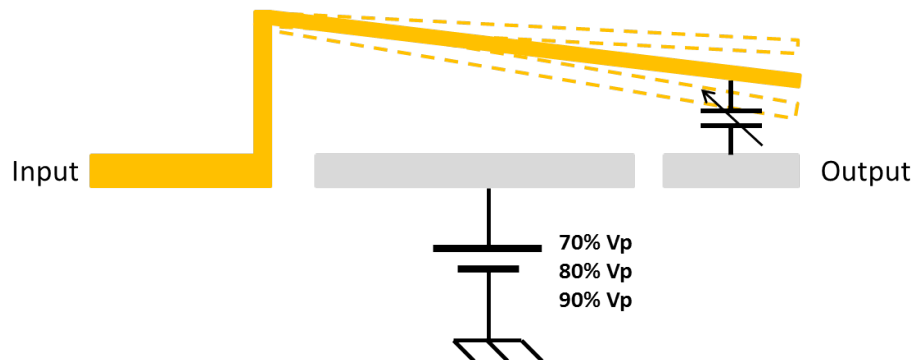


Figure 2.8: Cross-section of the switch and the different bias voltages applied on the structure to study the effect of creep.

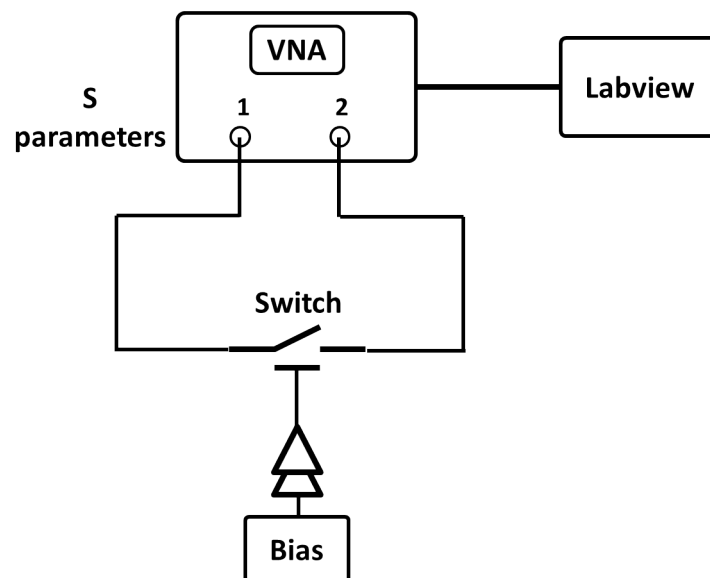


Figure 2.9: Test bench to assess creep consisting in partially biasing the switch and get the S-parameters via a Vector Network Analyzer (VNA) and save data with Labview.

It will appear later in sections 2.3.4.4 page 56 and 2.3.5.1 page 59 that the bench needs some modifications to handle temperature measurements but the principle will remain the same.

2.3.3 Precautions and approximations

Before going further, an explanation about approximations done here has to be detailed in order not to miss important details that the reader might consider.

2.3.3.1 Drift of constant constraint

Some elements in theory of parallel plates actuator are going to be exposed in order to understand how electrostatic force is linked with the gap between both electrodes.

Let us consider two parallel metallic plates, one is fixed and the other is mobile, anchored by a spring constant. Applying a voltage between them will generate a force that makes them to come closer. This is the electrostatic force F_e expressed in equation (2.3).

$$F_e = \frac{1}{2}Q.E \quad (2.3)$$

Where Q is the charge between fixed electrode and mobile electrode, and E is the electric field between them. The electric field is defined in equation (2.4).

$$E = \frac{V}{h} \quad (2.4)$$

Where V is the voltage applied between electrodes as known as the bias voltage and h is the gap between the electrodes. So the formula of the electrostatic force can be rewritten as in equation (2.5).

$$F_e = \frac{Q.V}{2h} \quad (2.5)$$

On the other side the spring constant generates a restoring force F_r that is opposite to the electrostatic force. The restoring is expressed in equation (2.6).

$$F_r = k.(h_{up} - h) \quad (2.6)$$

Where k is the spring constant of the suspended structure, h_{up} is the height of the beam at the rest state and h is the height of the beam under constraint. So the term $(h_{up} - h)$ represents the shift of the beam from its original position, i.e. when the bias voltage equals 0 V. At steady state, when the beam is immobile, the electrostatic force equals the restoring force (equation (2.7)).

$$F_r = F_e \quad (2.7)$$

Then equation (2.7) is developed using equations (2.5) and (2.6).

$$k.(h_{up} - h) = \frac{1}{2}Q.E \quad (2.8)$$

$$k.(h_{up} - h) = \frac{1}{2}C.V\frac{V}{h} \quad (2.9)$$

$$k.(h_{up} - h) = \frac{C.V^2}{2.h} \quad (2.10)$$

C is the capacitance value of the switch that is dependent on the distance between the metallic plates h . So the capacitance is expressed as a function of its physical parameters in equation (2.11).

$$C = \frac{\epsilon_0 \epsilon_r . S}{h} \quad (2.11)$$

Where ϵ_0 is the vacuum permittivity and S is the surface of facing plates. Considering the air, the relative permittivity ϵ_r equals 1. The capacitance is replaced in equation (2.12).

$$k.(h_{up} - h) = \frac{\epsilon_0 . S . V^2}{2.h^2} \quad (2.12)$$

Thus developing the formula allows us to express the bias voltage V as a function of the height of the beam in equation 2.13.

$$V = \sqrt{\frac{2.k.h^2(h_{up} - h)}{\epsilon_0 . S}} \quad (2.13)$$

Thus, the bias voltage V is proportional to the gap h and the spring constant k . So if the spring constant decreases (because of creep), as the bias voltage is fixed, the gap shall decrease in order to compensate the disequilibrium in the equation. But the electrostatic force is inversely proportional to the square of the gap. So the gap will decrease faster than the spring constant so the switch will pull in down state accelerating. As a consequence, the results of experiment will be a superposition of creep together with a progressive increase of electrostatic force over time. Being aware of that, the technique has been employed anyway and one improvement of this test bench would be to use a servo loop between the VNA and the bias generator to keep the electrostatic force constant. The VNA would catch the transmission parameter, then send it to a computer that would interpret the results and order eventually a new voltage to the bias generator. Later, this idea has been tried out in the second measurement technique in section 2.4 page 62.

To summarize the main idea, mechanical creep is going to be assessed at constant temperature, under constant bias voltage but in reality, the constraint, depending on the electrostatic force, will not be constant.

2.3.4 Creep measurements at room temperature, varying bias voltage

A campaign was done on 4 types of RF-switches. Three of them are fabricated in the lab and the last comes from the Omron company. They are presented in figure 2.10.

- The 5 anchors fixed-fixed circular structure known as S5.
- The symmetrical cantilever known as SYM.
- The asymmetrical cantilever known as ASYM.
- The commercial RF-MEMS 2SMES-01 from Omron.

The asymmetrical cantilever is not represented here but it has almost the same dimensions that the symmetrical one. The only difference is between the two anchors where one is longer than the other that makes an asymmetric design. A detailed description of symmetric and asymmetric switches are given in chapter 4 section 4.1 page 108.

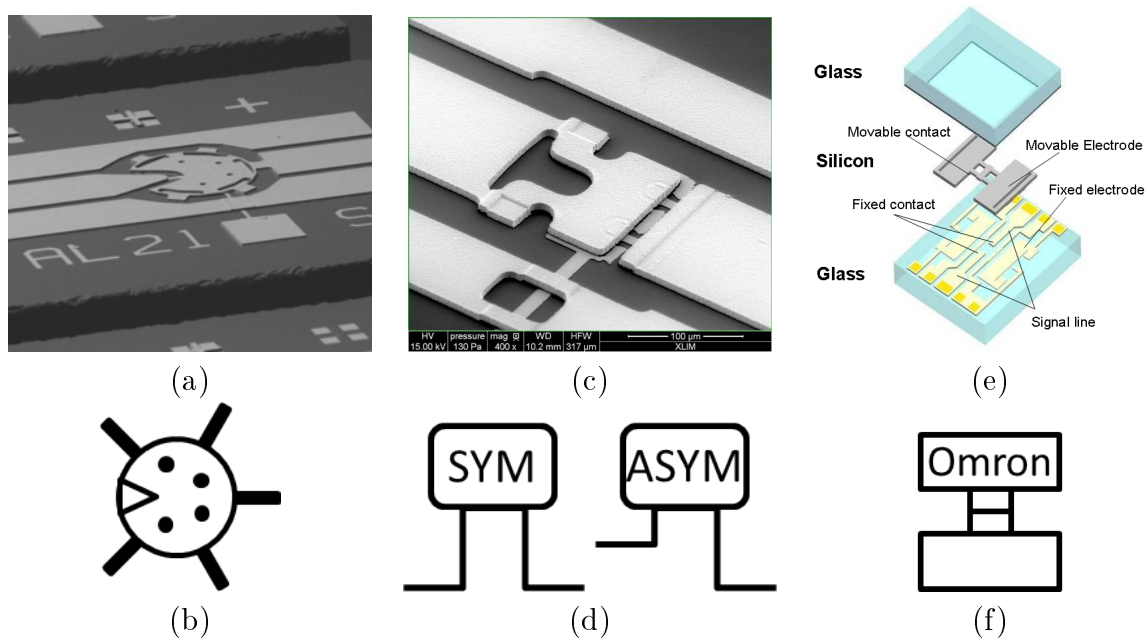


Figure 2.10: (a) and (b) The 5-anchors circular structure, S5-switch from Xlim (c) and (d) The 2-anchors symmetrical cantilever, SYM-switch from Xlim (e) and (f) The Omron RF-MEMS.

The S5-switch is a very robust switch with a circular suspended structure with 5 anchors in gold evaporated by electrons beam and then electroplated. It gets a high contact force to get low contact resistance and a high restoring force to prevent stiction.

The SYM-switch is a cantilever anchored in one side with two orthogonal anchors also in gold evaporated by electrons beam and then electroplated. The orthogonality of the

anchors allows us to avoid residual stresses between layers due to fabrication process. The suspended cantilever is particularly thick to get a high restoring force and it is wider than it is long in order to limit short-circuits between bias pad and RF-lines.

The ASYM-switch gets the same characteristics as the SYM-switch except in the length of one of the anchor that is longer than the other. The aim of the asymmetry is to modify the movement of the bridge during pull-down so as to prevent bounces.

The Omron switch is described later in this thesis at section 2.3.4.4 page 56.

All families of switches coming from our fabrication process were chosen so that they get almost the same parameters defined in table 1.4, i.e. less than 10% drift and the procedure of selection was done by applying a unique bipolar triangle waveform on the bias pad to get these parameters via the $T(V)$.

2.3.4.1 Measurement results on S5-switch

The first tested switches are the S5. S5-switches have about 38 V of pull-down voltage and results are presented in figure 2.11.

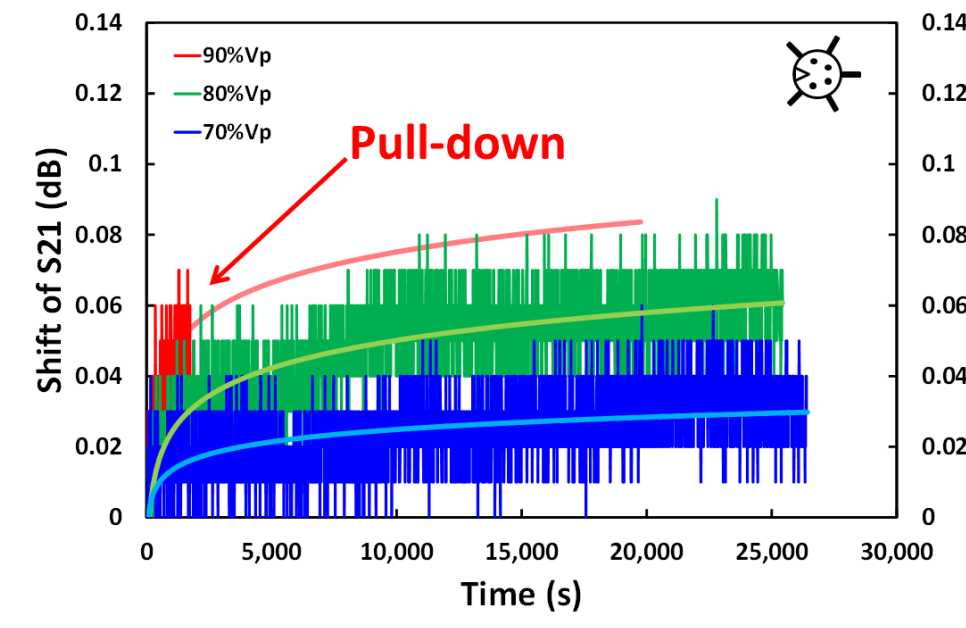


Figure 2.11: Measurement results of the transmission parameter shifting over time for three S5-switches biased at 70%, 80% and 90% of their pull-down voltage.

Due to the sampling of the VNA and the low level of measurement (about 31 dB of loss at 2 GHz) blue, green and red lines have plotted to fit the measured points. Plotting the shift of the transmission parameter S_{21} at 2 GHz over time allows us to confirm that more the applied voltage is close to the pull-down voltage V_p and faster the switch falls in down state. That is why the red curve is very short, the test lasted half an hour

before reaching the down state. In first approximation the fitted curves are described by a natural logarithmic function given in equation (2.14).

$$\Delta S_{21} = a \cdot \ln(\text{Time}) + b \quad (2.14)$$

Where a is the speed of the shift i.e. the slope of the fitted curve in a log-log graph and b is the y-axis intercept. The slopes for the measurements at 70%, 80% and 90% are respectively 5.04×10^{-3} dB/ln(s), 11.3×10^{-3} dB/ln(s) and 12.5×10^{-3} dB/ln(s) that confirms the acceleration of creep with a higher constraint. The natural log function has been chosen to fit the shift because of its easiness and quickness compared to creep model.

2.3.4.2 Measurement results on SYM-switch

The second type of tested switch is the SYM-switch. It is a two-anchors cantilever instead of the previous one with five anchors circular structure. These second switches have a pull-down voltage about 92 V and get loss about 17.5 dB at 12 GHz. The measurement was done at 12 GHz because it was not exploitable at 2 GHz. It is not a big deal because the behavior (i.e. the shift in transmission) remains the same between 2 GHz and 12 GHz. The measurement results are shown in figure 2.12.

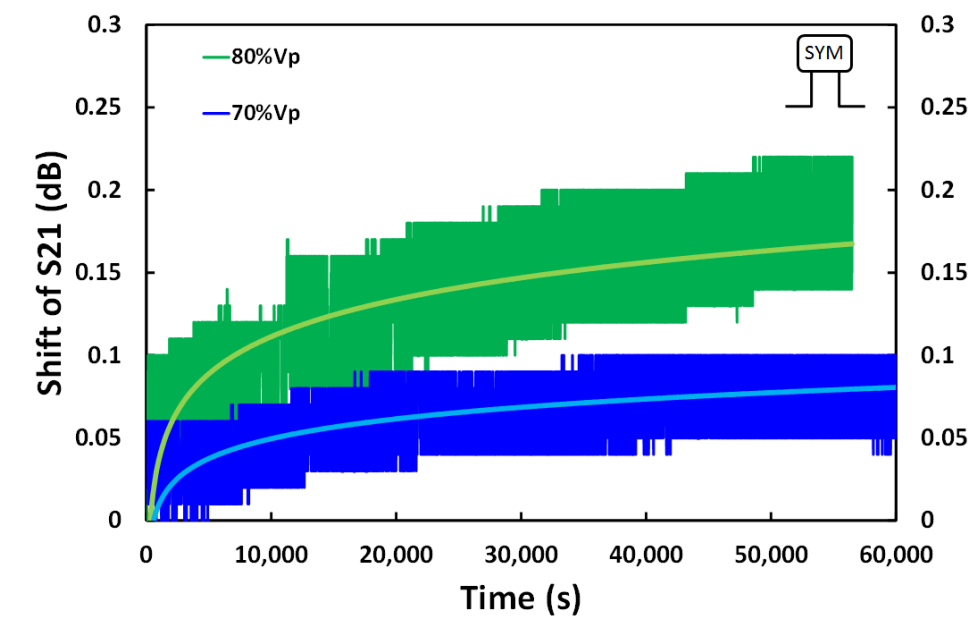


Figure 2.12: Measurement results of the transmission parameter shifting over time for two SYM-switches biased at 70% and 80% of their pull-down voltage.

Also in this case, the shift of the transmission parameter is more important for 80% than 70% still indicating the acceleration of creep with a higher constraint. However here this is another kind of structure (two-anchors cantilever) and looking more precisely on

the curves it allows us to note that the bending of the beam is faster than in S5-switches (fixed-fixed structure). In fact, the slope for the 80% curve (green) is $32.4 * 10^{-3}$ dB/ln(s) and the slope for the 70% curve (blue) is $17.3 * 10^{-3}$ dB/ln(s). It appears that a suspended beam anchored in one side (SYM-switch) suffers more from creep compared to multiple anchored circular structure (S5-switch). There may be more mechanical constraints on this type of switch.

This difference in creep behaviour may come from the structure itself since the S5-switch and the SYM-switch have a different thickness of movable part leading in a different spring constant leading in different pull-down voltage (38 V for S5-switch compared to 92 V for SYM-switch). Actually the same technique is used to deposit these layers, beginning by electron beam deposition and finishing with gold electroplating. But, the cantilever of the SYM-switch is thicker than the S5-switch.

Second, there is a matter considering creep regarding the design. While the bias is applied, electromechanical simulations allows to know how much the material is stressed and where, because some points may endure very high strain like twisting, compression, bending [38]. That kind of problems has to be mitigated as much as possible. Here this is a free suspended cantilever (SYM-switch) compared to a five anchors circular structure (S5-switch) where the degrees of freedom are limited and mechanical stress may be different.

Finally, considering the complexity of some layers in the fabrication process, due to multi-layers stacking (adhesive layer, evaporated layer, electroplated layer, sacrificial layer, ...) this may foster creep. Eventual residual stresses created during fabrication may remain between two different layers, because of considerations like temperature deposition and matching compatibilities. More generally, a good-understanding of materials used in the process are utmost importance and a complete study of each material deposited is necessary.

2.3.4.3 Measurement results on ASYM-switch

The following results consider the ASYM-switch structure which is almost the same as SYM-switch except in the length of one of its two anchors. This test will help us to confirm if the conclusions between S5 and SYM are consistent and if the results obtained with the SYM-switch are reproducible with ASYM-switch.

These switches have a pull-down voltage about 87 V and get loss about 17.5 dB at 12 GHz. The measurement results are shown in figure 2.13.

Once again, higher the applied force on the structure is and bigger the shift of the transmission parameter S_{21} is over time. Here the green curve obtained with 80% of pull-down voltage has a slope about $42.0 * 10^{-3}$ dB/ln(s) compared to the blue curve (70% of

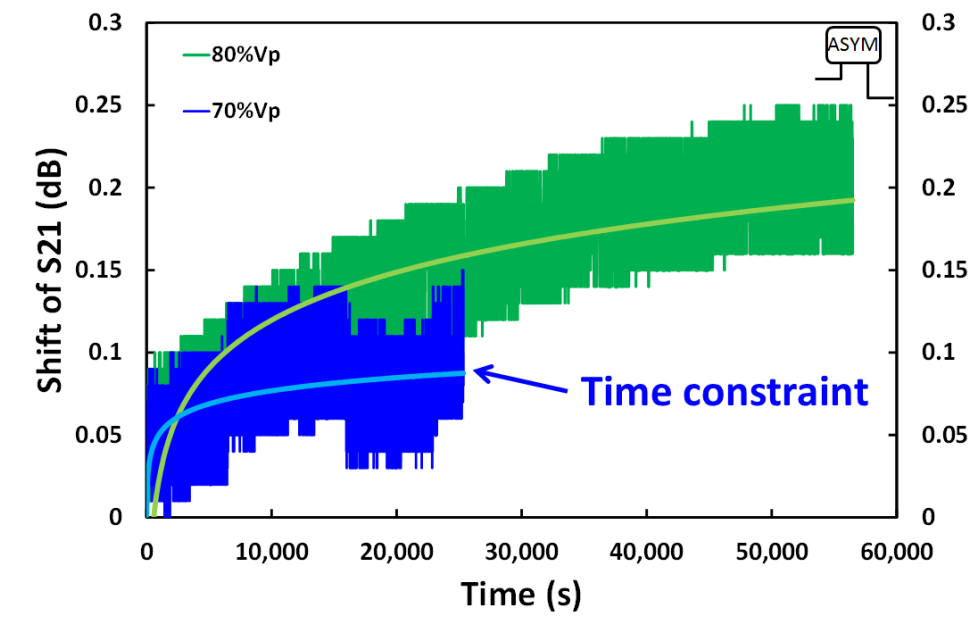


Figure 2.13: Measurement results of the transmission parameter shifting over time for two ASYM-switches biased at 70% and 80% of their pull-down voltage.

V_p) with $11.5 \times 10^{-3} \text{ dB}/\ln(s)$.

Generally, suspended beams such as SYM and ASYM-switches are more sensitive to mechanical creep than multi-anchors circular type S5-switch.

2.3.4.4 Measurement results on Omron switch

The last type of switch tested with this technique is a commercial component that gets a completely different fabrication process compared to Xlim. The Omron RF-MEMS switch is a Single Pole Double Throw (SPDT) switch, it has a monocrystalline silicon suspended structure bi-anchored. This kind of material is supposed to have a near perfect structure, letting it not to be susceptible to creep in particularly. As this switch is packaged, the measurement was not done on a probe station as it has been done until now. So the bench was changed so as to get the transmission parameter by another method. The switch has been mounted on a Printed Board Circuit (PCB) with SMA connectors according to the figure 2.14.

The testing method consists in applying an RF signal from an RF source at 12 GHz and 10 dBm on the RF-com port of the switch. The RF-output 1 is connected to a detection diode that converts the RF power into a voltage and this voltage is gotten via an oscilloscope driven by a computer that saves the data every 6 seconds. The bias is provided by the same generator connected to the bias connector of the PCB. So the set up is minimalist as previous one, however the RF power is higher in this case (the VNA is between about -10 dBm and 0 dBm) because the diode is not as accurate as the VNA,

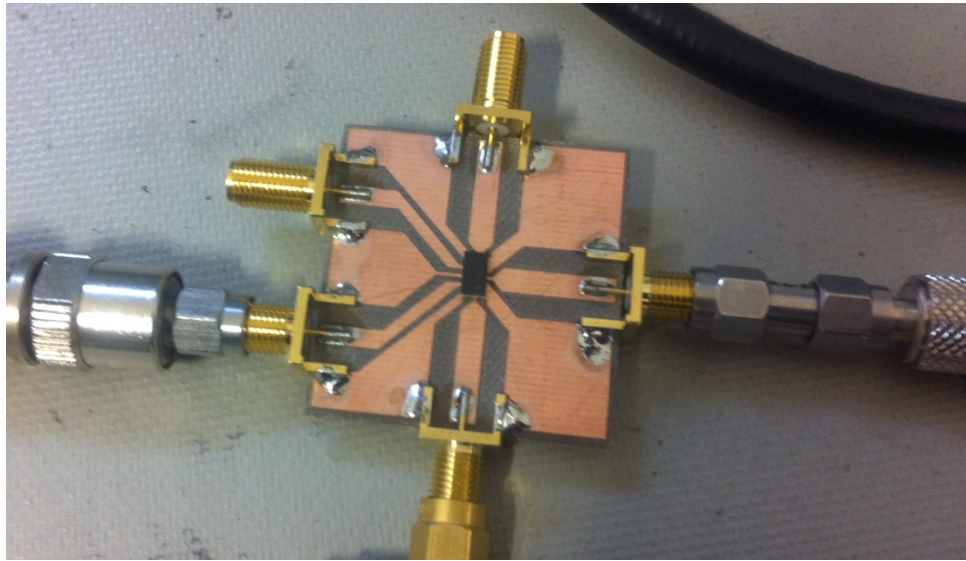


Figure 2.14: Photograph of PCB mounted Omron switch with connectors.

so the input power has to be increased to get a signal in output with acceptable noise. It is assumed that the increase of power at the input of the switch does not affect its operation, since it is still a low level of power compared to the maximum power (30 dBm) given in the data sheet [39]. The updated test bench is shown in figure 2.15.

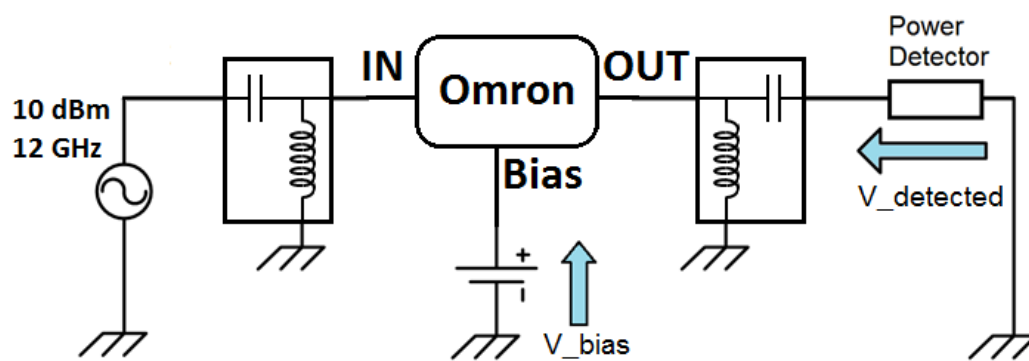


Figure 2.15: Photograph of PCB mounted Omron switch with connectors.

The given voltage in output of the diode was re-converted in dB so as to make a comparable data with the others switches. The Omron switch has a 24 V pull-down voltage and 21 dB of loss at 12 GHz biased at 80% of V_p . The test was held during 70 hours and is presented in figure 2.16.

Whereas all the other switches biased at 80% ended in down state, the Omron is the only one that stays stable and did not switch during the whole test. Due to the monocrystalline structure, at constant room temperature and constraint, the Omron RF-

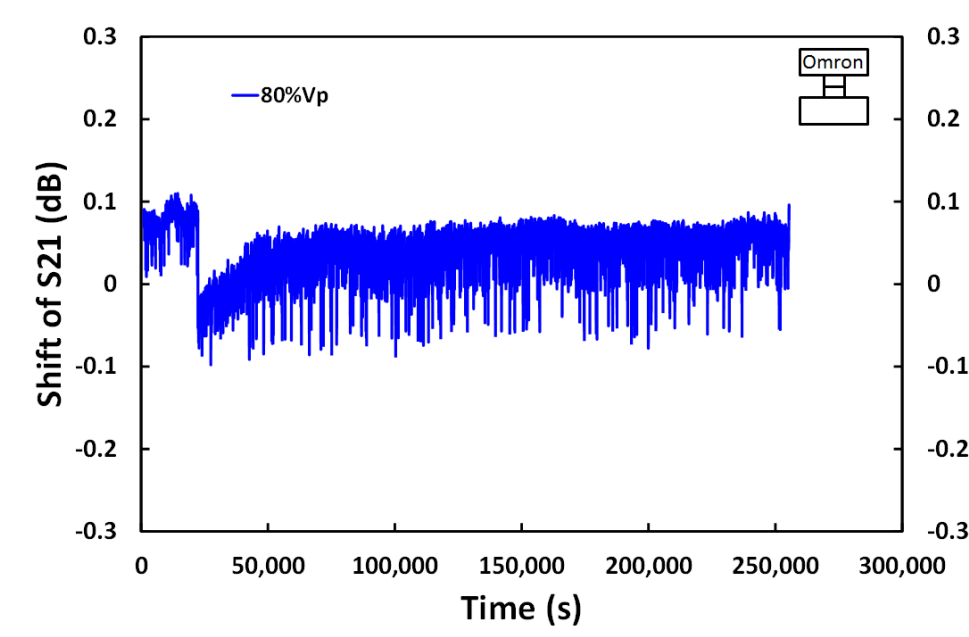


Figure 2.16: Measurement result of the transmission parameter shifting over time for the Omron RF-MEMS switch 2SMES-01 biased at 80% of its pull-down voltage.

MEMS switch has demonstrated an extreme low sensitivity to mechanical creep.

2.3.4.5 Discussion

All the results regarding the measurement of creep at several constant constraints are summarized in table 2.2.

	S5	ASYM	SYM	Omron
V_p	38 V	87 V	92 V	24 V
$70\%V_p$	5.04	11.5	17.3	-
$80\%V_p$	11.3	42.0	32.4	≈ 0
$90\%V_p$	12.5	-	-	-
Unit	$\times 10^{-3}$ dB/ln(s)			

Table 2.2: Summary of the slopes measured on several switches at several constant constraints.

Materials used in S5, ASYM and SYM switches are electroplated gold. There is a big difference between electroplated gold structures and monocrystalline structure (Omron), thus an important influence of the material is noticed. Then, there is a significant difference between S5-switch (which is a membrane) and the cantilevers (SYM and ASYM). So the switch design has an important impact on the immunity to creep. One assumes that, due to different geometric structures, the stress is distributed differently. Moreover, S5-switch is bigger than cantilevers in terms of size, allowing a distribution of stress more wide, so less dependence on mechanical creep. Finally, one can say that the deformation

rate depends on material and also on design that is confirmed by results obtained with Omron switch that has a very different structure.

2.3.5 Creep measurements at constant bias voltage ($80\%V_p$) varying temperature

The impact of bias voltage on mechanical creep in RF-MEMS switches has been demonstrated. Now, using the previous technique, the dependence on temperature will be presented. The test bench is modified to allow temperature measurements in a vacuum station and presented in figure 2.17.

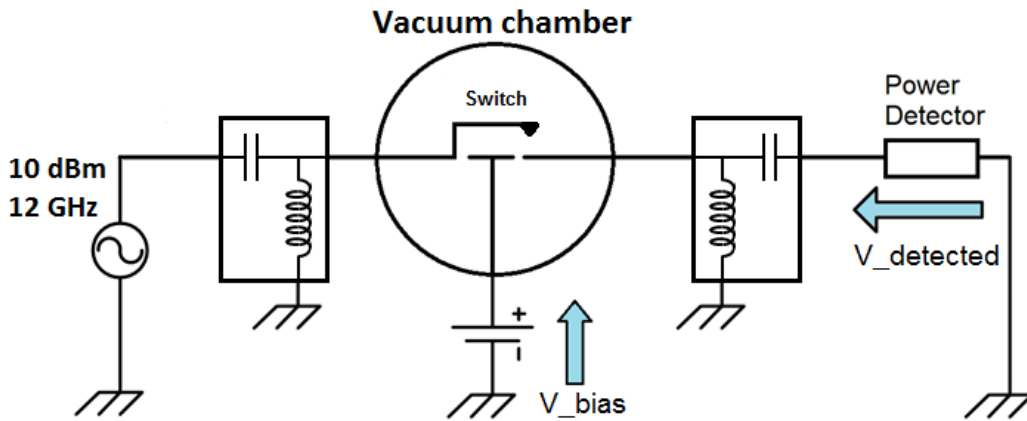


Figure 2.17: Photograph of PCB mounted Omron switch with connectors.

2.3.5.1 Measurement results on SYM-switch

Here, the main idea is, with the technique used for Omron switch (with detection diode), to study the effect of temperature on SYM- and ASYM-switches². Their sensitivity to creep is expected to be accelerated with temperature conducting tests at 60°C, 80°C and 120°C. The switches are all biased at 80% of V_p to get a constant constraint and are put in a controlled environment to avoid disruptive effects affecting temperature. In figure 2.18 are presented the results for the SYM-switch.

Here the first observation is that creep is accelerated with temperature. Indeed, the sudden increase in the shift of S_{21} at 120°C first and then at 80°C, can be explained by the fact that the switches fell in down state because the spring constant k decreased and F_e became much higher than F_r (see for the demonstration section 2.3.3.1 page 50). The test of the switch at 60°C was stopped due to the slow drift and long time spent without switching.

²At that time, these temperature tests could not be done on S5 and Omron switches due to availability of components and/or testing equipments.

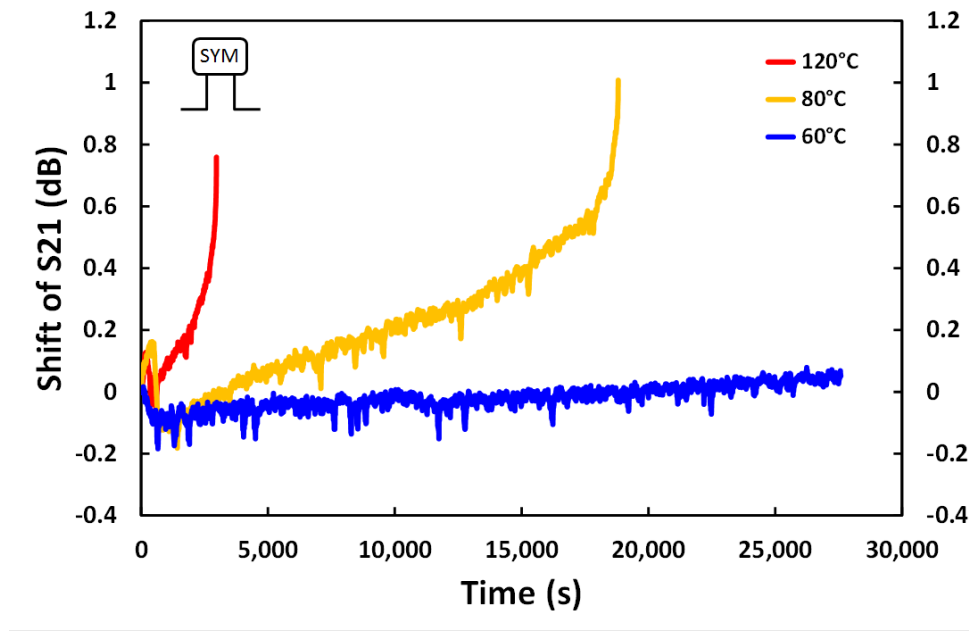


Figure 2.18: Evolution of the transmission parameter shifting over time for the SYM-switch at different temperatures. The bias voltage is 80% of the pull-down voltage.

On a second observation, the shift of S_{21} is faster with increasing temperature [40], in fact the 60°C curve fits a linear function in its linear section estimated at 4.27×10^{-6} dB/s, whereas the 80°C curve gets a slope about 3.59×10^{-5} dB/s and the 120°C gets a slope about 1.53×10^{-4} dB/s. So higher the temperature is and faster is the shift of the transmission parameter S_{21} .

On a third observation, the shift is larger and takes a longer time before switching. In other words, the 80°C curve needs about 20,000 seconds and a shift of 0.6 dB to switch whereas the 120°C curve gets the switching about 2,000 seconds with a shift of only 0.4 dB. As only two curves is not representative, the test was repeated on the ASYM-switch.

2.3.5.2 Measurement results on ASYM-switch

In figure 2.19, measurement results of the ASYM-switch biased at 80% of pull-down voltage V_p are presented. The operation conditions are the same as for SYM-switch at 60°C, 80°C and 120°C. The shift of the transmission parameter S_{21} over time is obtained.

As expected by the previous test, here the results are quite similar considering almost the same structure. The difference between SYM- and ASYM-switch takes place in the speed of the drift and on the quickness of the switching down. Indeed, the 120°C curve gets a slope about 4.26×10^{-4} dB/s and falls in down state after 0.3 dB of S_{21} shifting. Regarding the 80°C curve, it gets a slope about 3.38×10^{-5} dB/s and falls in down state after 0.6 dB of S_{21} shifting. Finally, the 60°C curve gets a slope about 9.43×10^{-6} dB/s and what confirms our supposition given before is that the switch does not fall in down

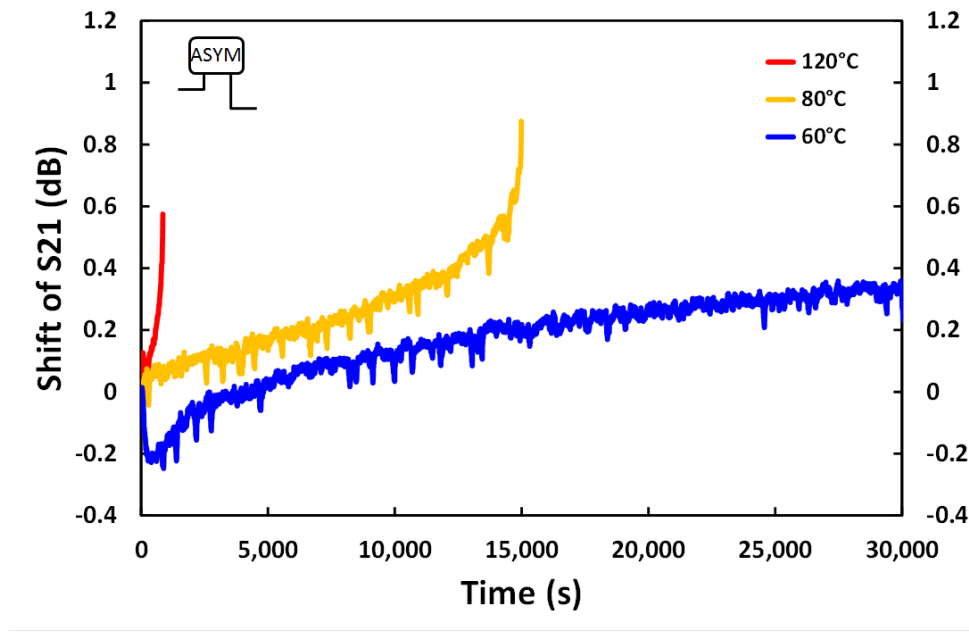


Figure 2.19: Evolution of the transmission parameter shifting over time for the ASYM-switch at different temperatures. The bias voltage is 80% of the pull-down voltage.

state even after a S_{21} shifting of 0.6 dB (the test was conducted up to 57,000 seconds but was truncated in figure 2.19 for ease of reading). So with a rise in temperature the shift of S_{21} becomes shorter before ending in a down state.

On another hand one can suppose that the dissymmetry in anchors is more sensitive with temperature, since the structure might suffer from particular internal stresses following the fabrication process and as a consequence may lead in a release of constraints during the test revealing a less robust device. It would be interesting to conduct more testing to investigate potential explanations.

All the results regarding the temperature measurements are summarized in table 2.3.

	ASYM		SYM	
	Time to pull-down (s)	Slope (dB/s)	Time to pull-down (s)	Slope (dB/s)
60°C	> 50,000	$9.43 * 10^{-6}$	> 25,000	$4.27 * 10^{-6}$
80°C	15,000	$3.38 * 10^{-5}$	19,000	$3.59 * 10^{-5}$
120°C	850	$4.26 * 10^{-4}$	3,000	$1.53 * 10^{-4}$

Table 2.3: Summary of slopes and lifetimes measured on SYM- and ASYM-switches at different temperatures.

2.3.6 Discussion

In this section a measurement technique has been presented. It monitors the transmission parameter S_{21} of RF-switches whilst applying a constant force on their beam or submitting

them to different temperatures. Actually, the constraint force is not constant since the spring constant decreases over time, decreasing the electrostatic gap, thus the electrostatic force increases. As a consequence, the results have to be modified before taking any conclusions on the nature of creep and its evolution law. However, this technique clearly demonstrates the influence of creep in RF-MEMS switches using an easy and quick test bench setup. The tested structures are very similar, fabricated with the same material and a large influence of temperature on the pull-down of switches has been observed. A recommendation regarding these results is to conduct testings at higher temperature than room to get accelerated failures.

For future works, these results open a question regarding biasing, which is how to convert this shift duration into a lifetime using normal operation at 50% duty cycle for instance. Moreover, this study focuses on the pull-down voltage V_p whereas it will be more accurate to do on the release voltage V_r . Indeed, considering figure 1.12, where is explained the evolution of the $T(V)$ curve of a switch suffering from creep, the time when the switch will fail is given for V_r that will reach 0 V (that will happen in first). In the next section a study of mechanical creep is investigated monitoring the release voltage.

Another fact that is not explained, is the use of a natural log function to fit the curves with several constant constraints and the use of a linear function to fit the curves on temperatures. If the same model is not used to fit the curves, this is because these models looked more appropriate in those cases. That is why no comparison is done between the two tables 2.2 and 2.3.

2.4 Second measurement technique: Assessment of creep using constant contact force based on the servo controlling of the contact resistance

In this section, a second innovative measurement technique that surpasses the first one, is presented. The section is divided as follow: first of all, some theoretical issues are explored related with the electrical contact. Then the test bench and the principle of the technique will be detailed and finally, results are exposed and discussed.

2.4.1 Introduction

As concluded in the previous section, the assessment of creep requires an accurate acquisition system and independence on any other phenomena. Here, the developed technique is still about applying a constant constraint on the beam of the switch and getting its deflection over time. On the opposite of the previous technique, the release voltage V_r

instead of V_p will be used to assess mechanical creep. But before going further some theoretical elements have to be exposed so as to understand every theoretical issue required later. Firstly, the topic will deal with contact resistance which is deeply involved in ohmic micro-switches. It will be shown that the metal contact is subjected to temperature and adhesion that may end in failure. Moreover an introduction to theory of electrostatic force on parallel plates will be presented. Finally, the last section on the theory introducing the new technique, is dedicated to results on the contact resistance as a function of the bias voltage.

2.4.2 Elements on the theory of electrical contact

This section related to theory of electrical contacts is presented to figure out what happens in the region of contact in ohmic RF-MEMS switches during operation.

2.4.2.1 Constriction resistance

Major studies of contacts between two metals were done by Holm in the 60s' for macroscopic contacts [41]. For ohmic switches the critical point is the contact between metals. At micro-scale, facing surfaces are not perfectly flat but rough. It means that the contact is realized on a distribution of points instead of the entire surface. In such a system, current flow lines have to cross over the interface through these single points (figure 2.20). Each single contact spot induces a constriction resistance $R_{constriction}$ that when all are added together reveal the contact resistance R_c . Smaller the contact surface is, higher is the resistance.

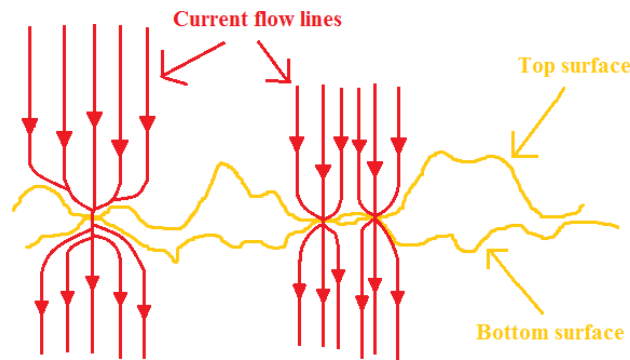


Figure 2.20: Schematic of two rough metallic surfaces in contact crossed by a current.

In Holm's theory, the predicted constriction resistance is given by equation (2.15) considering a circular constriction in bulk interface. This equation is valid on first approximation.

$$R_{constriction} = \frac{\rho}{2r} \quad (2.15)$$

Where ρ is the electrical resistivity and r is the radius of contact disk.

2.4.2.2 Contact mechanics

A model of contact was developed by Hertz to describe the behaviour of two metals in contact under applying force [42]. This model considers two ellipsoids perfectly smooth in elastic deformation. The contact area A is given in equation (2.16) according to figure 2.21.

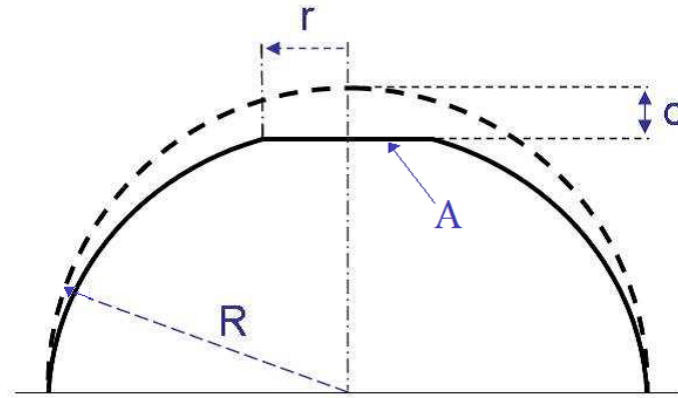


Figure 2.21: Deformation of hemispherical contact asperity [5].

$$A = \pi R \alpha \quad (2.16)$$

Where R is the radius of the hemispherical contact asperity, r is the radius of contact disk and α is the vertical deformation of the asperity. Following calculations gives the normal contact force depending on Hertzian modulus which is defined by Young's modulus and Poisson's ratio of both metals [43]. After calculations, the effective radius of contact is given by equation (2.17).

$$r = \sqrt[3]{\frac{3F_c R}{4E}} \quad (2.17)$$

Where F_c is the contact force and E is Hertzian modulus. From r the contact radius, the constriction resistance can be calculated. What is important is that the constriction resistance or by extension the contact resistance is depending on the contact force, i.e. the bias voltage. On the opposite, a high contact force will squeeze the asperities, increase the contact surface and induce a low contact resistance.

The Hertz' model considers that the solids in contact are in elastic regime and does

not consider adhesive forces based on the contact itself. So the Hertz' model is good on first approximation.

2.4.2.3 Supertemperature and the Wiedemann-Franz law

An increase in contact resistance what means a rise in current density involves a rise in temperature. As the temperature cannot easily dissipate in the air, the excess temperature will be evacuated by current flow. Depending on voltage applied on the contact, either charge transport or heat transport leads. Indeed, higher voltage increases the velocity of electrons in spot contact but also increases the number of collisions i.e. a shorter mean free path; therefore the heat transport is leading. While a lower voltage leads on the other hand to charge transport. This phenomenon follows a simple rule named the Wiedemann-Franz law and was expressed by Lorenz in equation (2.18).

$$\lambda\rho = LT \quad (2.18)$$

Where λ is thermal conductivity, ρ is electrical resistivity, L is the Lorenz constant and T is the absolute temperature. Under these conditions and using equation number (10) in [44] the voltage drop V can be expressed as in equation (2.19).

$$T_{max} = \sqrt{\frac{V_c^2}{4L}} + T_0 \quad (2.19)$$

The maximum temperature T_{max} is proportional to the contact voltage V_c . The term $(T_{max} - T_0)$ represents the contact supertemperature which is relative temperature between bulk and contact spot. This critical temperature due to the contact spot makes the metals to get into softening regime that causes failure. This expression does not consider that electrical resistivity and thermal conductivity are depending on temperature. It does not consider also that Lorenz constant depends on materials. The results may slightly vary by taking into account these considerations until 50 mV. Under conditions of classical uses and measurement of electrical contact, these equations are sufficient. It is important not to forget that approximations cannot hold anymore in case where the contact radius is about the electron mean free path i.e. when there are exchanges between electrons and other particles (like defects or phonons in the conductor) and for intermediate temperatures [45]. Anyway, the voltage drop across the contact involves an increase in temperature which can lead to thermal runaway.

2.4.2.4 Softening, melting

A rise in temperature leads to physical deformations but the deformation is not clearly defined. Several works point out on possible explanations nevertheless opinions are not

unanimous. The main phenomena encountered and demonstrated after softening are necking, material transfer and surface contamination [46] [47] [48] besides everybody notice that the contact resistance increases over cycles. Depending on whether materials dissipate slowly or quickly the heat to reach thermal equilibrium, the thermal runaway occurs which causes contact melting. As the stability of the contact resistance is linked with temperature, the table 2.4 given in the following extracted from [10] lists softening voltage and melting voltage for common electrical materials. The voltage drop for gold softening is 80 mV what is very limiting in our applications considering that gold is widely used in electrical contacts.

Metal	Softening		Melting	
	Voltage mV	Temperature °C	Voltage mV	Temperature °C
Au	80	100	430	-
Ru	-	430	-	-
Al	100	150	300	600
Fe	190	500	190	1539
Ni	160	520	160	1452
Cu	120	190	430	1083
Zn	100	170	170	419
Mo	250	900	750	2620
Ag	90	180	370	960
W	400	1000	1100	3390

Table 2.4: Softening and melting voltages and temperatures of some common metals [10].

2.4.2.5 Contact resistance as a function of bias voltage

The idea of the technique developed in this section comes from observations done on $T(V)$ of several switches that get different metal contacts. In figure 2.22 is shown an $R(V)$, i.e. a contact resistance as a function of the bias voltage applied on the switch. Compared to the $T(V)$, it is a reciprocal function that gets the minimum of the curve when the transmission is the best and it is very convenient to assess the contact resistance quickly. In other words, when the losses of an ohmic switch are very low, the transmission is done almost without loss that means a low contact resistance at DC and low frequencies. As these curves are not perfectly flat and straight, it will be possible to control the contact resistance of switches by modifying the bias voltage. If one can control the contact resistance and make it stable (which is the aim of the second technique of this chapter), it means that a constant force will be applied on the contact, because the force is proportional to the surface contact and so proportional to the contact resistance.

Depending on the materials in contact, the curves have different shapes. Harder

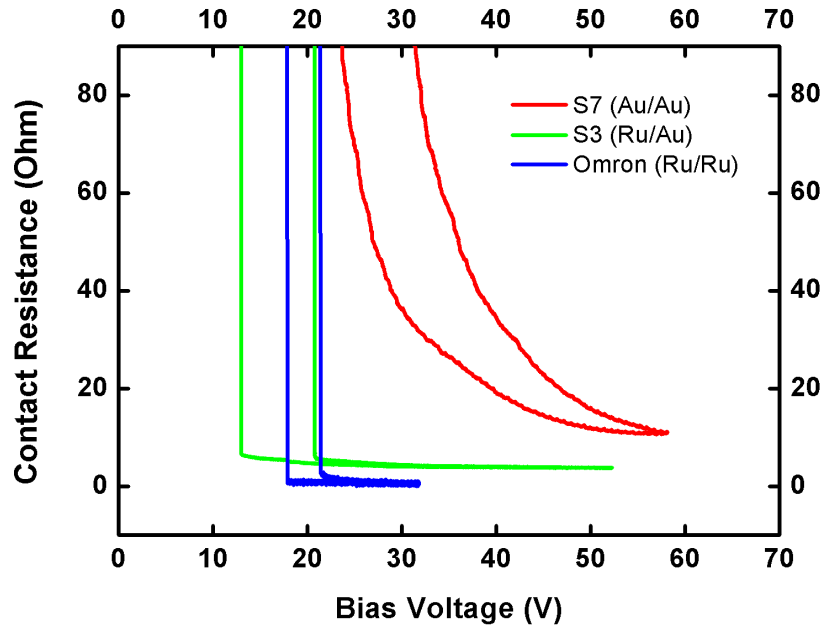


Figure 2.22: Contact resistance versus bias voltage for 3 switches that get different metallic contacts, evidence of hysteresis of switches and hardness of metals.

contact metal results in straight slopes and sharp transitions. Indeed gold (Mohs hardness 2.5 [49]) is softer than the Ruthenium (Mohs hardness 6.5 [49]).

Another noticeable point regards the gap between pull-down and release voltages defined as the bias voltage value for the first value of contact resistance (to get V_p) or the last value of contact resistance (to get V_r). The data are summarized in table 2.5.

Switch	S7	S3	Omron
V_p	30 V	21 V	22 V
V_r	18 V	13 V	17 V
V_p/V_r	1.67	1.61	1.29

Table 2.5: Comparison of pull-down and release voltages for 3 switches giving the ratio V_p/V_r .

The gap between V_p and V_r gives us information about how is built the switch in the region of the electrostatic gap and contact points. Indeed, if the beam crosses the unstable point of the electrostatic gap during actuation, the release voltage shall be less than if it does not cross. For the Omron switch it means that the displacement of the beam does not exceed $\frac{1}{3}$ of the electrostatic gap, whereas S3- and S7-switches cross the unstable point, come to a low position and need more restoring force to re-open. This explains why S3- and S7-switches get a lower V_r than the Omron (comparatively to their V_p). On the other side, Omron switch does not get $V_p = V_r$ because of adhesive phenomenon that

occurs for very flat surfaces and make the metal contacts to stick together.

One peculiarity that one may remark is the conductivity of metals in contact in these switches. Indeed, gold has a better conductivity than Ruthenium (Au: $4.5 * 10^7$ S/m, Ru: $1.4 * 10^7$ S/m [49]) but the gold/gold contact gets a higher resistance in our tests compared to Ru/Ru contact. This has already been observed in micro-switch because of contamination effects and intrusive species that create thin dielectric layers that the contact has to break before touching the bottom electrode.

2.4.3 Presentation of the test bench

Taking into account all the previous considerations, the test bench set up is going to be detailed. The idea is to pull-down the switch and keep it in down state as close as possible to the release voltage V_r . Then the value of contact resistance of the switch is monitored and the bias voltage is modified if the value of contact resistance changes. A test point is defined for the contact resistance in the setup as the first value of contact resistance when the switch closes (typically between 1Ω and 100Ω). If the contact resistance increases compared to this point, the bias voltage is increased and the contact resistance decreases. Conversely, if the contact resistance decreases compared to this point, the bias voltage is decreased in order to decrease the contact force and increase the contact resistance. The stages of technique are summarized in figure 2.23.

If the contact resistance remains constant during the entire test, it involves a constant contact surface, and a constant contact force. For these considerations and for fixed test bench parameters (humidity, pressure, temperature, current, light) it is admitted that creep is the only physical phenomenon that can occur in the experiment. The test bench is presented in figure 2.24.

The measurement of contact resistance is done on an external series resistance as forming a voltage divider where the voltage across this external resistance is constant. The voltage value is detected by an analog input of an Arduino micro-controller board that converts the voltage into a contact resistance and then sends it to a computer running Labview. The Arduino code is written in Annex A of thesis. All voltage generators of the bench are driven by Labview and are modified according to the value given by the Arduino board. The servo loop thereby created is executed every 100 ms.

To make an analogy of this technique, let us consider a car going on the road at a fixed speed. The use of dampers allows the car to be stable and to have a constant force applied on the wheels. When the car encounters dips and swells, the force generated by the car weight changes punctually and dampers counteract the effect to make the car stable. The suspended beam is considered as a car and the servo controlling is considered as dampers to keep the contact resistance constant.

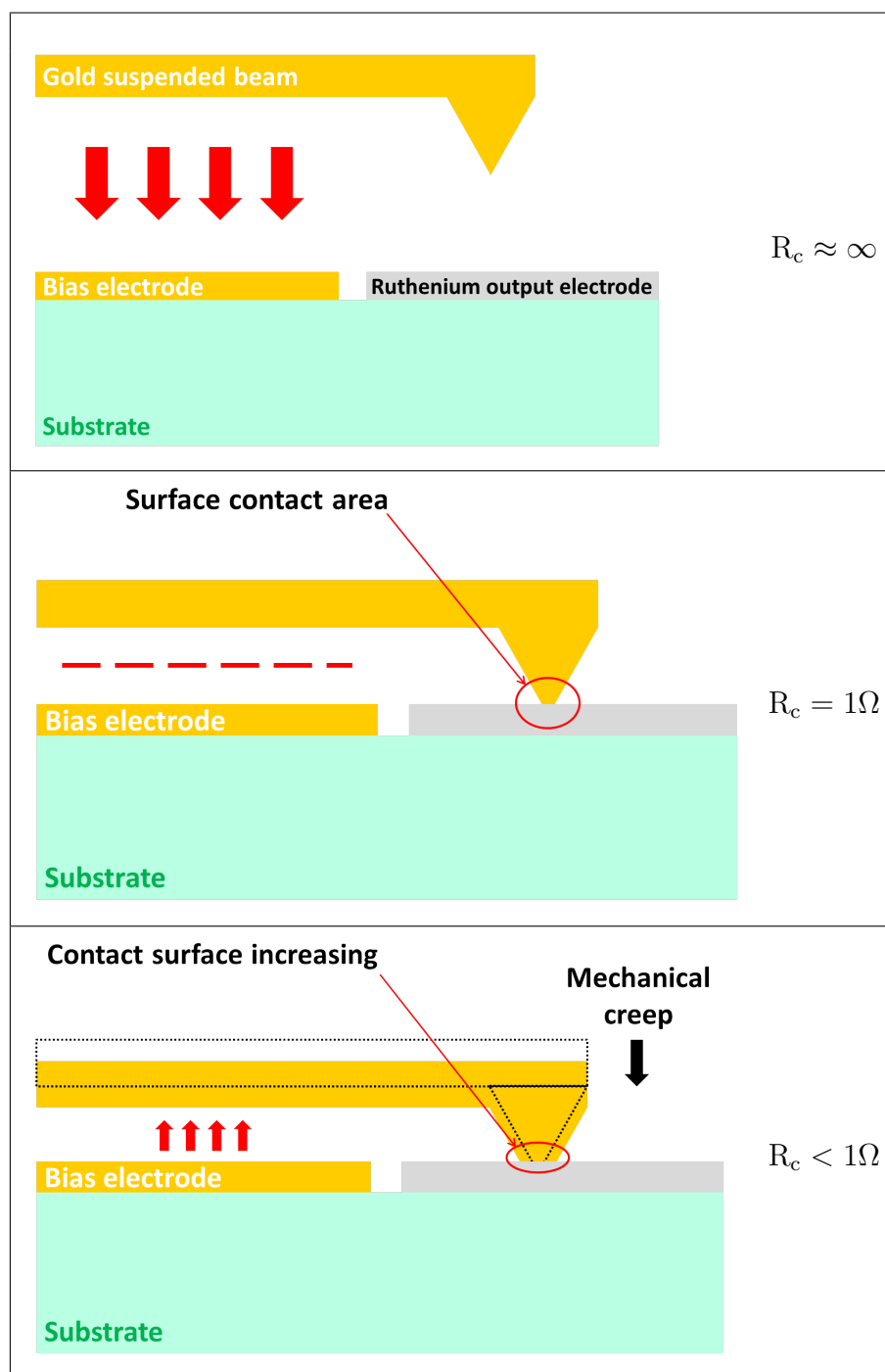


Figure 2.23: Principle of assessment of creep servo controlling the contact resistance.

Carefulness is required about the interpretation of results because mechanical creep will occur on suspended beam but may also occur on contact dots. The contact dots made of asperities will deform while contacting facing asperities on the other side of contact. Moreover, the environmental conditions are considered very stable because of the use of a temperature controller and since all the tests are conducted in vacuum, contaminations should be minimal.

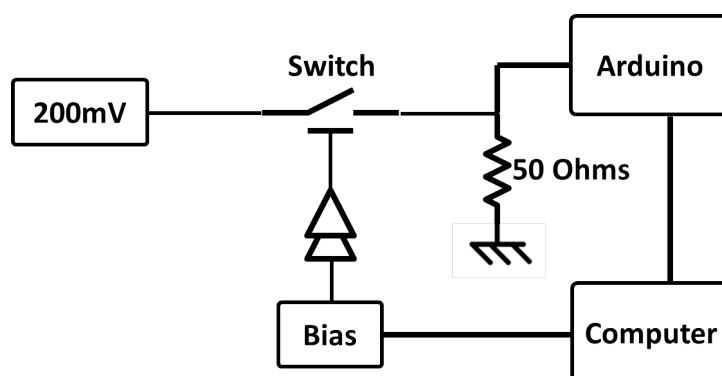


Figure 2.24: Test bench to assess creep consisting in servo controlling the contact resistance of switch with bias voltage.

2.4.4 Results on S5-switches

Testings have been conducted on S5-switch having in mind the first tests done with partially biasing technique, and it is expected that the bias voltage will decrease over time and will decrease faster with the rising of temperature. The shift of bias voltage over time is plotted for 20°C, 40°C, 80°C and 120°C, for 4 switches with the same characteristics (less than 10% drift). The results are showed in figure 2.25.

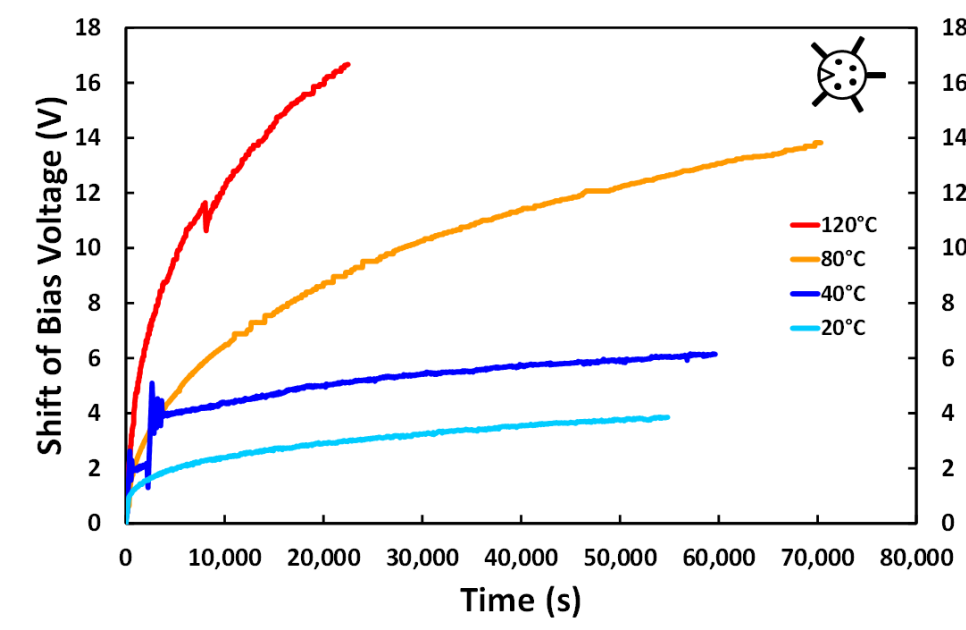


Figure 2.25: The shift of bias voltage at different temperatures for a constant contact resistance demonstrating the behavior of creep on S5-switches.

In fact, a decrease³ of the bias voltage over time is obtained. For higher temperature than room temperature the decrease is accelerated. Unfortunately the curve at 120°C

³The shift of the bias voltage is positive but really the bias voltage decreases over time.

was stopped because the test bench, at that time, could not record a shift in bias voltage higher than 20 V.

As it was a new technique, during measurements the bench was constantly in progress in order to improve its performances. At first, only one bias generator was used and a compromise should be done between the variation range and the resolution. Then, a second generator was set up coupled with the first one. Now one generator is dedicated for a wide variation range (0 V to 120 V) and a second generator is dedicated for the resolution (1 mV of resolution from 0 V to 20 V). It is assumed that from 1 mV to 5 mV of resolution is required to modify the contact force as precisely as possible to be close to the contact resistance setpoint. In section 3.3.3.2 page 102 a way to improve the resistance measurement with the Arduino using a link from Atmel is detailed.

To go further, it is interesting to assess how much creep is activated by temperature. Creep and the temperature are linked by the Arrhenius' law which is given in equation (2.20) [50].

$$\dot{\epsilon} = A. \exp^{-\frac{\Delta F}{kT}} \quad (2.20)$$

Where $\dot{\epsilon}$ is the strain rate, A is a constant, ΔF is the activation energy, k is the Boltzmann's constant (in eV) and T is the absolute temperature.

From this equation (2.20), a network of curves is plotted in figure 2.26. Every curve is defined by three points⁴ 20°C, 80°C and 120°C, and for these three points the strain rate is measured. Time is fixed for every curve; it means that after 5,000 seconds since the beginning of the test, the data of strain rate are collected (with different temperatures). Finally, every 5,000 seconds the same procedure is repeated up to 20,000 seconds (so 4 curves are obtained in total).

In the Arrhenius' theory, the predicted model shows that strain rate versus energy follows a straight line. So a good agreement is noticed between theory and our system. Moreover, the curves stay parallel over time (i.e. all along the measurement) meaning that only creep is involved in our system. To complete the results of these measurements, the activation energy has been extracted from the straight lines of figure 2.26. Found with the slope of the straight lines, the activation energy equals 0.22 eV with a $8.8 * 10^{-3}$ eV standard deviation. To conclude on these values, the S5-switch is sensitive to temperature because the activation energy is very low. Suspended structures made from gold might be sensitive for applications requiring independence on temperature variations, like in space for instance.

⁴The 40°C curve was not taken into account for the data processing because the curve seems to be faulty compared to others and we suppose that something went wrong in the beginning of testing.

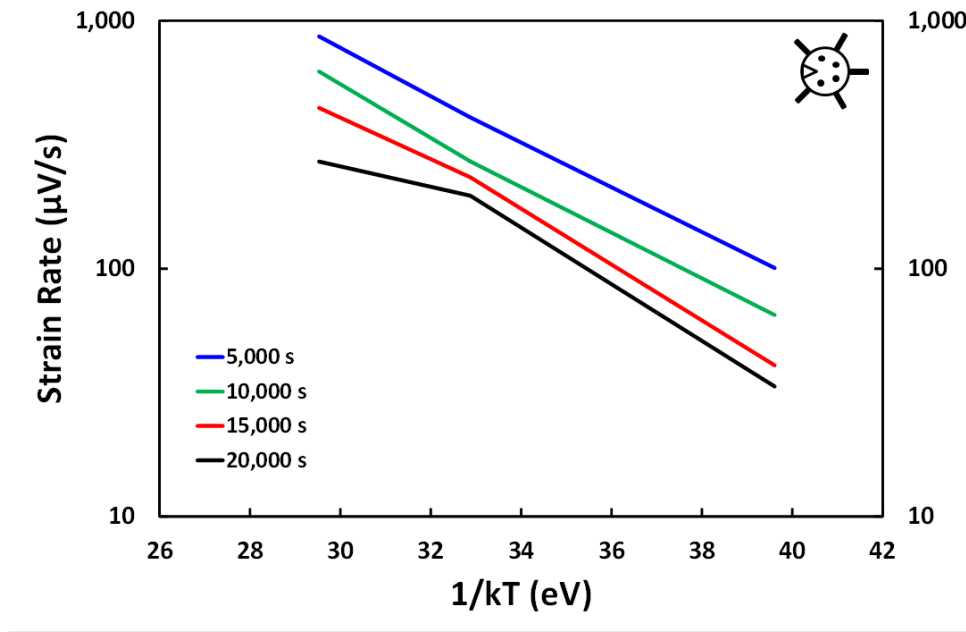


Figure 2.26: Evidence of creep accelerated by temperature given by an Arrhenius' plot.

2.4.5 Results on SYM- and ASYM-switches

As it has been done systematically during the thesis, as many test as possible are conducted to widen our global comprehension on RF-MEMS switches and their failure mechanisms. Previously, testings were conducted on all the switches available in the lab to make comparisons between them in order to provide relevant conclusions. Nevertheless, the availability of SYM- and ASYM-switches at the time to continue testing was on a renewal so not enough results can be provided compared to expectations. Moreover, it was the first switches on which has been tried out the new measurement technique based on the servo controlling of the contact resistance. The bench was not completely optimized like it is now so, some clues are given in this section to improve the quality of the measurement.

In figure 2.27 are presented the results for SYM-switch at 25°C et 40°C.

It is tough to interpret the curves but some explanation is given in the following. In both cases sawtooth appeared that can be explained by the fact that the software cannot find the value of contact resistance ordered by the setpoint contact resistance. So every time the software is close to the setpoint, it continues to decrease the bias voltage. Because the setpoint is so close to the release voltage that the contact just re-opens and all the procedure has to be re-initiated. Restarting the procedure means that first, the software increases the bias voltage (the curve goes up) because the value of the contact resistance is higher (open circuit) than the setpoint value. Then the switch reaches the down state. Second, the bias voltage is decreased (the curve goes down) because the value of contact resistance is lower than the setpoint value. It may be explained by the fact that

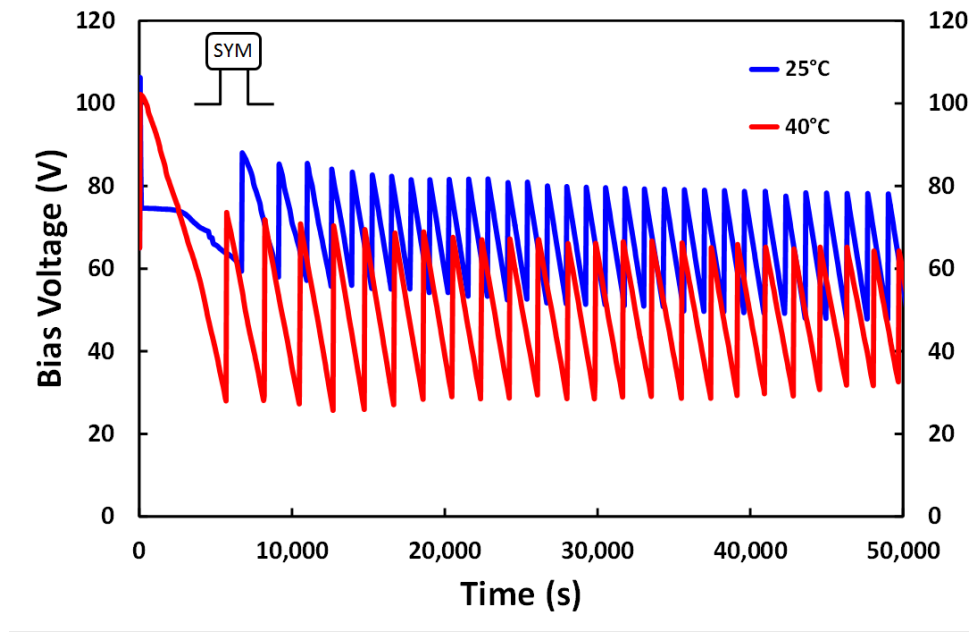


Figure 2.27: Evolution of the bias voltage to maintain the SYM-switch at a constant contact resistance over time at 25°C and 40°C to observe creep phenomenon.

the point of contact resistance was not chosen very wisely and it was too high compared to our expectations. Anyway, a natural log trendline was extracted for both curves and the slope of trendline at 40°C is higher ($-6.91 \text{ V}/\ln(\text{s})$) than at 25°C ($-3.34 \text{ V}/\ln(\text{s})$).

Even though the results are coarse, the expected trend is here. However due to the slightly randomness of the curves it is hard to extract data from these measurements. A new measurement campaign with more samples will take place.

The results obtained for the ASYM-switch are presented in figure 2.28.

The curves have a better shape than for the SYM-switch. The sawtooth oscillations are drastically reduced and two reasons are given to explain that. First reason would be that a suited value of the setpoint of contact resistance has been found. The second reason would be that the structure itself allows more flexibility in its mechanical behavior that the setpoint of contact resistance can be chosen far from the value reached by the switch.

In the early ages of the bench, the setpoint of contact resistance was fixed by the operator (typically between 1Ω and 100Ω) as it is mentioned in presentation of the test bench (section 2.4.3 page 68). Actually, this is not the best way to proceed. Indeed, each switch has its own particularities, its own parameters, even tiny. So the correct procedure would be to select the appropriate setpoint of contact resistance according to the $R(V)$ gotten with bipolar triangle like it was done to sort switches.

Regarding the performances of the ASYM-switch, a natural log trendline was extracted

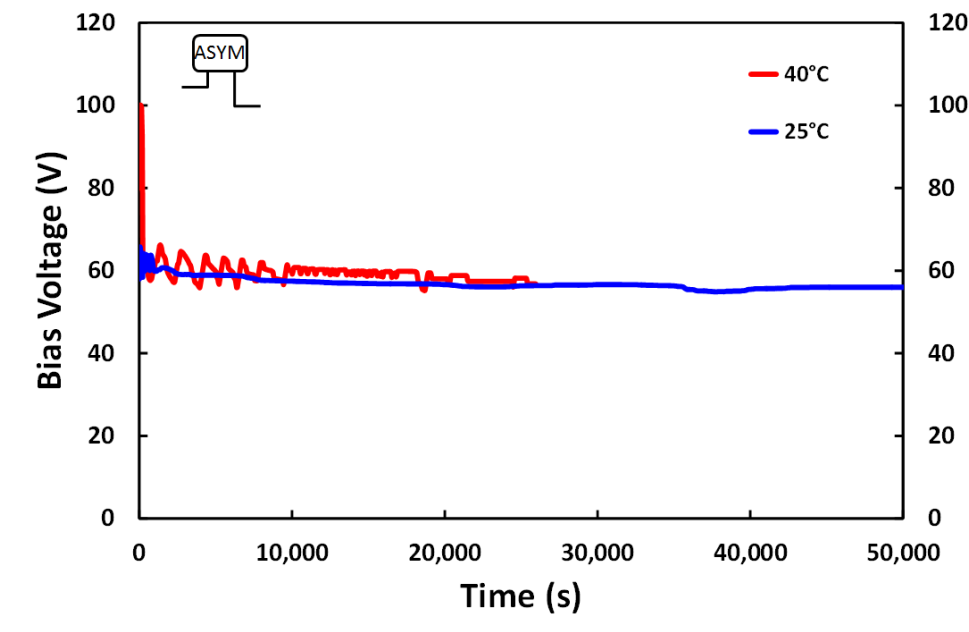


Figure 2.28: Evolution of the bias voltage to maintain the ASYM-switch at a constant contact resistance over time at 25°C and 40°C to observe creep phenomenon.

for both curves, the 25°C curve gets a slope about $-1.42 \text{ V}/\ln(\text{s})$ whereas the 40°C gets a slope about $-2.14 \text{ V}/\ln(\text{s})$. Generally, the trend according to higher the temperature is and higher the shift is, is confirmed. But the slopes of the ASYM-switch are lower in this case and it can be explained by giving an hypothesis such as the structure, because of its asymmetry, is able to bear mechanical stress without being too much affected.

In conclusion of these tests on SYM- and ASM-switches, a wide range of contact resistance values in the $R(V)$ are available before opening (like the S7-switch presented in figure 2.22). It makes our test bench very efficient. On the opposite, a switch that has a wide range of contact resistance values will not necessarily be a reliable switch (admitted by experience). Finally, the setpoint value of contact resistance was chosen as the minimum value of contact resistance gotten during the $R(V)$, i.e. the contact resistance value when the contact is stabilized.

2.4.6 Results on Omron RF-MEMS switch

Since the Omron RF-MEMS switch is a reference regarding low sensitivity to creep, the opportunity to conduct the test of servo controlling the bias voltage to get a constant contact resistance, was taken. At room temperature, the results are presented in figure 2.29.

The Omron switch was tested during more than 55 hours in down state enduring a constant contact force without exhibiting any dependency on mechanical deformations on its structure because of creep. The Omron switch with monocrystalline structure and

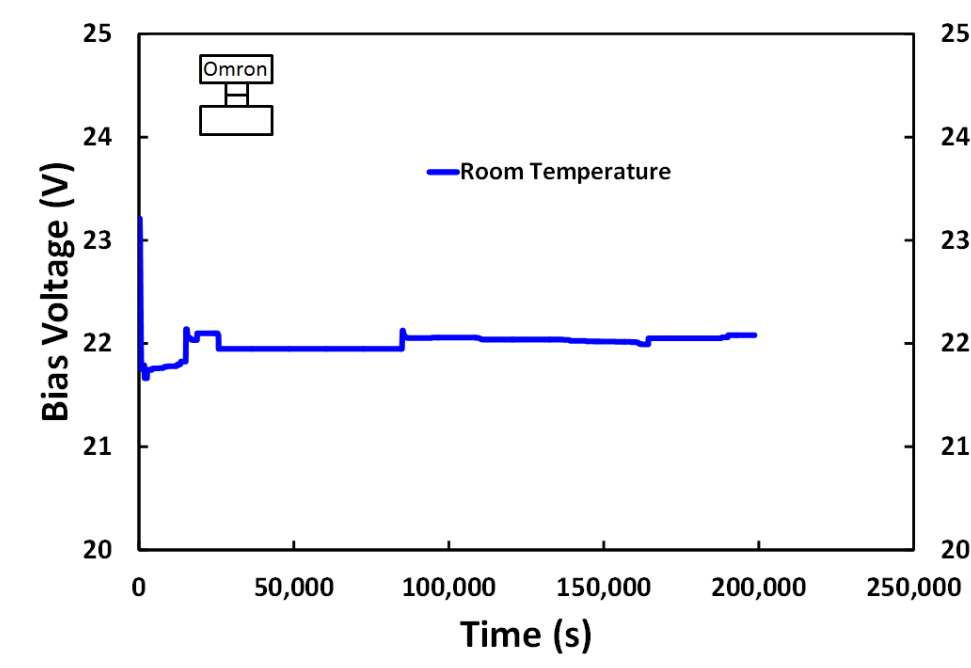


Figure 2.29: Evolution of the bias voltage to maintain the Omron switch at a constant contact resistance over time demonstrating the insensitivity of the switch on creep phenomenon for more than 55 hours.

Ruthenium contacts shows excellent performances, it confirms the conclusions seen in section 2.3.4.4 page 56.

2.4.7 Discussion

The technique based on servo controlling the contact resistance to assess creep in RF-MEMS switches showed interesting results. Electroplated gold structures are very sensitive to temperature variations and the activation energy has been extracted for these structures. The results obtained with ASYM and SYM cantilevers did not show particular behaviour. More testing are necessary to make further conclusions, choosing better set up parameters. It is important to notice that the bench assesses creep of the whole structure, i.e. the cantilever or membrane **and** the metal contacts. So the bench allows us to get a quick idea about the performances of the structure and performances of contacts at the same time.

The Omron switch did not show dependence on temperature during testing. It can be explained because of design, which is different between Omron, S5, SYM and ASYM. Moreover, the materials have an important influence and gold contacts are not likely the best candidates for RF-MEMS. However, Ruthenium contacts in Omron switch are rather efficient. None temperature measurements were conducted with this test bench for the Omron switch. It would be very interesting to do it at 120°C for instance and compare

with S5 switch.

Finally, the servo monitoring technique is very interesting because it works as an accelerated technique. Since it is quite easy to implement, this technique deserves to be developed.

2.5 Further testing conducted on Omron MEMS switch

Apart from the technique presented before, further testings were done on Omron switch to see its sensitivity to temperature during operation. For that a test bench has been assembled and is visible in figure 2.30.

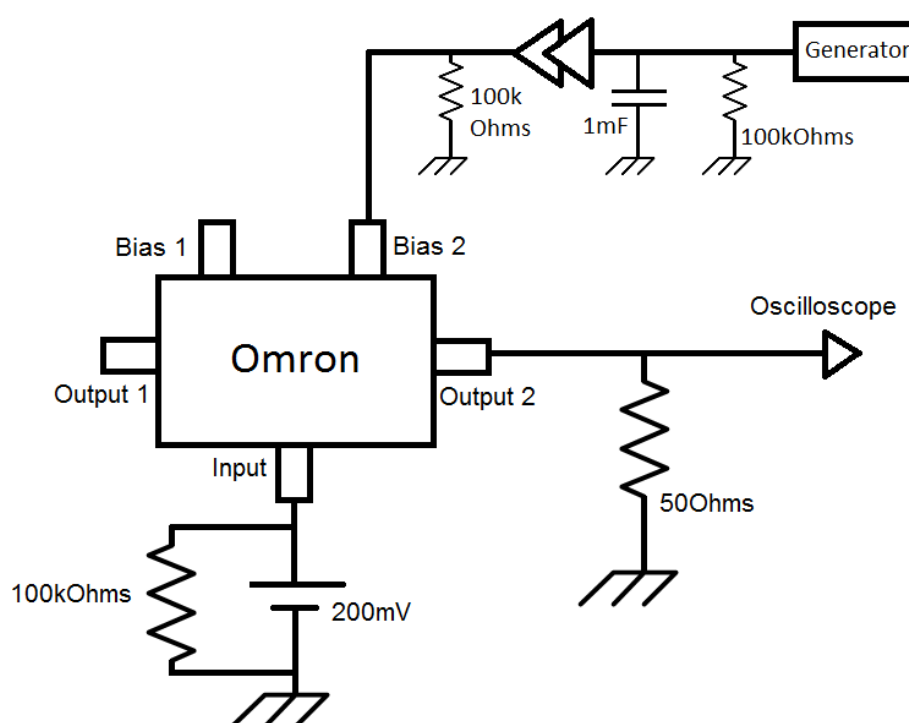


Figure 2.30: Complete test bench with lumped elements to assess the reliability of the Omron with DC testing at 25°C and 70°C.

So, only one⁵ switch was used at a time in this bench and lumped elements were implemented so as to prevent as much as possible transient events coming from the range changes of generators, that usually damage RF-MEMS switches. Then, the voltage drop on the 50 Ω output-2 resistance is gotten with an accurate oscilloscope driven by Labview and data are recorded on a computer, as usual.

⁵The Omron 2SMES-01 gets two switches inside its package, this is a SPDT switch (Single Pole Double Throw).

This long-term test was conducted at room temperature (25°C) and at 70°C. The test consists in pulling the Omron switch in down state for a while and checks its state every 30 seconds to follow its evolution under stress. The questioning consists in a bipolar triangle inserted every 30 seconds in the bias waveform as presented in figure 2.31.

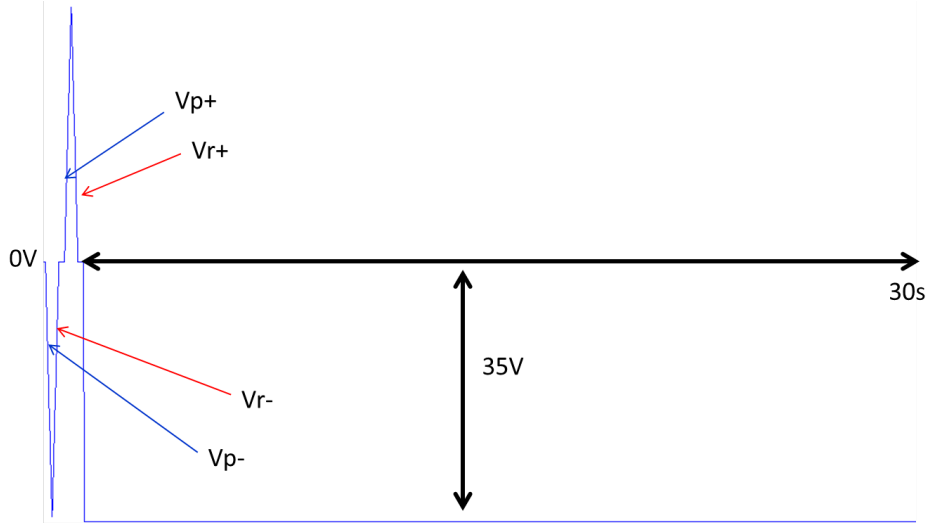


Figure 2.31: Waveform of the bias voltage applied on the Omron switch to follow the evolution of its parameters during a test held in down state.

The bipolar triangle allows to get positive and negative actuation voltages (V_{p+} , V_{r+} , V_{p-} and V_{r-}) as presented in figure 1.9. Moreover the triangle allows to get regularly the $T(V)$ of the switch (that is presented in figure 2.32 at room temperature) which is an important asset regarding the "health" of the switch.

The Omron gets as expected a very sharp $T(V)$ meaning that the hardness of the contacts is high (R_u/R_u). Moreover, the curves are very flat and close to the region of 200 mV, meaning after some calculations that the contact resistance is about 1 Ω or less which is considered as low loss. Finally, after 14 hours in down state, the switch has quasi none drift what proves the high reliability of this RF-MEMS. To get more information, the evolution of Omron actuation voltages is presented in figure 2.33.

Once again, the switch achieved the test without drifting and the test was stopped after 18 hours without any failure. Based on these references, the test will be reproduced in the same conditions at 70°C and compared with results at 25°C. In figure 2.34 is presented the $T(V)$ of the Omron at 70°C in the beginning of the test and after 62 hours.

The result at 70°C are very similar to those at room temperature, the contact resistance is also very good (the signal in down state is very close to 200 mV which is the input voltage) about 1 Ω and less. Looking at the evolution of actuation voltages at 70°C (figure 2.35), it can be seen that little or no drift is observed.

Indeed, the Omron switch remains very stable all along the test and the test has

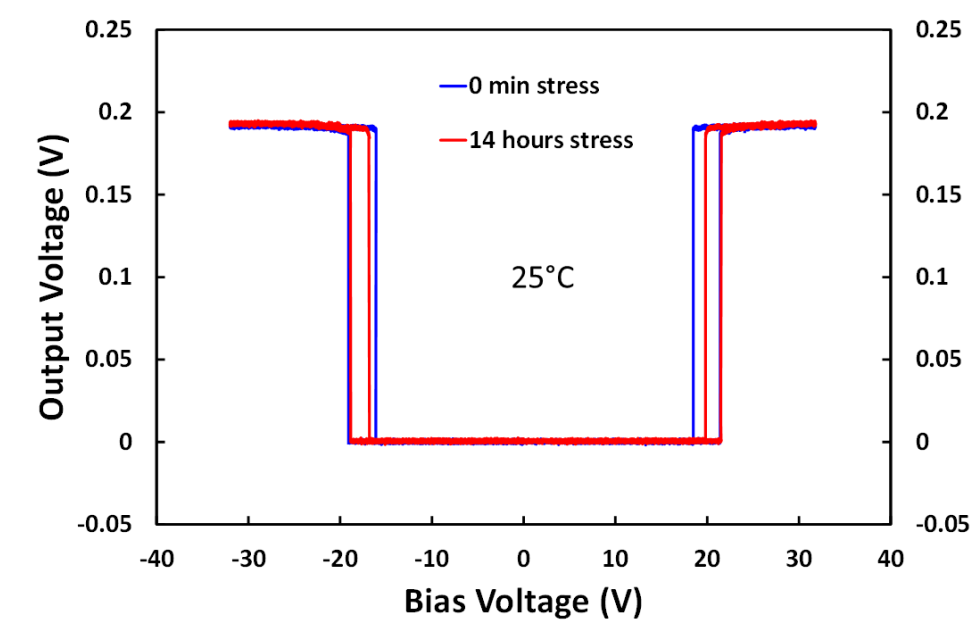


Figure 2.32: Transmission versus bias voltage $T(V)$ for the Omron switch at room temperature in the beginning of the test and after 14 hours in down state.

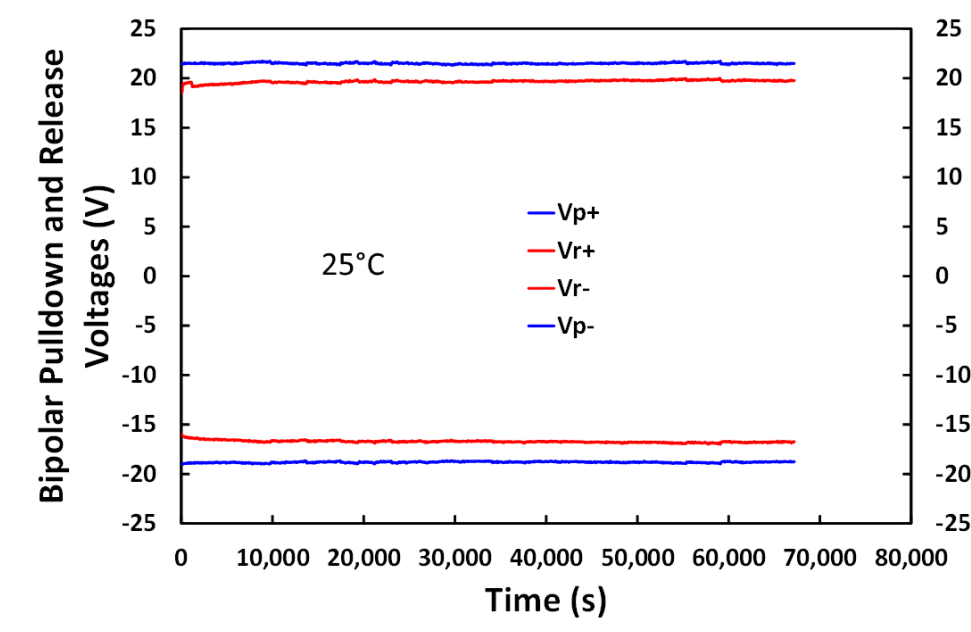


Figure 2.33: Evolution of actuation voltages versus time of the Omron switch held in down state at room temperature.

to be stopped to free the bench. Actually the Omron test was undertaken to assess a possible dielectric charging (related with section 2.2 page 44) since the composition of the Omron is not completely known. That is why, the test is held in down state with a negative waveform. If the switch had a dielectric layer, the charging would be accelerated with temperature [33] and it would have been possible to detect it in our measurement,

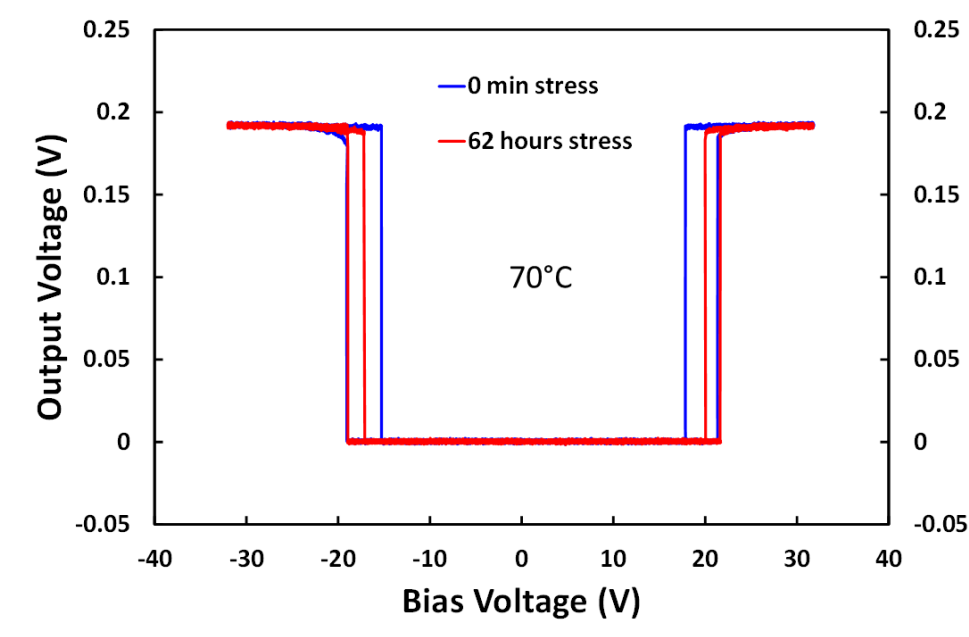


Figure 2.34: Transmission versus bias voltage $T(V)$ for the Omron switch at 70°C in the beginning of the test and after 62 hours in down state.

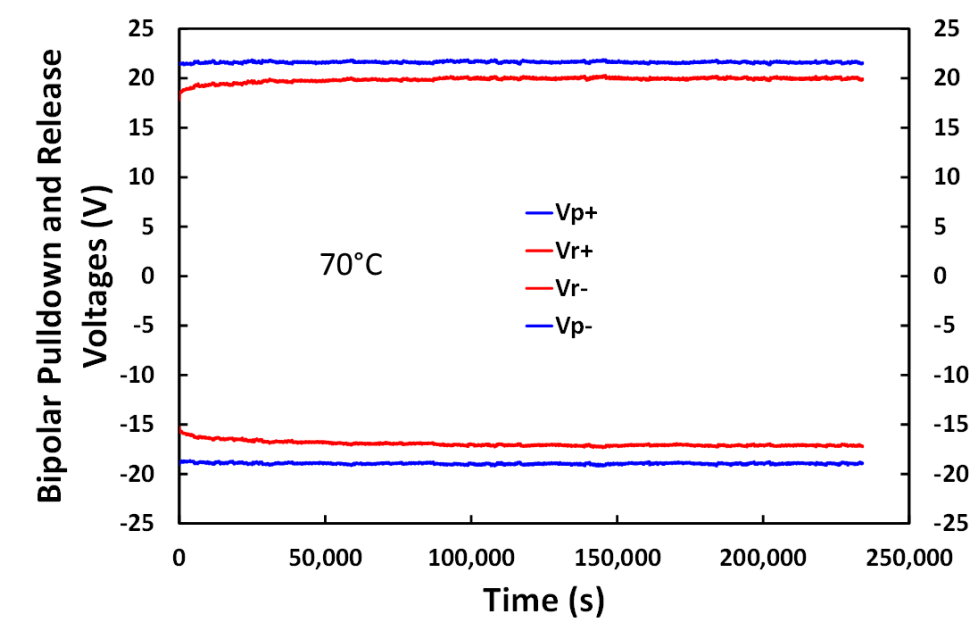


Figure 2.35: Evolution of actuation voltages versus time of the Omron switch held in down state at 70°C .

nevertheless it was not the case, charging did not occur. So at that time, the temperature of 70°C was chosen by default because it was convenient for the oven present in the lab.

2.6 Conclusion

This chapter was dedicated to creep phenomenon in ohmic-contact RF-MEMS switches. After a brief introduction on the theory, two methods were developed and were presented to assess creep. The first method is based on the partially biasing of the beam that makes it to pull in down state after a while. Creep is accelerated with temperature and applied force. Compared to our switches, the Omron switch performed the test without showing any sensitivity. It can be inferred that this is due to its monocrystalline beam compared to electroplated structures.

The second method is based on the monitoring of the contact resistance that allows us to apply a constant contact force on the switch contact thanks to the bias voltage. The results are in good agreement and show a better accuracy compared to the previous technique. Once again the sensitivity of monocrystalline beam is very low and seems to be a good candidate to remove creep problem.

Now the next chapter will present a global overview of the reliability of ohmic contact RF-MEMS switches and the results regarding operation conditions and accelerating factors.

Chapter 3 :

Reliability Assessment Methodologies

In the previous chapter the measurements took a very long time. The idea is to find key parameters that control lifetime of switches. It can be temperature, voltage, current, pressure, radiations etc. These key parameters called the acceleration factors allow to control the maximum lifetime of switches for given conditions. This chapter is dedicated to acceleration factors of the reliability of ohmic contact RF-MEMS switches. The chapter is divided as follow: first, some theoretical elements are given regarding the reliability as well as the models that are currently used to assess it. Then, the measurement results obtained for cycling testing under different operating parameters are presented. Finally, a quick and promising parallel test bench has been developed and will be presented. It allows to measure up to 48 switches at the same time on a 2 inches board and combined with acceleration factors, the test bench is the best achievement of the chapter.

3.1 Introduction to reliability

This section is dedicated to introduce the notion of reliability. A general definition is detailed in the first part and the second part is dedicated to an introduction to Weibull distribution. And finally the thesis will focus on practical examples found in the literature to get an idea about the use of the Weibull distribution.

3.1.1 General definition

Basically, the reliability gives the probability of an item to perform a required function under stated conditions for a specified period of time [51] [52]. The thesis deals with this topic because the reliability of RF-MEMS is the last step before industrialization and some steps remain before its complete successfulness. Currently most failure mechanisms of RF-MEMS switches have been studied and some solutions were given. The idea is to predict the lifetime of switches in given conditions in order to find the best suitable application.

The reliability has to be studied as soon as a component or a system goes out from a lab before going in the market. It is a critical step because all the work conducted till this step may come to an end if the reliability is not achieved.

To achieve reliability, the statistics are a paramount importance and a large number of components is required. In the life of a batch of components, the bathtub curve is generally associated to describe the failure rate for this batch all along its lifetime (figure 3.1 [53]).

At the beginning, there are the "dead-on-arrival" products caused by imperfections and random events in fabrication process. These products fail quickly so the failure rate starts high and decreases over time. This is the infant mortality. There are many ways to

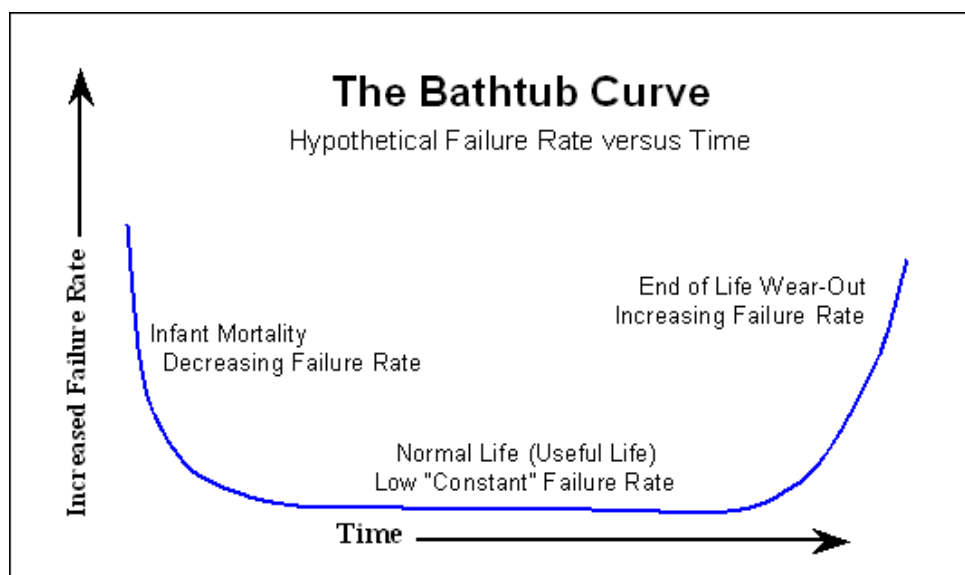


Figure 3.1: The bathtub curve describes the failure rate as a function of time, divided in three regimes, infant mortality, normal life and end of life.

mitigate infant mortality of components, for example, choosing appropriate specifications and tolerances that those "dead-on-arrival" components cannot pass. Another way is doing stress tests that can point out weaknesses of the devices that are invisible at a first look. Moreover, temperature accelerated tests allow to set aside those components or devices that will be sensitive to fatigue. These two last methods are regrouped in what is called a "burn-in" of devices. In our case where switches are built on a wafer, a complete sorting is done once the wafer comes outside the clean room, in order not to waste time in testing with deficient switches. Then, a map is drawn for every wafer coming out. A complete procedure has been developed in the thesis and is explained in section 3.4 page 104. For a decreasing failure rate $\beta < 1$. The definition of β will be presented later.

Once the failure rate reached a low and almost constant shape (i.e. the infant mortality is considered as ended¹) the regime of normal life of a population starts. This regime is ruled essentially by inappropriate uses out of the specifications, or unexpected events (drop of mobile phones ...) and must be as low as possible because this is the normal regime of the device where the customer is supposed to plenty enjoy its investment. For a quasi constant failure rate $\beta \approx 1$.

Finally the failure rate of a population of device will increase by the end of the bathtub curve because everything wears out. At that time, the customers were supposed to buy the new one before the device comes to its end. In this case $\beta > 1$.

It has to be taken into account that the bathtub curve gives only the appearance of a curve to understand the global behaviour of a population of devices, it is only a

¹The infant mortality can take many years depending on the devices, the bathtub curve is not scaled in time.

visual model that is not supposed to fit with in particular. To assess the reliability, it is convenient to refer to a model that can describe quasi all the behaviour of populations in Nature. This model is presented in the next section and it is called the Weibull's distribution.

3.1.2 The Weibull distribution

Before getting theoretical details, an analogy is presented to set the main idea and vocabulary.

Let us consider a batch of 100 tyres. The tyres get a wear indicator that states the lifetime. It is usual to define lifetime of tyres in number of kilometers. From the first tyre that failed to the hundredth, the lifetime may be very spread. One can understand that buying two tyres and one lasts half of lifetime of the other is not very pleasant. A parameter called the shape parameter β allows to quantify how much lifetimes of tyres are spread over time.

A second parameter called the scale parameter α is defined when 63 tyres over the 100 are failed. It is a kind of average that estimates the lifetime of tyres.

An example of cumulative failures versus the number of kilometers in a log-log graph, for tyres, is shown in figure 3.2. The shape parameter β and the scale parameter α are detailed in the next section.

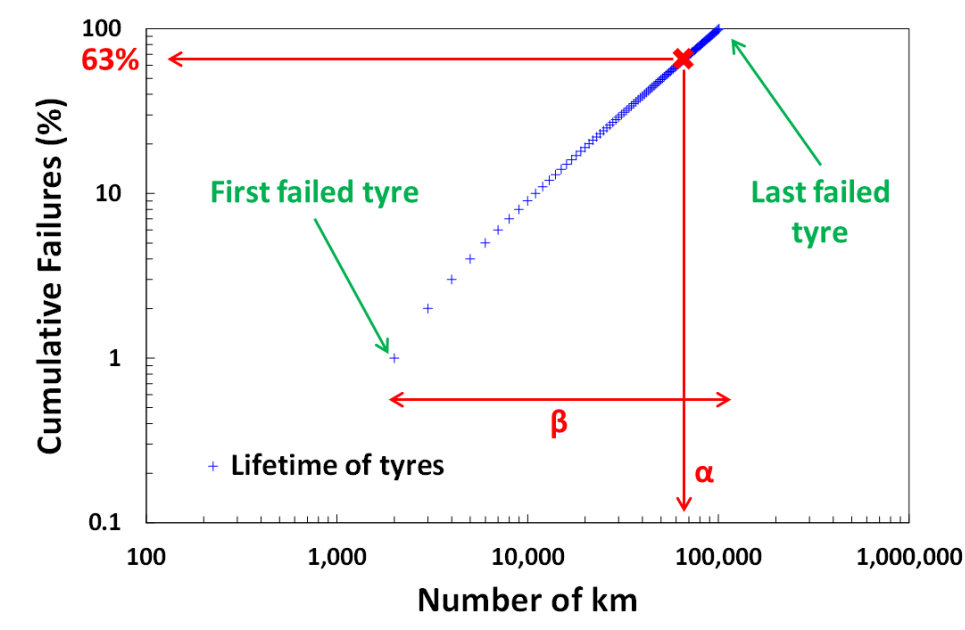


Figure 3.2: Example of lifetime of tyres plotted in a log-log graph with β and α representing the Weibull distribution parameters.

For switches, the lifetime is defined with number of switching or in hours of use. The switch does not get wear indicator but the contact resistance and operating voltages

allow to give a limit in operation of the switch. Once a voltage value is reached or a contact resistance is shifted, the switch is considered failed. As for tyres, the shape parameter β and the scale parameter α are extracted from the batch of switches that all failed. In the end, α and β are the indicators of reliability.

The Weibull's distribution refers to a statistical distribution function of wide applicability proposed by Waloddi Weibull in 1951 [54].

3.1.2.1 Theoretical elements

Usually the Weibull curve is an indicator of processes maturity and a way to assess the lifetime of a batch of components or systems. In this typical graph given in figure 3.3, the cumulative failures of these components are plotted as a function of the number of cycles. More the curve is vertically and shifted on the right and more reliable is the population of devices.

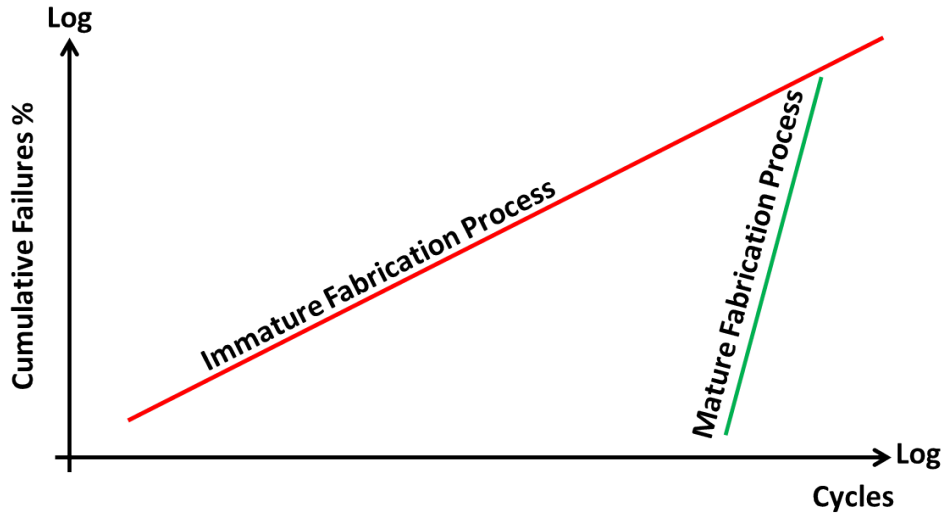


Figure 3.3: Two examples of reliability assessment of fabrication process plotted in a Weibull graph.

In terms of theory, the Weibull probability distribution function $f(t)$ is defined in equation (3.1) for $t \geq \gamma$.

$$f(t) = \frac{\beta}{\alpha} \left(\frac{t - \gamma}{\alpha} \right)^{\beta-1} \exp - \left(\frac{t - \gamma}{\alpha} \right)^{\beta} \quad (3.1)$$

Otherwise $f(t) = 0$ for $t < \gamma$.

Where t is time or the number of cycles, β is the shape parameter, α is the scale parameter and γ is the location parameter. The use of γ is not really representative in

reliability because failures always start from the beginning and the parameter γ shifts this beginning to a value of time higher than 0. So, for the following the Weibull distribution will be reduced to two parameters (α , β). Then, the cumulative distribution function $F(t)$ can be expressed in equation (3.2) considering $\gamma = 0$.

$$F(t) = 1 - \exp\left(-\left(\frac{t}{\alpha}\right)^\beta\right) \quad (3.2)$$

Moreover the reliability function $R(t)$ is defined in equation (3.3).

$$R(t) = \exp\left(-\left(\frac{t}{\alpha}\right)^\beta\right) = 1 - F(t) \quad (3.3)$$

And finally, the failure rate $z(t)$ can be found as in equation (3.4).

$$z(t) = \frac{\beta}{\alpha} \left(\frac{t}{\alpha}\right)^{\beta-1} \quad (3.4)$$

Regarding the application of theory, the shape parameter (β) and the scale parameter (α) have to be extracted from measurement results. The scale parameter α represents the time when 63.2% of the population of devices have failed². So it is a powerful indicator of the lifetime that can give an accurate estimation of the devices failed at a given time using equation (3.2). In figure 3.4 are presented the main functions of the Weibull distribution to get an idea about their shape. Regarding what was presented previously in section 3.1.1 page 82, here the impact of different values of β can be seen.

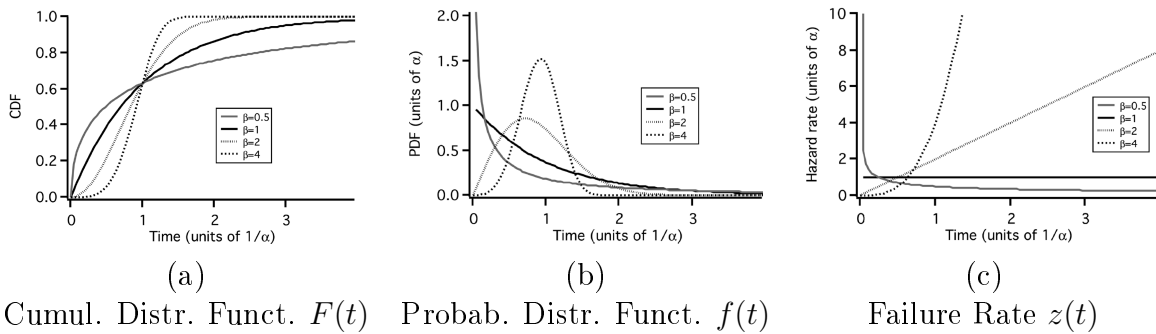


Figure 3.4: Main functions of the Weibull distribution [6].

In order to compare with other batches, the main steps to calculate α and β will be presented. The first step is to transform the previous equation (3.2). So the equation of the Cumulative Distribution Function is linearised by taking the natural log twice (equations (3.6) and (3.8)).

² $(1 - \exp^{-1} = 0.632)$

$$F(t) = 1 - \exp\left(-\left(\frac{t}{\alpha}\right)^\beta\right) \quad (3.5)$$

$$\ln(1 - F(t)) = -\left(\frac{t}{\alpha}\right)^\beta \quad (3.6)$$

$$\ln\left(\frac{1}{1 - F(t)}\right) = \left(\frac{t}{\alpha}\right)^\beta \quad (3.7)$$

$$\ln\left(\ln\left(\frac{1}{1 - F(t)}\right)\right) = \beta \ln(t) - \beta \ln(\alpha) \quad (3.8)$$

$$Y = aX + b \quad (3.9)$$

And finally putting equation (3.8) in a form of a linear function (as equation (3.9)) allows us to have a simpler system to solve.

$$Y = \ln\left(\ln\left(\frac{1}{1 - F(t)}\right)\right) \quad (3.10)$$

$$X = \ln(t) \quad (3.11)$$

$$a = \beta \quad (3.12)$$

$$b = -\beta \ln(\alpha) \quad (3.13)$$

Now α and β parameters³ can be found from Y and X that are obtained from measurements. Indeed, in equation (3.11) t is the time when the device fails or it could be a number of cycles. In equation (3.10), $F(t)$ can be calculating using the Median Rank equation based on the rank of the devices failing in a certain order. There are several techniques to calculate $F(t)$. This one was chosen because of its easiness to use and its accuracy considering the few number of devices available for each test. An approximation of the Median Rank equation is given in equation (3.14).

$$F(t) = \frac{j - 0.3}{n + 0.4} \quad (3.14)$$

Where j is the rank of the switch sorted by the failure order from the first that failed (#1) to the last (# n). Everything has been presented to plot data on a log-log graph,

³In literature, sometimes α and β are interchanged.

i.e. Y (as a function of $F(t)$) versus X (as a function of the number of cycles). All the points should follow a straight line on this graph otherwise it means that there is not only one failure mode involving in our devices and as a consequence the 3-parameters Weibull distribution will be needed to go further.

If the points follow a straight line therefore a linear regression will be computed using Excel for instance. From the software, a and b are gotten for the best straight line that fit our data. And finally the shape and the scale parameters are deduced using equations (3.12) and (3.13).

3.1.2.2 Acceleration factors

Using the Weibull distribution allows to get acceleration factors during reliability testing. In figure 3.5 is given an example of accelerated testing, in which the temperature could have been raised e.g. by 20°C . The consequence is, all the devices failed earlier, allowing a testing period reduced by a factor 10. Moreover, the straight lines remain parallel because the testing is assumed to be reproduced on the same components in the same conditions, except temperature.

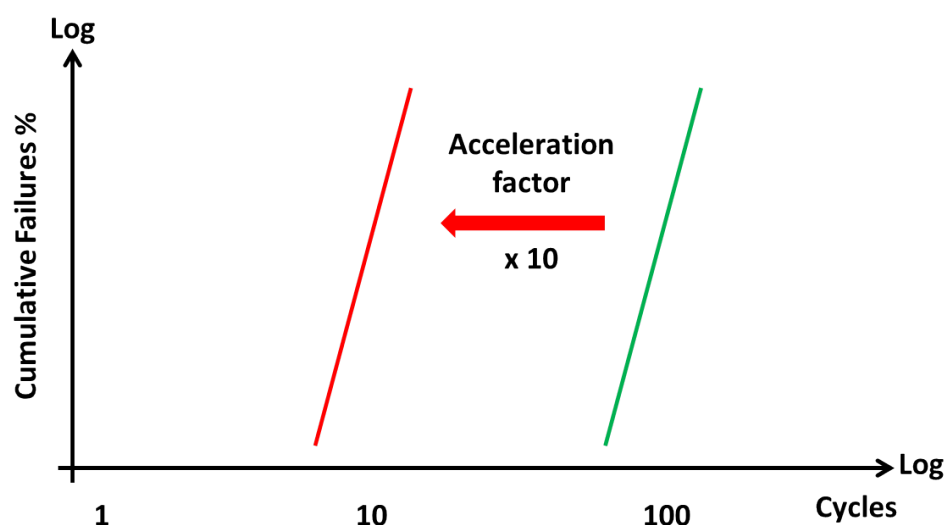


Figure 3.5: Example of acceleration factor extracted from the Weibull distribution.

The acceleration factors for reliability of RF-MEMS have not been published yet. Finding them will allow to better understand reliability of RF-MEMS.

3.1.2.3 Practical examples

Found in literature, the three next examples give an idea about the use of the Weibull curves.

In the figure 3.6, the authors tested in cold switching at 20 dBm, 32 switches from their fabrication process represented by the black dots in the figure. Cold and hot switching are operating modes of switches, for an exhaustive explanation of these modes, the reader can refer to section 3.5 page 104.

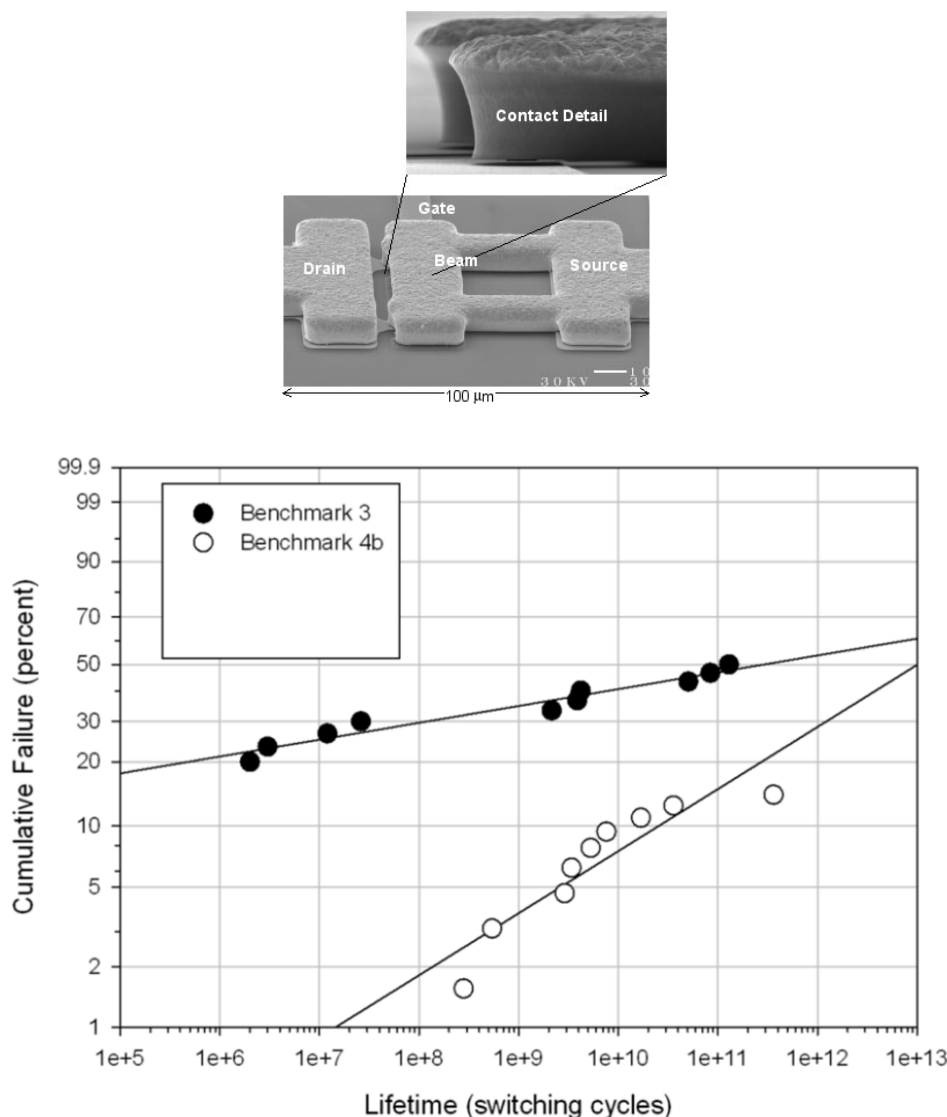


Figure 3.6: Weibull curves for a fabrication process improved, Radant RF-MEMS [7].

Not all the dots are presented in the figure but 50% of their switches reached 100 billion cycles and the mean of the cycles before failure is about 200 billion. Then, after improvements on the switch design, on the reliability of the contact and on the fabrication process to limit contaminations, they redid the reliability test in the same conditions. The lifetime of 64 switches are represented in white dots and 88% of them passed 100 billion cycles and the mean number of cycles is about 10 trillion. We suppose that a mistake was introduced in the paper regarding numbers. Anyway the slope of the Weibull line is higher and shifted on the right, this is an evidence of the improvement of

reliability and fabrication process. On the other hand they did not mention the scale and the shape parameters used to plot the Weibull distribution of the cumulative failures. Also they did not mention the criterion of failure nor the failure mechanism. More generally, the failures are spread on several decades meaning that the fabrication process might be improved.

In the second example in figure 3.7, Czaplewski et al. built switches with different contact material.

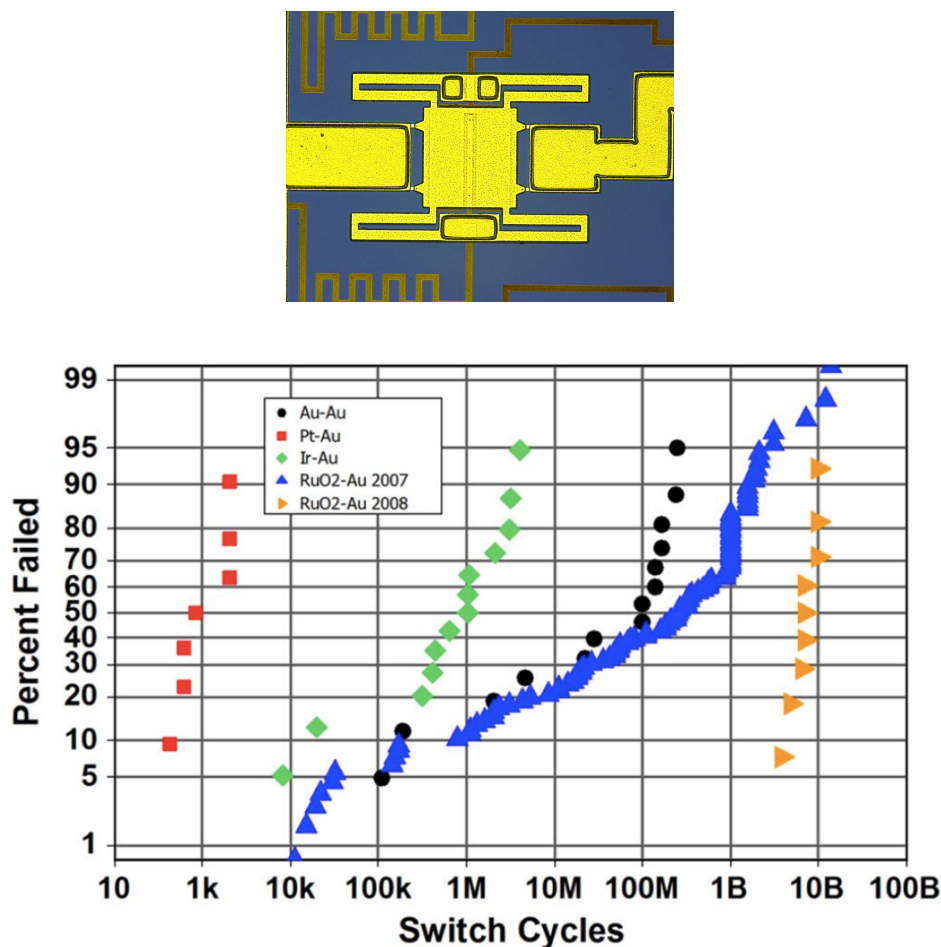


Figure 3.7: Weibull curves for a switch with different contact materials, Sandia National Laboratories, Argonne National Laboratory, USA [8].

Due to changes in the design and contact materials, they achieved with $\text{RuO}_2\text{-Au}$ contact metal a better reliability in 2008 than its contenders because the curve is straight vertically (all failures happened in the same decade) and the lifetime is better than 1 billion cycles. The specific shapes of blue and black dots have to be noticed because they do not follow a straight line. Either some switches with different natures were mixed or a second type of failure mechanism appeared in the test after 1 billion cycles for the

blue dots and 100 million cycles for the black ones. This kind of figure were briefly discussed in section 3.1.2.1 page 85. More generally, it is not mentioned if it was cold or hot switching neither the failure criterion as well as the shape and the scale parameters.

On the last example presented in figure 3.8, the authors show their results related with maturity of their fabrication process together with a Weibull distribution for reed relays.

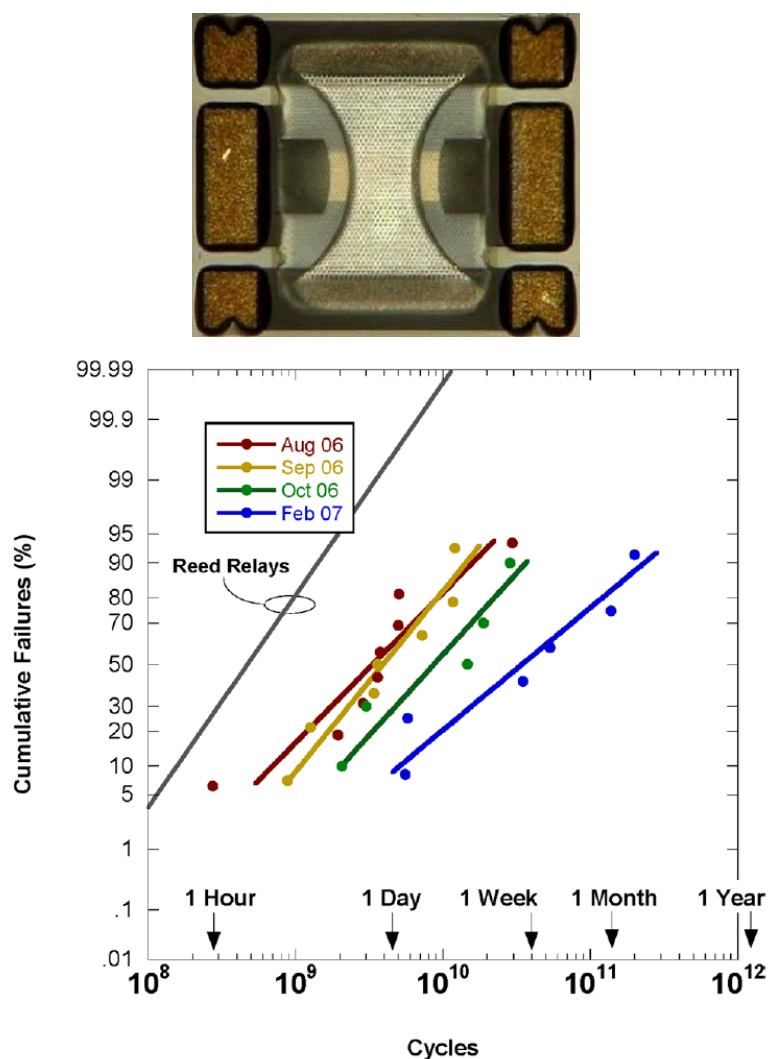


Figure 3.8: Weibull curves to assess the evolution of the fabrication process, Memtronics, LeHigh University, USA [9].

These results deal with capacitive RF-MEMS switches. The operating voltages are not mentioned neither if it is hot or cold switching. However they got an improvement in the lifetime of their switches but not in the slope of the straight line. They did not mention the failure criterion neither the failure mechanism. Also they did not mention what was improved in their fabrication process between August 2006 and February 2007. In addition the shape and the scale parameters are not mentioned and we suspect that

some points are missing regarding the dispersion of each family of points.

In the next section, the task will be to assess the lifetime of our switches in given operating conditions and plot on a log-log graph a Weibull distribution corresponding to their reliability. Extracting the scale and shape parameters of each family of curves, conclusions will be provided with regard to the reliability of the fabrication process and the switches.

3.2 Initial reliability testing on Xlim micro-switches

The Wiedemann-Franz law, seen previously in section 2.4.2.3 page 65, shows that a relay contact supertemperature only depends on the voltage across the metal contact. Melting degradation, and stiction are increased by applying a relatively large voltage between the input and the output of a switch. Typical voltages causing melting are 80 mV for soft metals like gold, up to 400 mV for harder metals (refer to table 2.4 page 66).

Under cold switching conditions, the contact resistance is either infinite or very small when a given voltage is applied across a loading impedance in series with the switch. Therefore, the contact never endures large voltage, and the contact ageing is much less than under hot switching conditions.

Let us consider the circuit presented in figure 3.9, this is a test bench that measure the number of cycles achieved by a switch. The bias voltage control the opening and the closure of the switch with a 50% duty cycle and a cycling frequency at 2.5 kHz, enough to reach steady states of the switch in open and close states. The control of voltage between the input and the output of the switch is controlled by changing V_{DC} . This control allows us to be in cold switching by a synchronisation between V_{DC} and V_{Bias} .

Under $V_{DC} = 5$ Volts between the input and the output of the switch, and under cold switching conditions, a device typically achieve more than 100 Million cycles (figure 3.10). Since large resistances are put in series with the RF-MEMS switch, little or no current passes through the switch contact. The contact voltage under cold switching conditions is minimal.

However, under hot switching condition, the voltage V_{DC} is present across the contact for a short time upon closure and opening of the switch, and locally melts the contact metals and causes rapid ageing of the relay, especially with thin metals like in RF-MEMS switches. Conversely, a reduced open/closure time as well as a low contact resistance fosters the switch endurance to hot switching events.

Using the set-up presented in figure 3.9, several switches were monitored under hot switching cycling with various bias voltages V_{Bias} . This test is simpler to settle than cold-switching testing because the contact resistance increase is the only failure mechanism

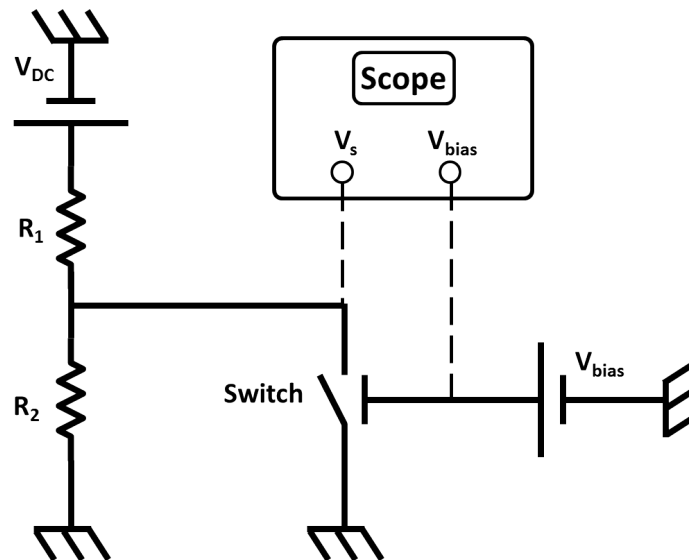


Figure 3.9: Schematic of the reliability bench to assess the lifetime of S5 RF-MEMS switches. R_1 is 10 k Ω and R_2 is 40 k Ω . The current in the switch is always less than 500 μ A.

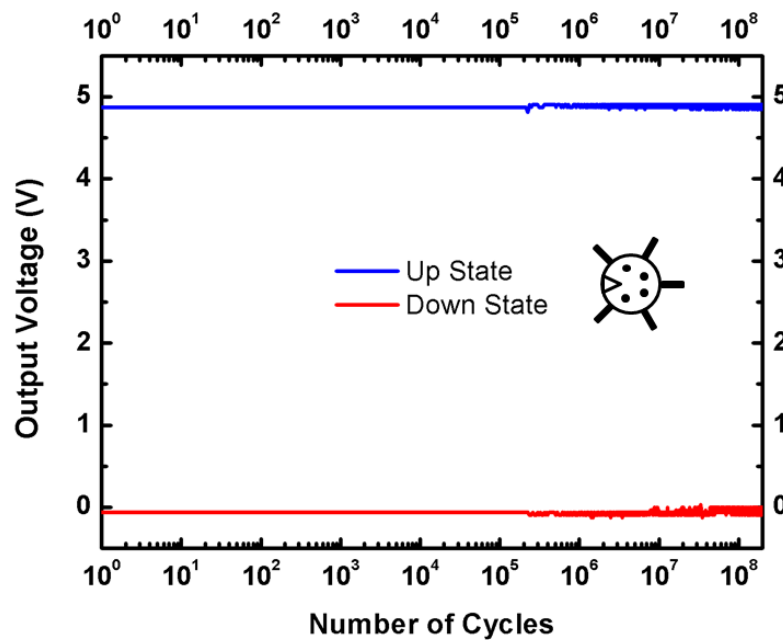


Figure 3.10: Recording of an S5 ohmic contact RF-MEMS switch during cold switching under 5V.

observed.

It has been decided that the device fails when the detected voltage was more than 0.5 V with the switch in the closed state (red curve in figure 3.10). This criterion could be easily detected and is followed by a quick increase in the contact resistance and ends to the failure of the relay in open circuit.

4 sets of 5 devices have been tested under various bias conditions. All devices were taken on the same wafer and were tested one after another, taking a long time. The bias voltage varied between 37 V, slightly above the pull-down voltage, up to 55 V, that is more than doubling the electrostatic force on the device. In three cases, the input-to-output voltage is 5 V, and a last test was conducted with an input-to-output voltage of 0.5 V. In this case the failure criterion was reduced to 0.05 V.

The results are presented in figure 3.11 and summarized in table 3.1. It can be seen that the device fails a lot quicker than under cold switching conditions.

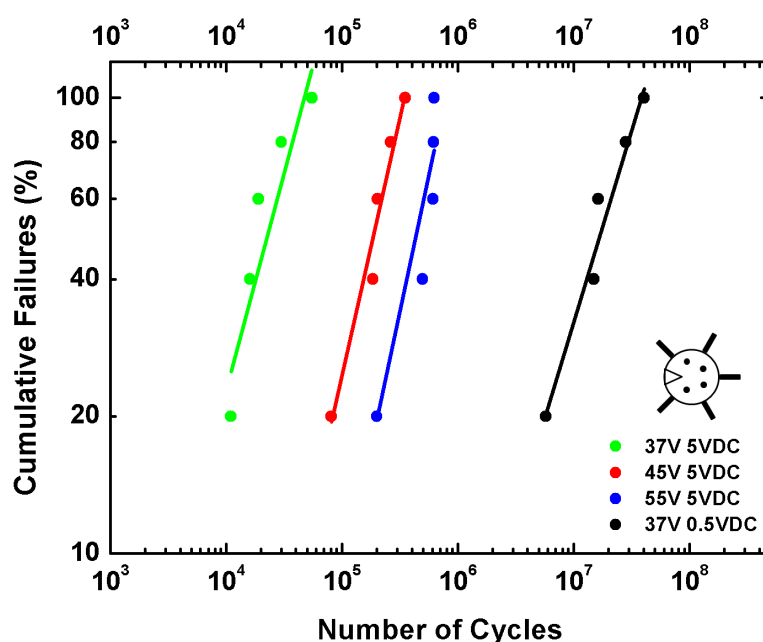


Figure 3.11: Cumulative failures versus number of cycles for 20 S5-type RF-MEMS switches.

V_{Bias}	V_{DC}	Average numb. of cycles	α Scale param.	β Shape param.	β Error
37 V	5 V	26,200	30,300	1.60	0.28
45 V	5 V	216,600	254,300	1.84	0.23
55 V	5 V	508,900	611,800	1.88	0.57
37 V	0.5 V	21,140,000	24,865,000	1.38	0.14

Table 3.1: Summary of measurement testing and computed parameters.

Also, it can be seen that increasing the bias voltage from 37 V up to 45 V, increases the lifetime nearly by a factor 10, and by a factor 20 when increasing the bias voltage up to 55 V. This is partly because the contact resistance is reduced, but also because the switch closes faster, effectively reducing the transient time of the switch. For 37 V

bias voltage, reducing the input-to-output voltage from 5 V down to 0.5 V increases the lifetime nearly by a factor 1,000.

Few comments are given regarding the shape and the scale parameters obtained. First β tends to increase with bias voltage though this increase is relatively low. It would mean that the failure rate is more spread for higher bias voltages. Actually, β should not be dependent on operating parameters, β is related with the maturity of fabrication process. Taking into account the error on β , the variation of the shape parameter β are not relevant and β can be considered as constant, meaning that the fabrication process is mature. The error on β represents how much the Weibull distribution parameters fit with data. Second, the input-to-output voltage V_{DC} has also an influence on the shape parameter β in the same trend as the bias voltage V_{Bias} , but only two values are available to compare and it would be interested to check these trends with more measurements. Third, with reference to the scale parameter compared with the average number of cycles, one can say that the values are quite similar and the same trend is followed. In conclusion a simple average is not far from a statistical value calculated by the Weibull's distribution but the difference is that the scale parameter is more difficult and longer to get.

In conclusion, this experiment showed how to accelerate measurements varying bias voltage and input to output voltage. The time spent in testing can be reduced up to 1,000 times. Temperature has an important role in lifetime of switches and will be studied in future works.

Considering that all of these tests were done in series, a lot of time was spent doing one thing at a time. Because not many events happen during the switching testing of RF-MEMS, from the point of view of an engineer, there were wasting time because something else could be done in parallel. Taking this into account the next section presents how to conduct testing in parallel using PCB and Arduino boards to improve efficiency of reliability testings.

3.3 Parallel test bench

Under specific operating parameters, the ohmic RF-MEMS switches can achieve a large number of cycles, where only the mechanical behaviour is solicited. This is what happens in cold switching especially. In cold switching, the electrical failure modes due to transient phenomena are avoided because, during actuation, the current flow is not allowed through the contact. The current flow is allowed only during steady states (ON and OFF states established). So testings were conducted in cold switching on the S5-switch with a high power signal (28 dBm at 2 GHz), the results are reported in figure 3.12. The switch is in series configuration. After 9 hours of testing and more than 82 millions of cycles achieved,

the switch did not show any weakness nor changes, so the test was stopped because of the long-term use of the test bench. Clearly this task takes too much time.

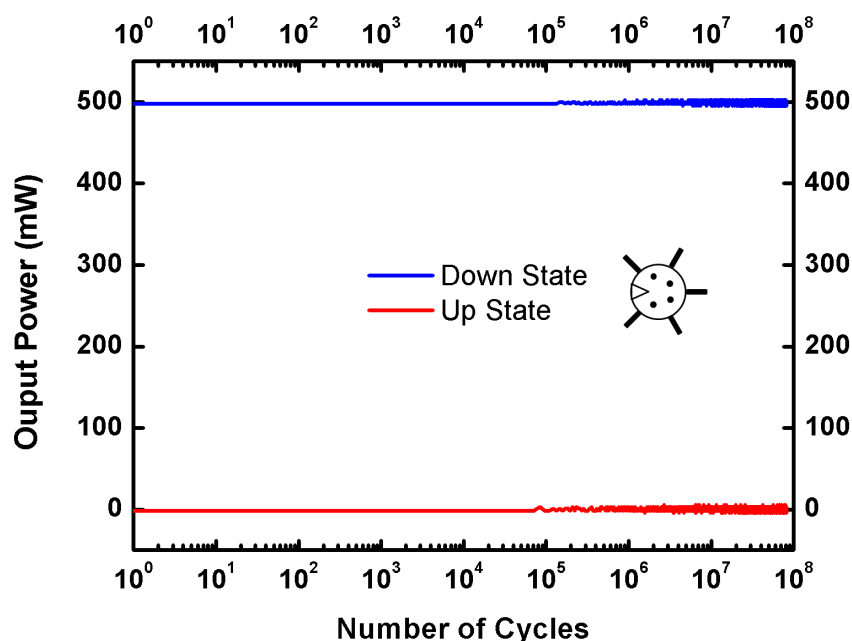


Figure 3.12: Recording of an S5-type ohmic contact RF-MEMS switch during cold switching under 28 dBm.

3.3.1 Introduction

As seen previously, accelerated testings are expected in a way that the RF-MEMS will be poised to be in the market after succeeding in reliability testing. In our perspectives, accelerated testing have to be combined with parallel testing to improve efficiency. Later in the thesis is presented a bench to perform tests in parallel, from 8 channels up to 48 for instance. On the other side, accelerated testing would be pursued by applying different kind of stress on the component. The combination of both is compatible and recommended.

This is in this frame that takes place the stress accelerated testing. The idea is to foster the degradation of a device putting it in stress conditions. There are two options for that, one option is applying temperature stress and the other is to apply operating parameters stress.

Depending on the type of device the operating parameters stresses may be mechanical, electrical, thermal etc. For RF-MEMS switches we mostly act on the bias voltage, the input to output voltage, the duty cycle and the pressure as the operating parameters

stresses (that was presented in section 3.2 page 92). However the maximum level of stress admissible by the component has to be watched in order not to activate a failure mechanism that is not involved on nominal operation. Related to that, an example [55] of an empirical equation is presented, that was developed to estimate the lifetime of electromechanical relays. In equation (3.15) the empirical equation that gives the lifetime (in number of cuts) as a function of operating parameters for *alternative* voltages, is presented.

$$t_a = K_a V^{n_a} I^{m_a} (\cos \phi)^{q_a} \quad (3.15)$$

Where V and I are RMS (Root Mean Square) voltage and intensity respectively, $\cos \phi$ is the power factor L/R or $1/RC$, K_a , m_a , n_a and q_a are parameters unique for a type of relay. Calculating the ratio between data obtained at two different operating conditions allows us to deduce easily the acceleration factor. In equation (3.16) is presented the empirical equation that gives the lifetime (in number of cuts) as a function of operating parameters for *continuous* voltages, where all the parameters are analogous as equation (3.15).

$$t_c = K_c V^{n_c} I^{m_c} \exp\left(\frac{q_c L}{R}\right) \quad (3.16)$$

For purely electronic components, the Arrhenius law (equation (2.20) in section 2.4.4 page 70) is very efficient for accelerating tests with temperature. Calculating a ratio between two values of lifetime with their respective temperature allowed us to find easily the acceleration factor.

Since our devices are composed with an electrical part together with a mechanical part, the continuity of this work would be to couple the acceleration factor studied in electronic components with the acceleration factor for operating parameters stress in mechanical devices to get a final acceleration factor including all the parameters involved in the reliability of RF-MEMS switches. This is a work currently in progress.

After this introduction on perspectives of acceleration factors, a specific test bench for parallel measurement has been developed. We estimate that 50 switches tested in parallel are required to lead properly an efficient reliability testing.

3.3.2 Design of PCB (Printed Circuit Boards)

Reliability measurements can take a long time and a simple test bench has been developed that allows us to accelerate the measurement procedure with DC voltages. The idea here is to set this test bench in parallel so as to conduct more efficient testings.

Based on the bench presented in figure 3.9, a circuit was designed on a 2 inches Printed Circuit Board (PCB). It allows the measurement of 8 switches at the same time. The elementary pattern is shown in figure 3.13.

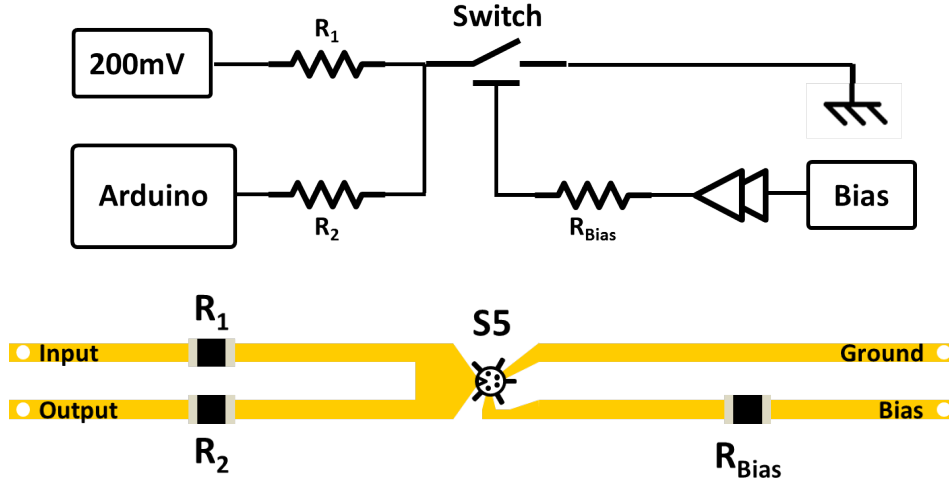


Figure 3.13: Elementary pattern of the 8 channels PCB design for parallel testing. R_1 is 10 k Ω and R_2 is 40 k Ω . R_{Bias} is large enough to prevent current in the bias line.

For each channel, the Input is connected to the input-to-output generator, the output is connected to an analog channel of the Arduino board, the ground is connected between all instruments and the bias is connected to the bias voltage.

Some holes are drilled through the substrate to weld output and input pins. The switches are flip-chip with a pick-and-place machine and together with the SMD (Surface Mounted Devices) resistances, are stuck with soldering paste in clean room before going into the oven to fix the soldering paste. An SMD resistance is a small electronic component that allows to be mounted on small circuits like PCB. A schematic view of an SMD resistance is shown in figure 3.14.

Basically, each channel is composed by four tracks. One track is for biasing where a series resistor is connected to prevent short circuits with other channels. There is a risk because only one bias generator is used to bias the eight channels. A second track for sensing the state of the switch (i.e. its contact resistance) with high value series resistance. On the same track there is the input voltage across a lower resistance (this is R_1) compared with the sensing one, so this is the third track. And the last track provides the ground.

The first step consists in reporting all the switches in one substrate to connect them to the measurement system only once. A duroid substrate was chosen from Rogers Corporation among RO4000 series. It has a 3.4 dielectric constant, a copper thickness about 17 μm and a substrate thickness about 1.5 mm. Then the copper is etched by photolithography process according to the design visible in figure 3.15 where the board side

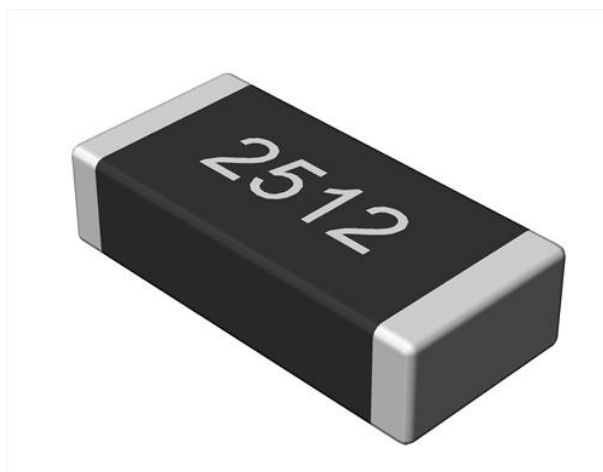


Figure 3.14: Surface Mounted Devices (SMD) resistance.

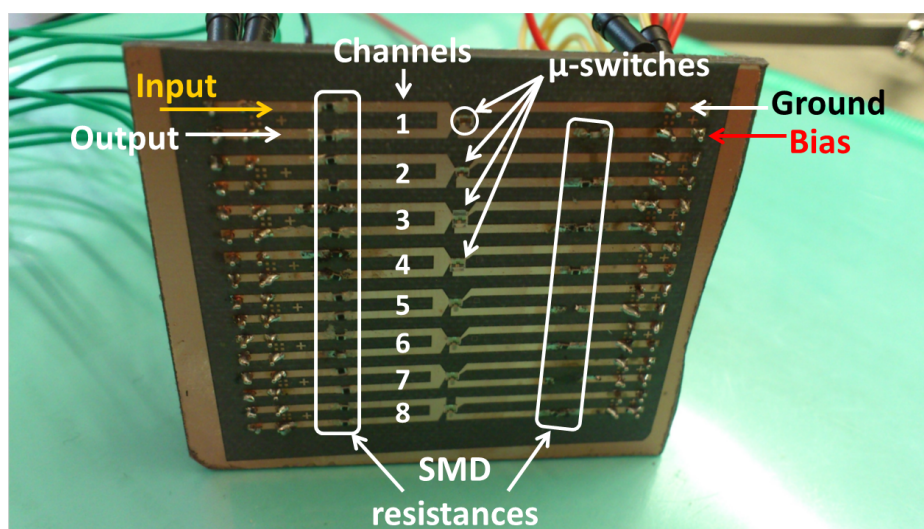


Figure 3.15: Photograph of the duroid board mounted with switches and resistances exhibiting 8 parallel channels.

size is 2 inches. The design consists in 8 channels in parallel reproducing the test bench presented in figure 3.9.

Some tests were conducted but there were some problems regarding the flip-chip technique that was not fully successful and led to non-readable results. But we could certify that the bench was operational using commercial variable resistors. Now, efforts have to be done to improve the technique that reports switches on the duroid substrate.

To reach more compactness, a second design has been drawn to measure 48 switches at the same time on a 2 inches PCB. The elementary pattern is given in figure 3.17. The circuit is the same as for the 8 channels, just more compact. It contains all the spaces for SMD resistances and switches in the minimum surface. It has been thought in order to

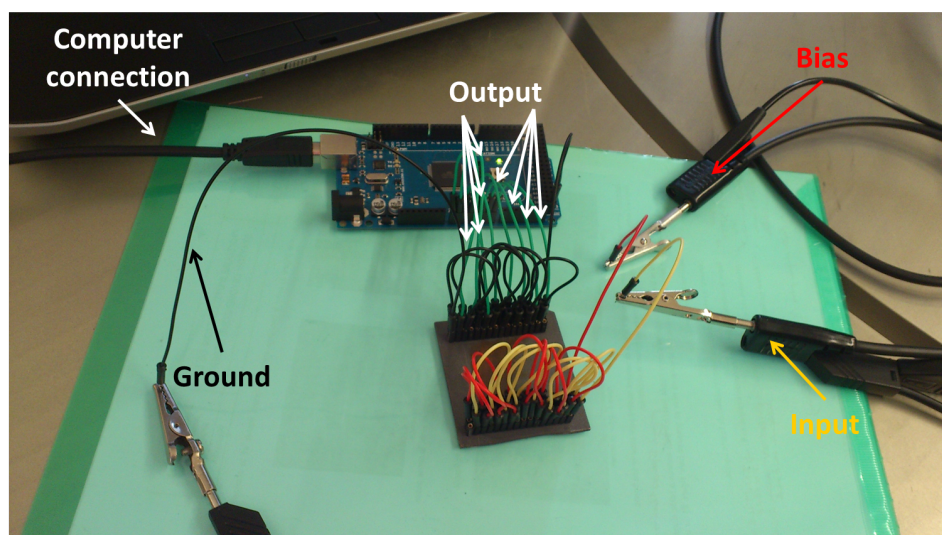


Figure 3.16: Photograph of the parallel test bench running with Arduino board getting output voltages from the duroid PCB where are mounted the switches.

save the wires and hole connections between the different boards. The color green in the figure represents SU-8 layer so as to prevent short-circuit between the different paths.

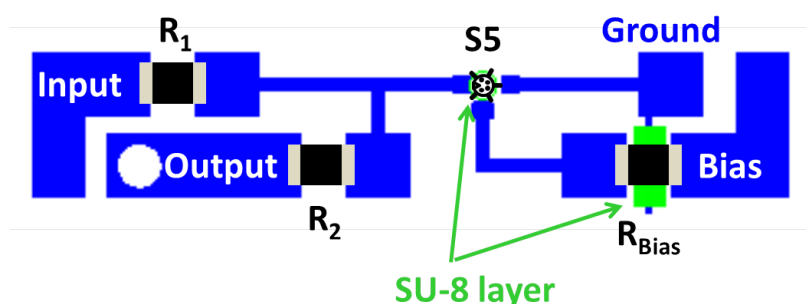


Figure 3.17: Design of elementary pattern to test 48 switches in parallel on a 2 inches PCB.

The final design with the 48 switches is shown in figure 3.18 and the fabrication is under progress.

3.3.3 Test with micro-controller

Arduino is an Italian company who makes Printed Circuit Board (PCB) based on Atmel micro-controller. With an open source software any program can be developed and upload that can help us to manage measurements. The model used is the Arduino Mega2560 board based on the Atmel ATMEGA2560 micro-controller (figure 3.19). What is interesting for us in Arduino board especially are the 16 analog input pins, the 54 digital input/output pins, its size and the "getting started". The board is powered and con-

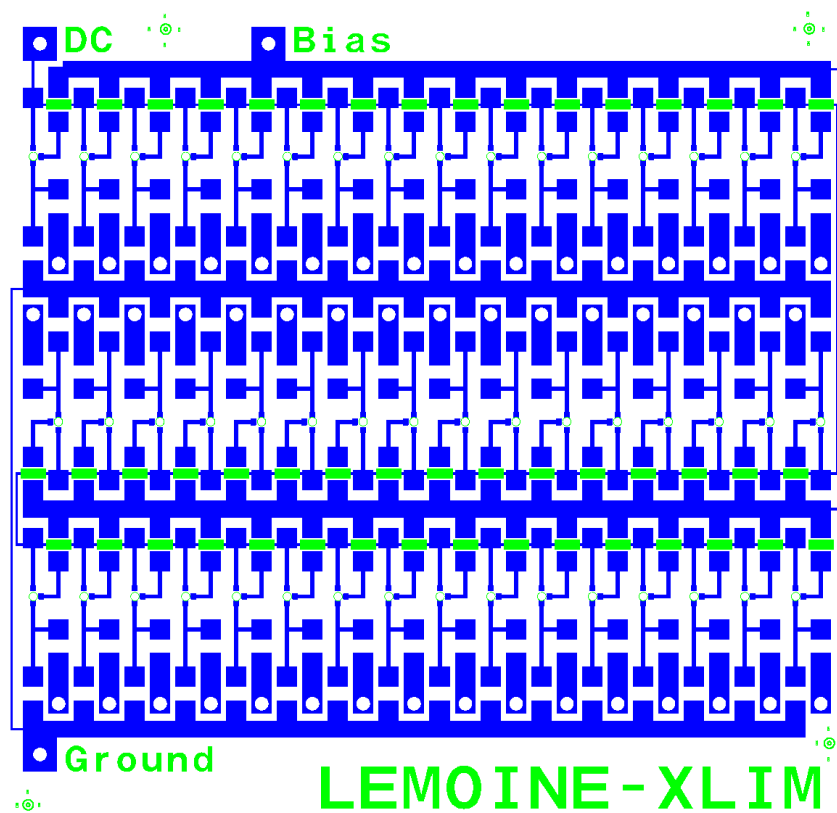


Figure 3.18: Design of the next duroid board to test 48 switches in parallel.

trolled by 5 V USB-series connection. Arduino boards are very convenient to get and deal with a signal quickly and accurately. It works at 16 MHz clock speed and has a native resolution of 10 bits on the analog inputs that is expendable up to 17 bits using the technique presented in section 3.3.3.2 page 102. At 17 bits of resolution measurement takes about 0.1 ms to be executed. So to proceed faster, the resolution can be decreased meaning that the accuracy would be lower, thus a compromise is required at this stage.

The sensing pins for measuring the output voltage of the switch on the duroid substrate will be connected to the analog input pins of the Arduino board. The Arduino will calculate the contact resistance and compare to a reference value. If the one state (up or down) is not included in the range, the Arduino stops counting the switching and displays on the computer through the USB cable the number of cycles with the number of the channel.

The Arduino code that allows to count the number of switching is presented in Annex B. The flowchart related with the code is given in figure 3.20.

The procedure starts by reset of boards and a trigger to switch ON the input-to-output voltage generator. Then a trigger is sent to the slave boards and every channel checks the state of one single switch. If the switch is not "ON", the channel number and the number of switching are displayed on the computer screen, the switch failed. If the switch is

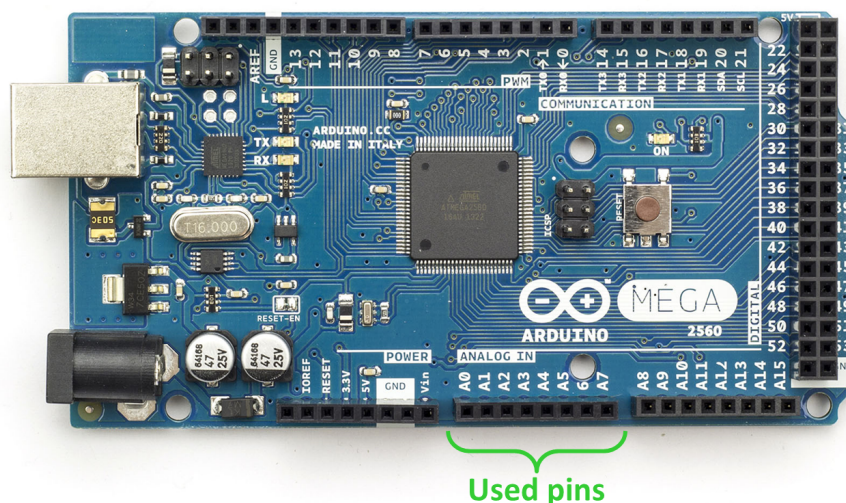


Figure 3.19: Photograph of the Arduino Mega2560 board based on an Atmel AT-MEGA2560 micro-controller showing all the different inputs and outputs.

"OFF", the bias is applied on all switches. Once again, the state of switches is tested. In this case, if the switch is "OFF", it means the switch failed and the number of switching is displayed on the computer screen. Otherwise, if the switch is "ON", the switch passes and the loop is restarted.

3.3.3.1 Presentation of test bench

Once everything is connected the bench looks like the figure 3.16. The biasing is provided on the top right corner and is distributed through all the red wires on the duroid PCB. Below the biasing cable is the input to output voltage distributed through the yellow wires to the inputs of the 8 switches on the PCB. And in the bottom left corner there is the ground connected to all the circuits. Finally the 8 sensing channels of the PCB are connected to the 8 analog input pins of the Arduino by the green wires.

3.3.3.2 Increasing accuracy of measurements with help coming from Atmel

Considering the low number of acquisition bits (10 bits), Atmel presents [56] a way to increase virtually the number of bits. Based on a mathematical rule in binary calculations, this point will be explained in this subsection.

The technique is called "Enhancing Analog-Digital Converter resolution by oversampling". It is well-known as long as you work in the field of special signal processing techniques. It consists in taking many samples of the wanted value to calculate an aver-

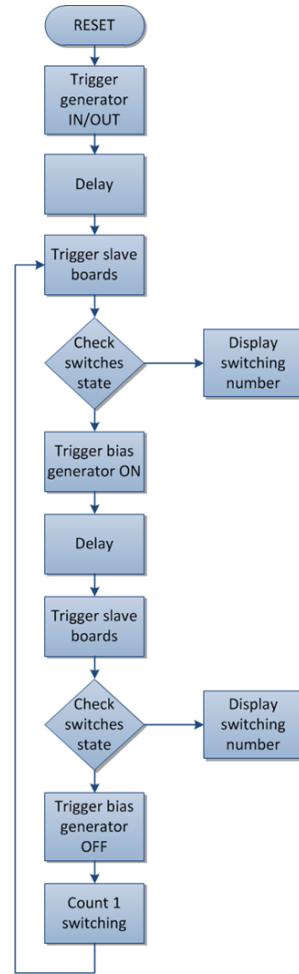


Figure 3.20: Flowchart of Arduino code that allow to count the number of switching done by micro-switches.

age and thus increase the accuracy. Because of the theory of oversampling and decimation, measuring four times the same value allows us to increase the acquisition resolution by one bit according to equation (3.17). Thus the number of possibilities is multiplied by two which means that the voltage resolution is divided by two.

$$f_{oversampling} = 4^n \cdot f_{nyquist} \quad (3.17)$$

Where n is the additional number of bit to reach the desired voltage resolution and $f_{nyquist}$ is the Nyquist frequency defined as the minimum sampling frequency to get the maximum frequency of a signal according to equation (3.18).

$$f_{nyquist} \geq 2 \cdot f_{max} \quad (3.18)$$

In practice, a loop is set so as to get the output voltage of the switch 16,384 times ($= 4^7$), then all the values are adding together and a geometric average is calculated which

consists in shifting the chain of bits by 7 steps on the right. It corresponds to a division but for binary digits. Ultimately, an acquisition system of 17 bits (10 native + 7 due to oversampling) is obtained representing a resolution about 38 μV theoretically. The drawback of this technique is the time spent in measuring 16,384 times the same value which is about 0.1 ms.

3.4 Initial sorting of switches on wafer

A procedure has been developed to sort RF-MEMS switches once they leave the clean room. The importance of sorting has come as an evidence to avoid preliminary potentially failed switches from our reliability tests. Because it appeared sometimes a switch that seems like good but after few minutes of testing led irremediably to a failure. So this procedure allows us to put aside those inexplicable events allowing us not to waste time.

The test consists in measuring the off-capacitance C_{off} for 5 seconds, then the contact resistance R_{on} is measured also for 5 seconds and it ends by applying a bipolar triangle to get the four actuation voltages ($V_{\text{p+}}$, $V_{\text{r+}}$, $V_{\text{p-}}$ and $V_{\text{r-}}$). The procedure allows to insert burn-in cycles or any waveform that would improve the sorting. This procedure is considered by far non-destructive, moreover it does not affect much the switches in their life since the test is done with the minimal configuration close to nominal operation.

For each step of the sorting procedure, the data are saved in a file that is treated with Excel. So once the set is launched the Excel file is filled semi-automatically waiting for the instructions of the operator. The data are entered in the worksheet according to the map of the wafer, preliminary set up by the operator, where he just has to tell the position of the switch to the computer.

The Excel file allows us to have a quick overview of the wafer and on the failure rate giving the key parameters. Thus, switches that do not get into the specifications can be put aside easily and quickly.

3.5 Presentation of hot and cold switching

Hot and cold switching are terms widely used in switches measurements. Here a definition of these two modes is given.

Two modes are distinguished to operate a switch. The first one that is called the hot switching is the normal operation of a switch where the switch has to stop (or not) a continuous signal, like for instance a continuous wave (CW). The second mode is called the cold switching where the current is allowed to pass through the contact only when the steady state of the mechanical part is established. It is a way to avoid transient phenomena like material transfer, electric arc, breakdown, field emission and so on during

opening/closing of the contact. Regarding the voltage generators, there must have a synchronisation between them to provide the cold switching, whereas nothing is required in hot switching. In other words, when the beam is moving (because of biasing), either a voltage is allowed across the contact (hot switching) or not (cold switching). This is represented in figure 3.21.

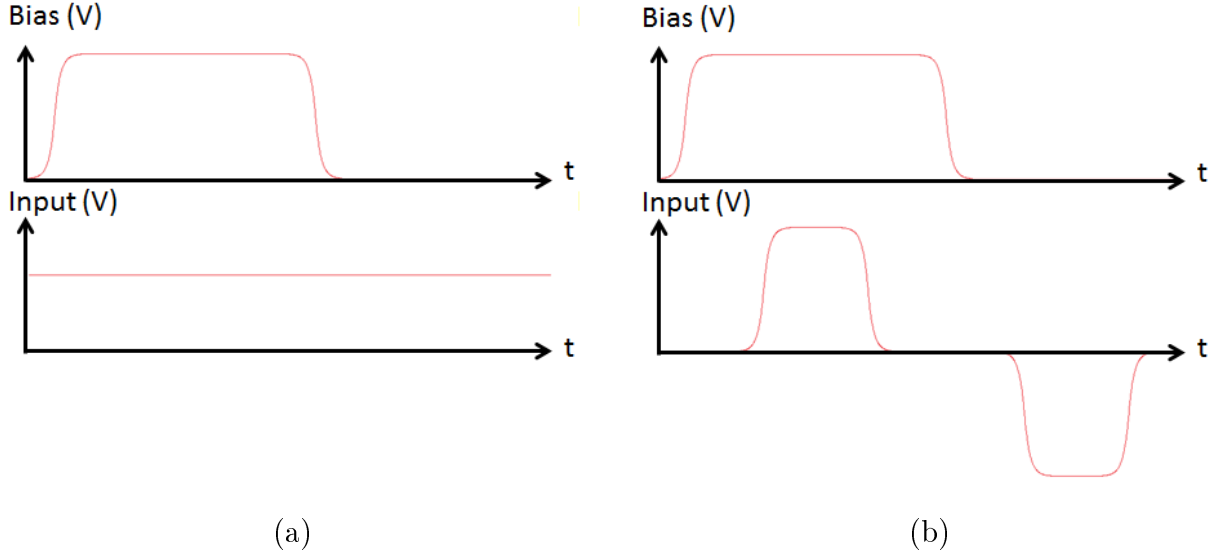


Figure 3.21: (a) Voltage generators waveforms for **hot** switching, (b) Voltage generators waveforms for **cold** switching.

In hot switching the input to output voltage is independent on the bias voltage. In cold switching the input to output voltage "waits" for the steady state of the switch to supply voltage/current. In other words, the cold switching requires a synchronisation between bias generator and input-to-output generator. As presented in the thesis, the hot switching accelerates the failure of switches.

To get a long lifetime of the switch it is suited to present testing conducted under cold switching, because the switch is less solicited and the failures are drastically reduced. In literature [7] [13] [57] some commercial RF-MEMS switches have reached a tremendous number of cycles tested under hot switching with a very low current. In fact, this is really close to reproduce cold switching, hence the results are better. As it was presented before, the voltage across the contact is a major factor affecting the lifetime of switches.

3.6 Conclusion

There are two ways to improve efficiency of testing of RF-MEMS switches, which are the operation parameters and the parallel test bench. Both of these topics have been explored opening in the continuity of the experiments. Indeed, these tasks require a great amount

of switches and a lot of dexterity to mount switches on the boards. The bias voltage and the input to output voltage have shown a great impact on the lifetime of the switches telling us that optimized operation parameters have to be found to reach a high number of cycles. The sorting of the switches is utmost importance to guarantee useful and efficient measurements. And finally some tracks were suggested to improve the reliability of the switches based on the previous works and on those conducted here.

Chapter 4 :

Possible Improvements for Reliability of RF-MEMS

The following chapter deals with the main results collected all over the thesis as possible improvements for next works on the topic. On a first section, an asymmetrical design will be presented that allows to prevent bounces of switches upon closure. Then, recommendations regarding improvements for reliability of RF-MEMS switches are detailed. This second section mainly exposes all the preliminary advices required to build reliable switches and extract main parameters. Finally the third section is dedicated to present three test benches that allow to get a full description of switches under various conditions.

4.1 Bouncing suppression using asymmetrical design

Contact bouncing is among the most critical phenomena reducing RF-MEMS reliability. Many RF-MEMS metal-contact switches suffer from multiple bounces when the contacts are closed upon actuation. Indeed, most reliable devices involve large contact forces, stiff mechanical structures and low damping.

Therefore, reliable, elastic metal-to-metal contacts are subject to bouncing upon closure, and the onset of the phenomenon is often linked to the applied bias voltage. For instance, well-known commercial switches have their bias voltage limited by the onset of bounces as voltage is increased.

This phenomenon is detrimental to the switch final reliability, since bounces are increasing the number of contact closures and openings required for one closure event.

This is even more critical when a significant electrical loading is present, and that contact reopening adds more cycles to a single one. Bounces can also happen as contacts are ageing, and the onset of bounces can be linked to reliability issues [57].

At the same time, most metal-contact switches are using two contacts at least, closing simultaneously when a bias is applied. The vast majority of structures are symmetrical with respect to contact positions, and this is in favor of bouncing.

This section will show that by slightly breaking the geometrical symmetry of the mechanical structure, bounces are suppressed and that the structure can withstand more bias voltage and more contact force without contact re-opening occurring.

4.1.1 Principle

For a better switch reliability, high contact force and high spring constant switch are needed. In these conditions, their mechanical structure can have low mechanical damping and because of high restoring force needed to avoid stiction, bounces appear after the first impact until the contact stabilizes. These multiples contacts in one actuation decrease the contact lifetime reducing the operation of switch. The phenomenon is even more apparent in low pressure environment and/or vacuum. The phenomenon is sketched in figure 4.1.

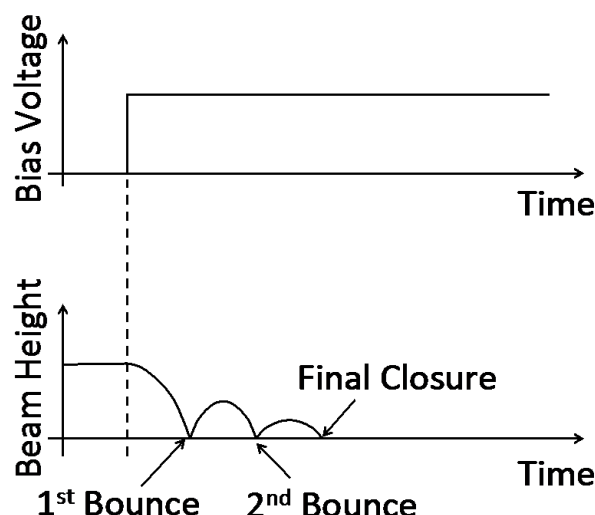


Figure 4.1: Beam height versus time for a step bias voltage, generating multiple bounces before final contact closure.

For a structure with symmetrical contacts and anchors, the mechanical deformation follows a simple flexural mode and when the contacts are touching the substrate, the kinetic energy is reflected mostly in this single flexion mode.

By breaking the symmetry of a MEMS structure with respect to the contact points, the kinetic energy of closure is spread into higher order mechanical modes instead of the first one, and their vibrations are less prone to re-opening the contacts.

The principle is illustrated in figure 4.2, on a basic RF-MEMS switch. The first one contacting is subjected to a lower stiffness due to the design and will contact first. The second one will close after attenuating the shock of the first contact during its flight. In these conditions, bounces will be extremely reduced.

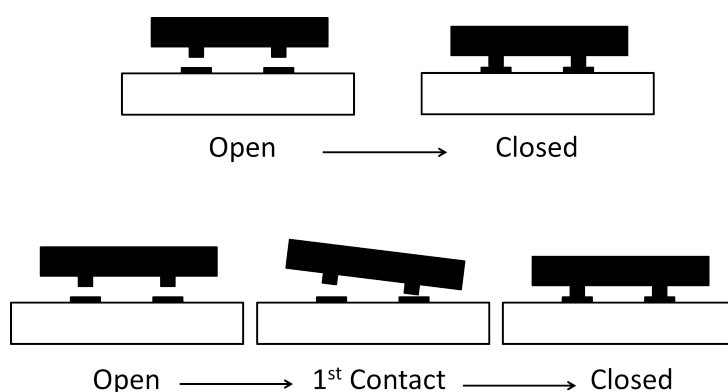
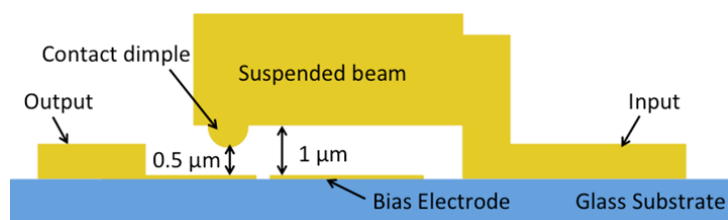


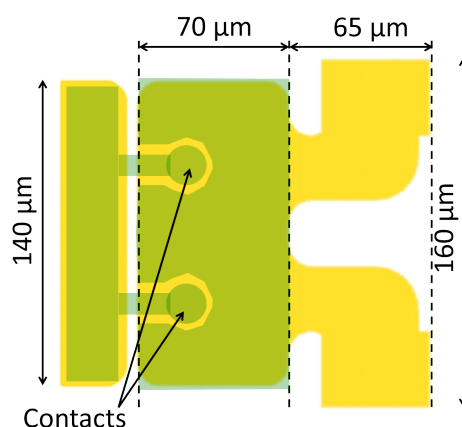
Figure 4.2: Front view of a symmetrical device contact closure (top) and asymmetrical device (bottom).

4.1.2 Design

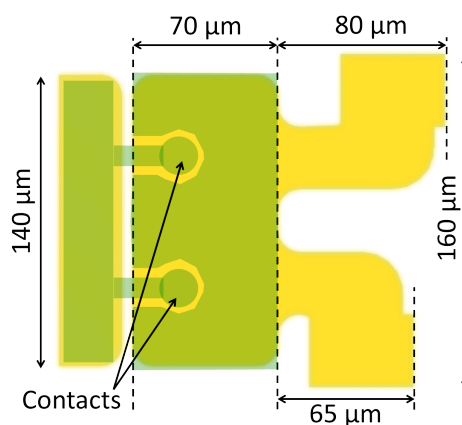
For demonstration purpose, a simple symmetric switch and its asymmetric version have been designed and fabricated on high resistive silicon. These designs, as shown in figure 4.3 are very similar to many RF-MEMS switches, and both versions have been fabricated on the same wafer, using the same fabrication process. The mechanical part is made of a thick electroplated metal cantilever (yellow) suspended above a bottom metal (green) acting as bias pad in one hand and contact line on the other hand.



Cross section of a simple switch.



Layout of the symmetric switch.



Layout of the asymmetric switch.

Figure 4.3: Design of switches.

Both switches have orthogonal anchors to prevent mechanical stress gradient to develop in the structure. The symmetry is simply broken by changing the length of one suspension

arm as shown in figure 4.3. The devices have pull-in voltages that are slightly different, between 85 and 90 Volts for the asymmetric version and between 95 and 100 Volts for the symmetric version. The symmetric version of the switch is slightly shorter.

4.1.3 Measurements

4.1.3.1 S-parameters

The measured S-parameters are given in the following figures. In up state, the switches reach 25dB of isolation at 5GHz (figure 4.4) and in down state, the insertion losses (figure 4.5) are less than 0.2dB at low frequencies. The rise in losses with frequency is attributed to a leakage of RF signal in the bias pad.

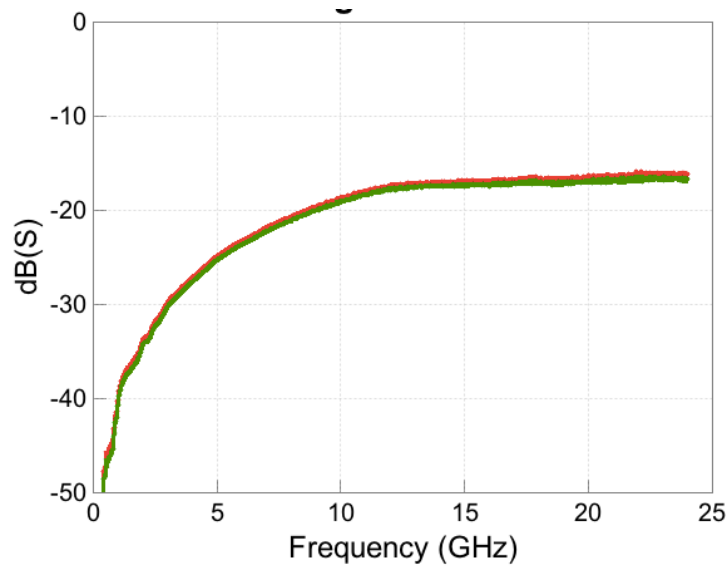


Figure 4.4: Isolation of the two switches with 100V bias voltage applied.

4.1.3.2 Dynamic behaviour

The switches are cycled using a 100Hz square bias signal, with variable amplitude. The input-to-output voltage is 200mV, the test bench is sketched in figure 4.6. The devices are tested in open laboratory environment, at atmospheric pressure.

The results of both switches are presented in figure 4.7, where the black line represents the bias voltage. Few microseconds after, the switch goes in down state having multiple bouncing in the case of symmetric switch. It finally closes after 4 bounces. The response time is approximately 40 μ s, 25 μ s and 20 μ s for respectively $1.05 * V_p$, $1.1 * V_p$ and $1.15 * V_p$, with V_p the pull-down voltage, meaning that larger the bias voltage is and faster the switch closes. It has already been demonstrated before [58] and a confirmation

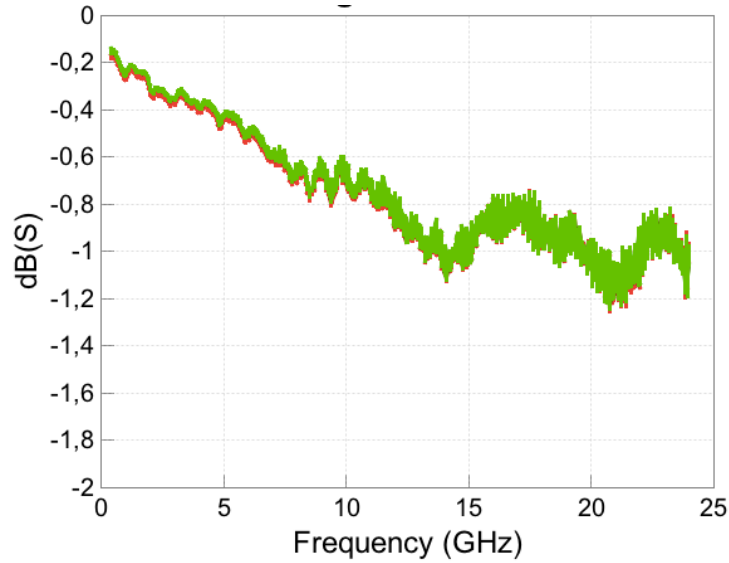


Figure 4.5: Insertion losses of the two switches with 100V bias voltage applied.

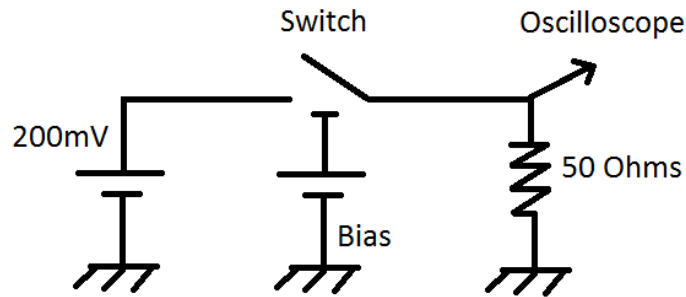


Figure 4.6: Test bench for the dynamic behaviour of the switch.

is done here.

Regarding the asymmetric switch, no bouncing is observed after actuation and the closing in down state. Moreover, one can notice that the switching time is shorter compared to symmetric switch. We may say that the switch closes faster due to asymmetrical flexion of the beam and resulting in a lower spring constant in one side of the beam. Indeed one contact touches the wafer before the other, and this contact is the one on the same side as the longest arm.

4.1.4 Conclusion

The use of asymmetrical structures for RF-MEMS switches allows suppression of bounces during contact closure. The proposed idea has been validated through measurements on a very simple design, with large contact forces.

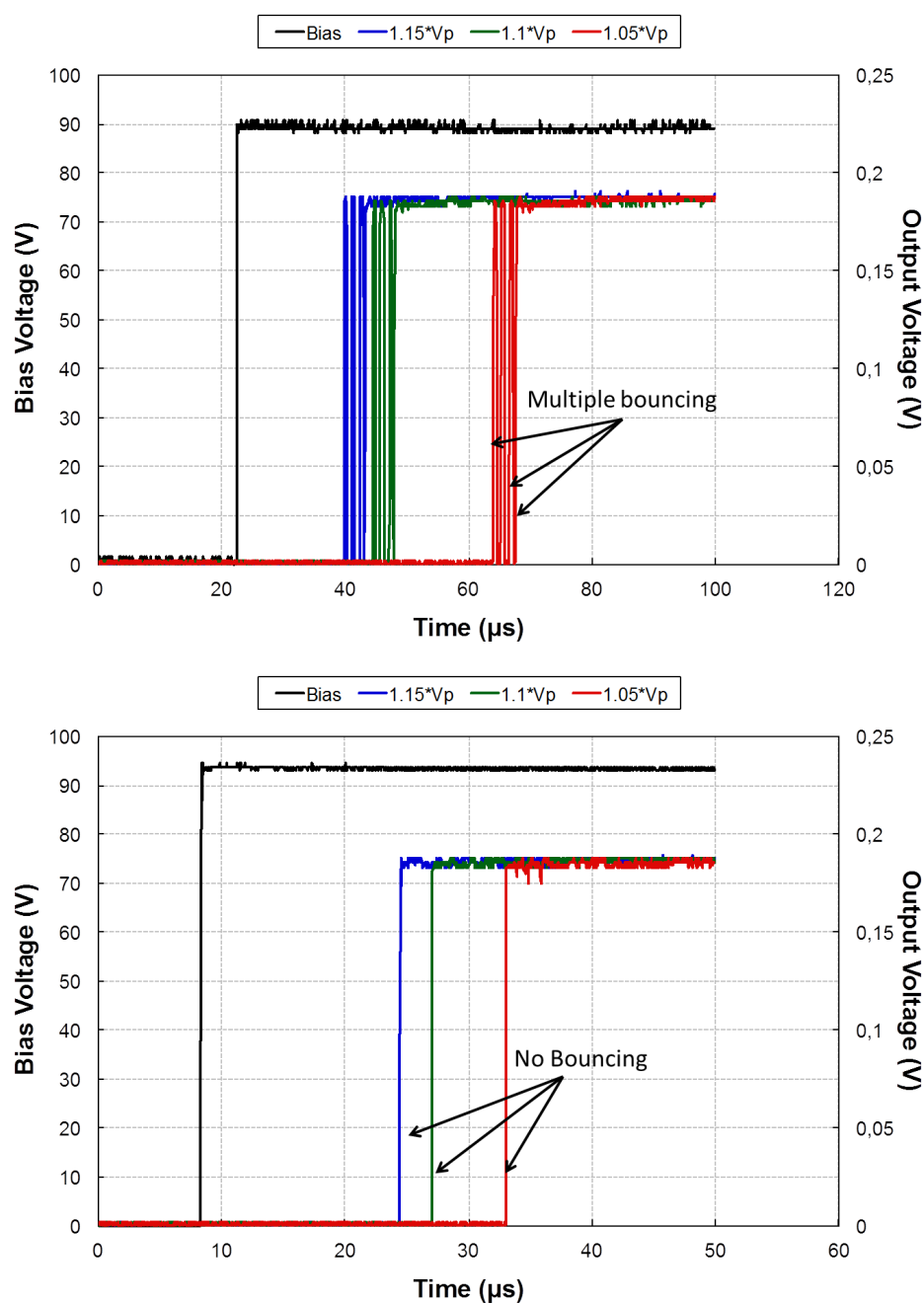


Figure 4.7: Measured responses for various bias voltages of the symmetric (top) and asymmetric (bottom) switches.

This approach can be applied to many other RF-MEMS designs to improve their dynamic behaviour. Future works will include advanced analysis of mechanical aspects of the switch.

4.2 Recommendations for improving reliability of RF-MEMS switches

With the contribution of previous works and those conducted here, some important points are marked down so as to help the next workers on this topic.

Design rules

- **High contact force**

A high contact force is required to achieve a low contact resistance. The contact surface is proportional to the applied force so a large contact force will result in a large contact area and a low contact resistance.

But, under large contact force, the contact metals have to remain in the same shape. It means that the metal contact must be harder than conductive. Typically Ruthenium which is hard, showed excellent performances in micro-switches compared to gold that is more soft. Under large contact force, the gold metal contacts tend to deform and result in a changing of contact area and thus contact resistance. But the contact force is related with bias voltage and a too large bias voltage is hard to implement in systems requiring low voltages.

- **High restoring force**

A high restoring force is necessary to avoid stiction of contacts which is a main failure mechanism. For that, the suspended structure should be preferably a monocrystalline structure, which can provide a good restoring force and avoid creep phenomenon at the same time. The monocrystalline structures is quasi free from defects, having a larger Young's modulus.

The anchors have a strong influence on the restoring force and there is a optimum number to find, not to increase too much the bias voltage. In any case, the anchors have to be built orthogonally to the suspended structure to release eventual stress resulting from the layers stack of fabrication process.

The two main shapes of suspended structure are divided in two categories, cantilevers and membranes. In testings presented in the thesis, the membrane-type structures showed a better reliability compared to cantilever, likely due to a larger surface that allows to spread stress nodes. So more the anchors are numerous and equally spread and better is the restoring force, and the reliability.

- **Contact area**

Regarding the region of the contact, it appeared that the switches which do not cross the instability point located at $\frac{1}{3}$ of the gap, have obviously a higher release voltage V_r than the others. It involves an hysteresis very tight because V_r is very close to the pull-down voltage V_p . Thus the reliability is greatly improved because if V_r starts to decrease because of the creep for example it will last longer than the switches which cross the instability point. This design rule also helps to fight against adhesive phenomena. Unfortunately C_{off} would be also affected like in the previous point.

Moreover, the switching time has to be as short as possible in order to limit the transient phenomena that are so destructive in hot switching. It can be done by shortening the travel distance of contact metal but the off-capacitance C_{off} will be degraded so a compromise has to be done.

The bounces have to be mitigated, because opening and closing three or four times during one actuation means that the switch lifetime will be reduced by a factor three or four. Each time the switch closes and opens, transient phenomena occur and wear the contact. To mitigate bounces, an high contact force helps as well as not crossing the instability point at $\frac{1}{3}$ of the electrostatic gap. Moreover, asymmetrical structures have shown independence on bounces.

Regarding the bottom electrode of the contact area (located on the substrate), it must be as thick as possible. Indeed, the top electrode will impact on the bottom one as many times as a switching is required. Purely mechanically, the bottom electrode will wear faster than the top one, like a nail that one hammers into wood. Combining impacts with current and temperature lead to faster wear of bottom electrode. Thus the solution is to make the bottom electrode thick, up to a certain limit, because the fabrication process may be affected to take this change in consideration.

- **Avoiding dielectric layers**

It is strongly recommended not to use dielectric layers or with carefully pay attention on risked areas. The risked areas are located where the electric field is focused. Usually the field is concentrated between bias pad and RF-lines. A risk of dielectric breakdown is present. The bias line has to be highly resistive to prevent leakage from RF signal to DC.

Repeatability in measurements

The reliability of RF-MEMS can be achieved only if a complete, accurate, methodical procedure is developed. Each step of the procedure has to be followed carefully, using every time the same equipment, same components.

None measurement equipment is ideal, involving imprecisions of measurement, thus constant repetition is a way to mitigate bad random events. Each equipment has to be completely known, its specifications, performances and limits.

The room conditions have demonstrated an influence in equipment and testing. So far, light, temperature and humidity have influenced our testings. If the lab does not allow to control these parameters, at least they have to be monitored.

Avoiding unique testing on single component

None testing shall be performed with one single component. It is not representative. The concept of micro-switches has already been demonstrated, it is important now to demonstrate the reliability of fabrication process and the ability to provide identical components.

Once a batch of components is available, after proper measurements, conclusions can be given.

Packaging required

It is mandatory to provide a packaging as hermetic as possible to avoid many failure mechanisms occurring because of ambient atmosphere. A temporary solution may be to conduct testing in a vacuum probe station like it was done in the thesis. But for long term analysis and industrialization, packaging remains unavoidable.

Related with space, packaging has to handle space environment, especially radiation effects and temperature. Wafer-on-wafer packaging has shown great performances on earth and will be a suitable candidate for space.

Acceleration factors

Acceleration factors are the keys parameters in reliability, they allow to predict lifetime of components. In the thesis, temperature, input-to-output voltage and bias voltage were identified as the stress factors that foster the failure of switches. The acceleration factors are easy to find using Weibull distribution, comparing scale parameter α for quite constant β .

- **Temperature**

Any mechanical structure is affected by temperature. Depending on the thermal expansion coefficient, some materials will not handle temperature constraint required in electronics or space applications. A rise in temperature is an acceleration factor as presented in chapter 2. All the materials involved in movement of the switch have to be monocrystalline (considering creep matters) with an high melting point (considering temperature matters).

- **Input-to-output voltage**

Since the thesis, the input-to-output voltage has become an acceleration factor for failure mechanisms of RF-MEMS. The input-to-output voltage is directly proportional to the contact voltage where transient phenomena occur. More the contact voltage is and more the temperature rises, leading locally in melting, dramatic for the contact materials.

The stress can be applied by high RF-power. The ageing will be accelerated as power increases. For the same reasons, the current increases, the temperature as well leading in super-temperature in the area of contact. Contact metals must be harder than conductive, for example by experiment, Ruthenium showed better results compared to gold.

- **Bias voltage**

The bias voltage is an acceleration factor for ageing RF-MEMS as seen in this chapter and in chapter 2. Switches have demonstrated a better reliability when the bias voltage is higher than the pull-down voltage. A large bias voltage implies a large contact force, then a large contact surface, leading in low contact resistance. If the contact resistance is small enough, there is not much dissipation of energy, which means a lower temperature in the contact zone and finally a better reliability.

To achieve an efficient estimation of acceleration factors, a mature fabrication process is required and must be repeated many times. The fabrication yield must be above 75% on each wafer. Finally a numerous quantity of switches are required, a Weibull distribution must be estimated with 50 switches at least.

- **Duty cycle**

For such structures as micro-mirrors, worth case ageing testing is usually conducted to study the reliability of video beamers. The worth case is biasing micro-mirrors 95% of the time at the maximum temperature. This allows to wear micro-mirrors very fast getting acceleration factors.

For micro-switches, it appeared that the duty cycle of bias voltage has an influence on the lifetime of switches. Usually, switching testings are operated at 50% duty cycle. It has been observed that during all testing campaigns, a larger duty cycle (above 50%) fosters reliability of RF micro-switches. Conversely, a duty cycle below 50% shortens lifetime of switches. Finally, an acceleration factor could be found in switching testing duty cycle.

Contact contamination

Contact contaminations occur in ambient room if the switch is not packaged. In ambient atmosphere, it is tough to control all the variables and extract relevant acceleration factor. Most of the time, the contamination due to ambient air is not predictable coming from random effects.

The package is still mandatory. But, depending on materials of the fabrication process, the switch can pollute itself. Because of operation, thin particles may move from one side to another and end in the contact area. Accumulating undesired particles may create a thin layer that prevents the optimum contact between ohmic electrodes.

To conclude, either the contact remains clean and the normal operation of the switch can be achieved. Or, the contact is dirtier and a larger contact force is needed to drill through parasitic thin layer.

Failure mechanisms

The failure mechanisms encountered during testing were the break of bias line, stiction and open circuit.

The bias line used to break when the bias voltage was large and the thickness of metal layer very thin. A bad fabrication process release or contamination may result in a short circuit between bias line and RF lines allowing the current through the circuit. The bias line then evaporates because of its low thickness and the circuit remains open in the end.

The stiction is almost predictable since the release voltage decreases before ending in stiction of the switch. The problem has been partly solved designing robust micro-switches with large restoring force.

The switch may end in open circuit if the first metallization is not thick enough. In the ohmic contact area, where the top electrode goes down to the bottom electrode, an impact is left on the bottom side. After numerous impact, the material is removed and a hole will remain instead. This ends in an increase of contact resistance until no material remains, leading in open circuit.

4.3 Three recommended testings for reliability assessment of RF-MEMS

Three testing methods are presented to conduct reliability assessment of RF-MEMS. Through these testing, the global behaviour of ohmic contact RF-MEMS switches will be assessed. It has to be mentioned that the operator must know and control at any time the current passing through the switch in order to avoid transient effects coming from generators.

Held in down state, assessing mechanical behaviour

The test set up presented here deals with the assessment of mechanical behaviour of the switch, i.e. the suspended structure as well as contacts deformation. The idea is to

put the switch in down state using 95% duty cycle for example, and heat it. Relevant temperatures for this kind of test would be 80°C and above. Every cycle, the pull-down and release voltages are recorded for positive and negative range. The following figures 4.8 give examples of curves obtained for switches that pass or not.

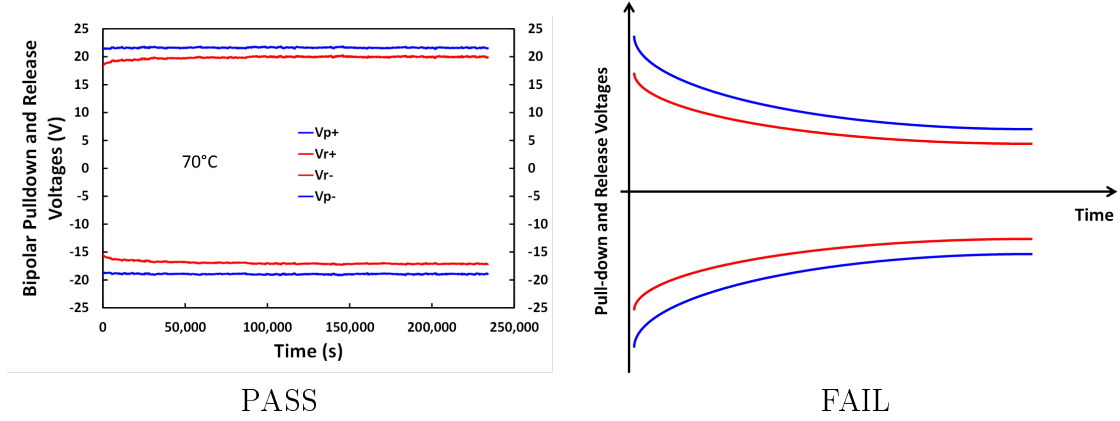


Figure 4.8: Example of curves for switches assessing the mechanical behaviour.

Another version is possible taking into account the innovative test bench developed in chapter 2, partially biasing the switch. The idea is to bias the switch close the pull-down voltage, typically 80% V_p as it was done previously, and monitor the movement of the beam. Examples are given in figure 4.9.

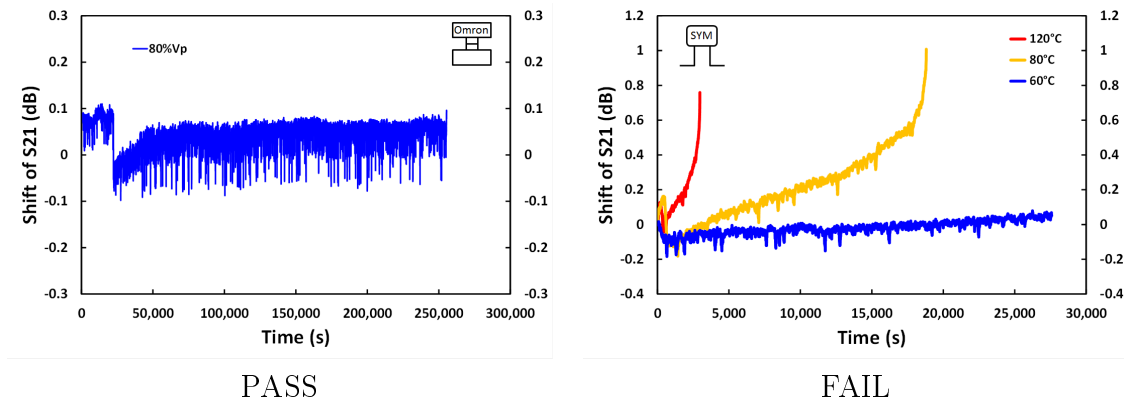


Figure 4.9: Example of curves for which the switches are partially biased and transmission parameter is monitored to know if the switch pulls in down state or not.

Assessing contacts contamination in packaged switch

The idea of this test set up is to check contacts contamination during operation. This is convenient to assess a packaged switch and to check if the packaging is hermetic. The testing will take place in room environment. Low signals are required, an RF-signal (typically 0dBm) or low DC input-to-output voltage (typically 50mV or less). The duty

cycle would be 50% with a switching rate about 1kHz or more. The monitoring of the contact resistance will allow to know if the contact degrades over time and cycles. In figure 4.10 two examples are given to get an idea of what can happen during operation.

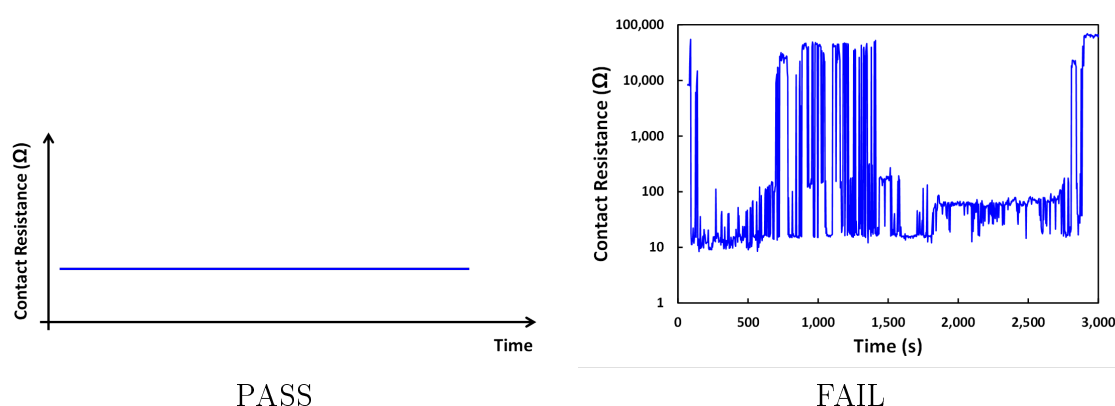


Figure 4.10: Example of curves for which the switches that are subjected to contamination. In the left case the contact resistance does not change over time, in the right case the contact resistance varies a lot meaning that contamination occurs and species are introduced in the contact.

Servo controlling the bias voltage monitoring the contact resistance

The idea is to reproduce the testing presented in section 2.4 page 62 where the contact resistance is monitored servo controlling the bias voltage. This testing will assess mechanical creep occurring in the switch. Despite the fact that mechanical creep is a slow phenomenon, the bench allows to get a quick response. The requirements for this bench regard an accurate acquisition of the contact resistance (typically $< 0.1\Omega$) and a fine control of bias voltage (typically $< 10\text{mV}$). Coupling higher temperature will allow to get quicker results extracting activation energy. Knowing the activation energy allows to quantify the dependence of the structural material on temperature. Example of curves are presented in figure 4.11.

Considering all switches tested during the thesis, the only one that passed all of these testings without showing any failure is the Omron MEMS switch. The design and materials used in this switch provide one of the best answer for reliability of RF-MEMS.

4.4 Conclusion

The aim of this chapter was to give guidelines for reliability of RF-MEMS. An asymmetrical design was presented to prevent bounces in micro-switches. Several advices have

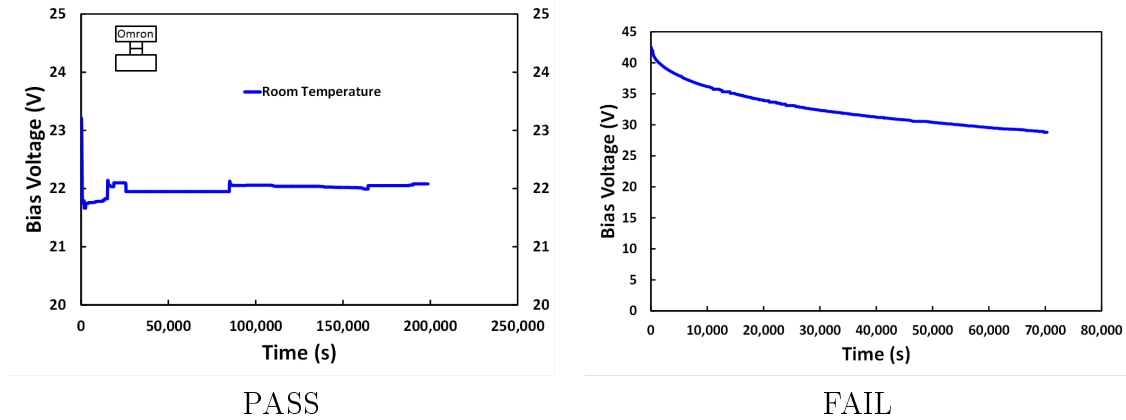


Figure 4.11: Example of curves for which the switches shows sensitivity to mechanical creep or not. The technique used is the monitoring of contact resistance servo controlling the bias voltage.

been exposed, regarding design, testing, fabrication, packaging and extraction of physical parameters. The last section is dedicated in presenting three test benches that allow to get a global behaviour of the switch.

General Conclusion

The objective of this work was to study the reliability of RF-MEMS switches which are potentially better candidates than the current technology in telecommunication satellites and radio-frequency mobile applications. From the measurements of failure mechanisms it has been pointed out that certain fabrication processes reveal a better reliability. In particular, micro-cantilevers with a monocrystalline structure have demonstrated a very low sensitivity to creep. Moreover it was found that the lifetime of the switches are strongly dependent on the operating conditions.

A better understanding of the phenomena involved in the reliability of RF-MEMS switches has been exposed and promising candidates can be selected quickly after few measurements. Especially the Omron RF-MEMS switches have demonstrated a great reliability.

In the first chapter, the MEMS technology and the MEMS for Radio-Frequencies, the RF-MEMS, were introduced. The pros and cons of these components have been detailed and the failure mechanisms were exposed. The more dramatic failure mechanisms have been pointed out and it has been proposed to focus on it. Some of them were already studied and the others were not. The study focused on mechanical creep phenomenon and methodologies to assess the reliability of ohmic contact RF-MEMS switches.

The second chapter was devoted to the study of creep failure mechanism in several switches. After exposing the theory of creep, two innovative test benches were presented to assessment mechanical creep. The first test bench assess mechanical creep by observing the evolution of the transmission parameter over time for a switch partially biased. The results demonstrated the influence of creep on switches, however the accuracy of the results were not so good, thus the second test bench was introduced. The second test bench is an original way to assess creep, in fact the switch is pulled in down state and by monitoring the contact resistance, the bias voltage is modified by servo controlling. The results showed the same trend as the first technique with more accuracy. The Omron switch that gets a monocrystalline suspended beam demonstrated a great insensitivity to creep at this stage compared to the switches fabricated in our lab.

In perspectives, these measurement capabilities can be extended on more different switches with a systematic extraction of the activation energy. On the other hand it would be interesting to develop a mathematical model that will predict the time when the switch will not be able to pull up in up state after being too long in down state and failing because of creep.

In the third chapter, the basics on the theory of the reliability are reminded, introducing the Weibull's distribution. Then, cycling testings on many switches under several

operating conditions were conducted and the results were plotted extracting the Weibull parameters for each condition. The results showed a great influence of the bias voltage and the input-to-output voltage on the lifetime of switches allowing to perform accelerated testing. On the other hand a parallel test bench was developed with a fast acquisition procedure permitting to get more results in one frame.

The combination of both test benches will be a promising perspective as long as the preparation of the samples can be improve. It would also be interesting to extract a mathematical model from the lifetime achieved by the switches depending on the operating parameters. In this case a high number of switches are required as well as a high number of testing to get as many data as possible and to improve the accuracy of the model that would be based on experimental results.

In the fourth chapter was presented a innovative design for suppression of bounces in RF-MEMS switches. Then, recommended rules were given to improve reliability of RF-MEMS. Finally, three test benches were presented so as to conduct full experiment on switches and extract all of their parameters.

In a final conclusion, the packaging of RF-MEMS switches has not been broached but only mentioned. Obviously it is utmost importance to guarantee a high efficiency of the components working on the "Earth" e.g. mobile applications under environmental conditions and this shall be achieved with an efficient hermetic package. But in space, the components even non-packaged will not suffer from atmospheric disturbance. So the cost of each component would be reduced since the packaging is really expensive and takes a big part in the total price of the switch.

What proves the high reliability of the switches developed at Xlim is the successful launched mission in the Athena Fidus satellite in the frame of the MEMO project by the beginning of the year 2014, where the switches were loaded on a reliability testing board to operate missions in real conditions. At the time when the thesis is written, our switches are operating in nominal conditions.

Annex A

Arduino code to get an accurate voltage value to send to Labview

```
float Rc = 0.0;
float Vc = 0.0;
long int digitVc1 = 0;
long int digitVc2 = 0;
void setup() {
    Serial.begin(9600);
    analogReference(EXTERNAL);
    delay(500);
}
void loop()
{
    digitVc1 = 0;

    for(int i=0; i<1024; i++)
    {
        digitVc1 = digitVc1 + analogRead(4) + 4;
        //Serial.println(digitVc);
    }
    digitVc1 = digitVc1 >> 5;
    //Vc = digitVc * (3.31 / 32767.0);
    //Rc = (0.2 - Vc) / (Vc / 50.0);
    //Serial.println(Vc);
    //digitVc = 10;
    //digitVc2 = 32768;
    Serial.write(digitVc1>>8);
    Serial.write(digitVc1);
    //Serial.write(digitVc2>>8);
    //Serial.write(digitVc2);
    //Serial.println();
    //Serial.print("\t");
    delay(100);
}
```

Annex B

Arduino code to count switching of switches

```
int digitaloutV = 0;
float analogoutV = 0.0;
float limupstate = 0.5;
float limdownstate = 0.2;
int polar = 52;
long timezero = 0;
long interval = 500;
int compteur[16] = {0};
int verif[16] = {0};

void setup() {
  Serial.begin(9600);
  pinMode(polar, OUTPUT);
  delay(3000);
}

void loop() {
  unsigned long timezero = millis();

  for(int i=0 ; i<16 ; i=i+1)
  {
    digitaloutV = analogRead(i);
    analogoutV = digitaloutV * (5.0 / 1023.0);
    if(analogoutV < limupstate && verif[i] == 0)
    {
      compteur[i]=compteur[i]+1;
    }
    else if(analogoutV > limupstate && verif[i] == 0)
    {
      int x = compteur[i]/2;
      Serial.print("Voie "); Serial.println(i);
      Serial.print(x);Serial.println(" commutations");
      verif[i] = 1;
    }
  }

  digitalWrite(polar, HIGH);
  unsigned long timeuno = millis();
```

```
        delay(1);

for(int i=0 ; i<16 ; i=i+1)
{
    digitaloutV = analogRead(i);
    analogoutV = digitaloutV * (5.0 / 1023.0);
    if(analogoutV > limdownstate && verif[i] == 0)
    {
        compteur[i]=compteur[i]+1;
    }
    else if(analogoutV < limdownstate && verif[i] == 0)
    {
        int y = compteur[i]/2;
        Serial.print("Voie "); Serial.println(i);
        Serial.print(y); Serial.println(" commutations");
        verif[i] = 1;
    }
}

    digitalWrite(polar,LOW);

while(timeuno-timezero<interval)
{
    delay(10);
    timeuno=millis();
}
}
```


Bibliography

- [1] H. Nathanson, W. Newell, R. Wickstrom, and J. Davis, "The Resonant Gate Transistor," *IEEE Transactions on Electron Devices*, vol. 14, no. 3, pp. 117–133, Mar. 1967. [Online]. Available: <http://ieeexplore.ieee.org/lpdocs/epic03/wrapper.htm?arnumber=1474635>
- [2] L. Robin, "MEMS for Mobile MEMS for Cell Phones and Tablets report," Yole Développement, Tech. Rep., June 2013.
- [3] J. Ruan, N. Nolhier, M. Baffleur, L. Bary, F. Coccetti, T. Lisec, and R. Plana, "Electrostatic discharge failure analysis of capacitive RF MEMS switches," *Microelectronics Reliability*, vol. 47, no. 9-11, pp. 1818–1822, Sep. 2007. [Online]. Available: <http://www.sciencedirect.com/science/article/pii/S0026271407003149>
- [4] D. Mardivirin, "Étude des mécanismes mis en jeu dans la fiabilité des micro-commutateurs MEMS-RF," Ph.D. dissertation, Université de Limoges, 2010. [Online]. Available: <http://www.theses.fr/2010LIMO4054/document>
- [5] M. Vincent, "Étude des mécanismes de défaillance du contact électrique dans un micro-interrupteur en technologie MEMS," Ph.D. dissertation, Université de Grenoble, 2010. [Online]. Available: http://tel.archives-ouvertes.fr/docs/00/53/58/11/PDF/These_Maxime_Vincent.pdf
- [6] A. Hartzell, M. da Silva, and H. Shea, *MEMS Reliability*, ser. MEMS Reference Shelf. Springer, 2010. [Online]. Available: <http://books.google.nl/books?id=AcIT5zE-BG4C>
- [7] J. Maciel, S. Majumder, J. Lampen, and C. Guthy, "Rugged and Reliable Ohmic MEMS Switches," in *2012 IEEE/MTT-S International Microwave Symposium Digest*. IEEE, Jun. 2012, pp. 1–3. [Online]. Available: <http://ieeexplore.ieee.org/lpdocs/epic03/wrapper.htm?arnumber=6258368>
- [8] D. A. Czaplewski, C. D. Nordquist, G. A. Patrizi, G. M. Kraus, and W. D. Cowan, "RF MEMS Switches With RuO₂-Au Contacts Cycled to 10 Billion Cycles," *Journal of Microelectromechanical Systems*, vol. 22, no. 3, pp. 655–661, Jun. 2013. [Online]. Available: <http://ieeexplore.ieee.org/lpdocs/epic03/wrapper.htm?arnumber=6425388>
- [9] J. Hwang and C. Goldsmith, "Robust RF MEMS switches and phase shifters for aerospace applications," in *2009 IEEE International Symposium on Radio-Frequency Integration Technology (RFIT)*. IEEE, Dec. 2009, pp. 245–248. [Online]. Available: <http://ieeexplore.ieee.org/lpdocs/epic03/wrapper.htm?arnumber=5383688>

- [10] T. Yamagiwa, H. Yamada, F. Endo, Y. Ohshita, S. Izumi, and I. Yamada, "Development of preventive maintenance system for highly reliable gas insulated switchgear," *IEEE Transactions on Power Delivery*, vol. 6, no. 2, pp. 840–848, Apr. 1991. [Online]. Available: <http://ieeexplore.ieee.org/lpdocs/epic03/wrapper.htm?arnumber=131143>
- [11] L. Marchand, "Micro & Nano Technologies at the European Space Agency," in *JAXA Micro-Electronics WorkShop, MEWS 19th*, October 2006. [Online]. Available: <https://eepitnl.tksc.jaxa.jp/mews/jp/19th/text/107.pdf>
- [12] P. Bacon, D. Fischer, and R. Lourens, "Overview of RF Switch Technology and Applications," *Microwave Journal*, vol. 57, no. 7, pp. 76–88, July 2014.
- [13] Y. Komura, M. Sakata, T. Seki, K. Kobayashi, K. Sano, S. Horiike, and K. Ozawa, "Micro Machined Relay for High Frequency Application," in *PROCEEDINGS OF THE RELAY CONFERENCE-NATIONAL ASSOCIATION OF RELAY MANUFACTURERS*, vol. 47, 1999, pp. 12–12.
- [14] D. A. Goins, R. D. Nelson, and J. S. McKillop, "Design of a 20 GHz Low Loss Ohmic Contact RF MEMS Switch," in *Microwave Symposium, 2007. IEEE/MTT-S International*. IEEE, 2007, pp. 371–374.
- [15] K. Segueni, L. Le Garrec, A. S. Rollier, R. Robin, S. Touati, A. Kanciurzewski, L. Buchaillet, and O. Millet, "Totally free-flexible Membrane for Low Voltage MEMS Metal Contact Switch," in *Microwave Integrated Circuit Conference, 2007. EuMIC 2007. European*, Oct 2007, pp. 355–358.
- [16] J. Bouchaud. (2012, January) IHS iSuppli Teardown Analysis Service Identifies First Use of RF MEMS Part, Set to be Next Big Thing in Cellphone Radios. [Online]. Available: <https://technology.ihs.com/389456/ihs-isuppli-teardown-analysis-service-identifies-first-use-of-rf-mems-part-set-to-be-next-big-thing-in-cellphone-radios>.
- [17] Z. Yang, C. Lichtenwalner, A. Morris, S. Menzel, C. Nauenheim, A. Gruverman, J. Krim, and A. Kingon, "A new test facility for efficient evaluation of mems contact materials," *Journal of Micromechanics and Microengineering*, vol. 17, no. 9, p. 1788, 2007. [Online]. Available: <http://stacks.iop.org/0960-1317/17/i=9/a=006>
- [18] Z. Yao, S. Chen, S. Eshelman, D. Denniston, and C. Goldsmith, "Micromachined Low-Loss Microwave Switches," *Microelectromechanical Systems, Journal of*, vol. 8, no. 2, pp. 129–134, Jun 1999.
- [19] C. O'Mahony. (2014) RF MEMS Capacitive Switch. [Online]. Available: <http://www.tyndall.ie/content/rf-mems-capacitive-switch>

- [20] V. Joshi, C. Khieu, C. G. Smith, C. Schepens, F. Csaszar, D. Lacey, T. Nagata, M. Renault, R. Van Kampen, R. Knipe, and D. Yost, "A CMOS Compatible Back End MEMS Switch for Logic Functions," *2010 IEEE International Interconnect Technology Conference*, pp. 1–3, Jun. 2010. [Online]. Available: <http://ieeexplore.ieee.org/lpdocs/epic03/wrapper.htm?arnumber=5510694>
- [21] W. Merlijn van Spengen, "MEMS reliability from a failure mechanisms perspective," *Microelectronics Reliability*, vol. 43, no. 7, pp. 1049–1060, Jul. 2003. [Online]. Available: <http://linkinghub.elsevier.com/retrieve/pii/S0026271403001197>
- [22] D. Mardivirin, A. Pothie, M. El Khatib, A. Crunteanu, O. Vendier, and P. Blondy, "Reliability of Dielectric Less Electrostatic Actuators in RF-MEMS Ohmic Switches," in *Microwave Integrated Circuit Conference, 2008. EuMIC 2008. European*, Oct 2008, pp. 490–493.
- [23] A. Broue, T. Fourcade, J. Dhennin, F. Courtade, P. Charvet, P. Pons, X. Lafontan, and R. Plana, "Validation of bending tests by nanoindentation for micro-contact analysis of MEMS switches," *Journal of Micromechanics and Microengineering*, vol. 20, no. 8, p. 085025, Aug. 2010. [Online]. Available: <http://stacks.iop.org/0960-1317/20/i=8/a=085025?key=crossref.cbec3adb6bcae863a141d04aa10202cc>
- [24] M. Cohn, R. Roehnel, J.-H. Xu, A. Shteinberg, and S. Cheung, "MEMS packaging on a budget (fiscal and thermal)," in *Electronics, Circuits and Systems, 2002. 9th International Conference on*, vol. 1, 2002, pp. 287–290 vol.1.
- [25] M. Douglass, "Lifetime Estimates and Unique Failure Mechanisms of the Digital Micromirror Device (DMD)," in *Reliability Physics Symposium Proceedings, 1998. 36th Annual. 1998 IEEE International*, March 1998, pp. 9–16.
- [26] R. W. Hertzberg, *Deformation and Fracture Mechanics of Engineering Materials*. Wiley, 1996, vol. 89.
- [27] CMU Defects Lab. (1999) Polygonisation experiment. [Online]. Available: http://neon.materials.cmu.edu/rohrer/defects_lab/polygoniz_bg.html
- [28] T. Courtney, *Mechanical Behavior of Materials: Second Edition*. Waveland Press, 2005. [Online]. Available: <http://books.google.nl/books?id=QcYSAAAAQBAJ>
- [29] M. F. Ashby, "On interface-reaction control of nabarro-herring creep and sintering," *Scripta Metallurgica*, vol. 3, no. 11, pp. 837 – 842, 1969. [Online]. Available: <http://www.sciencedirect.com/science/article/pii/0036974869901914>

- [30] G. Janssen, M. Abdalla, F. van Keulen, B. Pujada, and B. van Venrooy, "Celebrating the 100th anniversary of the Stoney equation for film stress: Developments from polycrystalline steel strips to single crystal silicon wafers," *Thin Solid Films*, vol. 517, no. 6, pp. 1858–1867, Jan. 2009. [Online]. Available: <http://www.sciencedirect.com/science/article/pii/S0040609008007669>
- [31] A. Broue, J. Dhennin, P. Charvet, P. Pons, N. Jemaa, P. Heeb, F. Coccetti, and R. Plana, "Multi-physical characterization of micro-contact materials for mems switches," in *Electrical Contacts (HOLM), 2010 Proceedings of the 56th IEEE Holm Conference on*, Oct 2010, pp. 1–10.
- [32] M. van Gils, J. Bielen, and G. McDonald, "Evaluation of Creep in RF MEMS Devices," in *2007 International Conference on Thermal, Mechanical and Multi-Physics Simulation Experiments in Microelectronics and Micro-Systems. EuroSime 2007*. IEEE, 2007, pp. 1–6. [Online]. Available: <http://ieeexplore.ieee.org/lpdocs/epic03/wrapper.htm?arnumber=4201200>
- [33] D. Mardivirin, S. Courreges, A. Crunteanu, A. Pothier, P. Blondy, F. Coccetti, and R. Plana, "Evidence of successive Fowler-Nordheim and Frenkel-Poole conductions in Si₃N₄ based RF-MEMS capacitive switches," in *Microwave Conference (EuMC), 2010 European*, Sept 2010, pp. 513–516.
- [34] Z. Peng, X. Yuan, J. Hwang, D. Forehand, and C. Goldsmith, "Dielectric Charging of RF MEMS Capacitive Switches under Bipolar Control-Voltage Waveforms," in *Microwave Symposium, 2007. IEEE/MTT-S International*, June 2007, pp. 1817–1820.
- [35] R. Modlinski, A. Witvrouw, and P. Ratchev, "Creep as a reliability problem in MEMS," *Microelectronics Reliability*, vol. 44, no. 9-11, pp. 1733–1738, Sep. 2004. [Online]. Available: <http://linkinghub.elsevier.com/retrieve/pii/S0026271404003117>
- [36] R. Modlinski, P. Ratchev, A. Witvrouw, R. Puers, and I. D. Wolf, "Creep-resistant aluminum alloys for use in MEMS," *Journal of Micromechanics and Microengineering*, vol. 15, no. 7, pp. S165–S170, Jul. 2005. [Online]. Available: <http://stacks.iop.org/0960-1317/15/i=7/a=023?key=crossref.362ee8ef49a0caa6c95356142f1cf20b>
- [37] C. Goldsmith, J. Ehmke, A. Malczewski, B. Pillans, S. Eshelman, Z. Yao, J. Brank, and M. Eberly, "Lifetime characterization of capacitive RF MEMS switches," in *2001 IEEE MTT-S International Microwave Symposium Digest (Cat. No.01CH37157)*, vol. 1. IEEE, 2001, pp. 227–230. [Online]. Available: <http://ieeexplore.ieee.org/lpdocs/epic03/wrapper.htm?arnumber=966876>

- [38] F. Barriere, A. Pothier, A. Crunteanu, M. Chatras, and P. Blondy, “A Zero-Level Packaged RF-MEMS Switch with Large Contact Force,” in *Microwave Conference (EuMC), 2011 41st European*, Oct 2011, pp. 1229–1232.
- [39] Omron Electronic Components. (2013) RF MEMS Switch: What You Need to Know. [Online]. Available: http://www.ttiinc.com/docs/IO/22190/2SMES-01_RFMEMSSwitch_Whitepaper.pdf
- [40] D. François, A. Pineau, and A. Zaoui, *Mechanical Behaviour of Materials: Volume 1: Micro- and Macroscopic Constitutive Behaviour*, ser. Mechanical Behaviour of Materials. Springer, 2012. [Online]. Available: <http://books.google.nl/books?id=h8mtGVa9ZUUC>
- [41] R. Holm, *Electric Contacts: Theory and Applications*. Springer, 1999. [Online]. Available: <http://books.google.nl/books?id=RBwIAQAIAAJ>
- [42] C. Brown, “Impact of Environmental Conditions on the Contact Physics of Gold Contact RF Microelectromechanical Systems (MEMS) Switches,” Ph.D. dissertation, North Carolina State University, 2008. [Online]. Available: http://books.google.nl/books?id=-mxTC5Fs_JQC
- [43] Z. Yang, “Contact Material Optimization and Contact Physics in Metal-Contact Microelectromechanical Systems Switches,” Ph.D. dissertation, North Carolina State University, 2008.
- [44] R. Timsit, “Electrical contact resistance: properties of stationary interfaces,” *IEEE Transactions on Components and Packaging Technologies*, vol. 22, no. 1, pp. 85–98, Mar. 1999. [Online]. Available: <http://ieeexplore.ieee.org/lpdocs/epic03/wrapper.htm?arnumber=759357>
- [45] H. Rosenberg, *The Solid State*, ser. Oxford Physics Series. Oxford University Press, 1995. [Online]. Available: <http://books.google.nl/books?id=CjmFNAEACAAJ>
- [46] D. Berman, M. J. Walker, and J. Krim, “Contact voltage-induced softening of RF microelectromechanical system gold-on-gold contacts at cryogenic temperatures,” *Journal of Applied Physics*, vol. 108, no. 4, p. 044307, 2010. [Online]. Available: <http://scitation.aip.org/content/aip/journal/jap/108/4/10.1063/1.3459893>
- [47] Z. Yang, D. Lichtenwalner, A. Morris, J. Krim, and a. I. Kingon, “Contact degradation in hot/cold operation of direct contact micro-switches,” *Journal of Micromechanics and Microengineering*, vol. 20, no. 10, p. 105028, Oct. 2010. [Online]. Available: <http://stacks.iop.org/0960-1317/20/i=10/a=105028?key=crossref.49e6e58f75610212736bc20974a27d04>

- [48] L. L. Chow and K. Kurabayashi, “Understanding and control of unstable contact resistance in RF MEMS gold-gold direct contact switches,” in *2010 IEEE 23rd International Conference on Micro Electro Mechanical Systems (MEMS)*. IEEE, Jan. 2010, pp. 771–774. [Online]. Available: <http://ieeexplore.ieee.org/lpdocs/epic03/wrapper.htm?arnumber=5442294>
- [49] D. Lide, *CRC Handbook of Chemistry and Physics, 85th Edition*, ser. CRC Handbook of Chemistry and Physics, 85th Ed. Taylor & Francis, 2004. [Online]. Available: <http://books.google.nl/books?id=WDlI8hA006AC>
- [50] F. Bayle and A. Mettas, “Temperature Acceleration Models in Reliability Predictions: Justification & Improvements,” in *2010 Proceedings - Annual Reliability and Maintainability Symposium (RAMS)*. IEEE, Jan. 2010, pp. 1–6. [Online]. Available: <http://ieeexplore.ieee.org/lpdocs/epic03/wrapper.htm?arnumber=5448028>
- [51] R. F. Stapelberg, *Handbook of Reliability, Availability, Maintainability and Safety in Engineering Design*. Springer, 2009.
- [52] D. W. Duma and K. J. Krieg. (2005, August) Department of defense guide for achieving reliability, availability, and maintainability. [Online]. Available: <https://www.dsia.org/sites/default/files/DoD%20RAM%20Guide%202005%20-%20Modified.pdf>
- [53] D. J. Wilkins. (2002) The Bathtub Curve and Product Failure Behavior. [Online]. Available: <http://www.weibull.com/hotwire/issue21/hottopics21.htm>
- [54] W. Weibull, “A Statistical Distribution Function of Wide Applicability,” *Journal of applied mechanics*, vol. 18, pp. 293–297, 1951. [Online]. Available: <http://web.cecs.pdx.edu/~cgshirl/Documents/Weibull-ASME-Paper-1951.pdf>
- [55] N. Yudewitz, “Predict Relay Life Reliably with Simple Empirical Equations,” *ELECTRONIC DESIGN*, vol. 27, no. 3, pp. 80–83, 1979.
- [56] Atmel Corporation. (2005) Enhancing adc resolution by oversampling. [Online]. Available: <http://www.atmel.com/Images/doc8003.pdf>
- [57] A. Fruehling, W. Yang, and D. Peroulis, “Cyclic Evolution of Bouncing for Contacts in Commercial RF MEMS Switches,” in *2012 IEEE 25th International Conference on Micro Electro Mechanical Systems (MEMS)*, no. February. IEEE, Jan. 2012, pp. 688–691. [Online]. Available: <http://ieeexplore.ieee.org/lpdocs/epic03/wrapper.htm?arnumber=6170280>
- [58] A. Verger, A. Pothier, C. Guines, A. Crunteanu, P. Blondy, J. Orlianges, J. Dhennin, F. Courtade, and O. Vendier, “Sub-hundred nanosecond reconfiguration capabilities

- of nanogap rf mems switched capacitor,” in *Microwave Symposium Digest (MTT), 2010 IEEE MTT-S International*, May 2010, pp. 1–1.
- [59] M. J. Madou, *Solid-State Physics, Fluidics, and Analytical Techniques in Micro- and Nanotechnology*. CRC Press, 2011. [Online]. Available: <http://books.google.com/books?id=d-dkI7VHikEC&pgis=1>
- [60] K. Petersen, “Micromechanical Membrane Switches on Silicon,” *IBM Journal of Research and Development*, vol. 23, no. 4, pp. 376–385, July 1979.
- [61] —, “Dynamic Micromechanics on silicon: Techniques and Devices,” *Electron Devices, IEEE Transactions on*, vol. 25, no. 10, pp. 1241–1250, Oct 1978.
- [62] R. Herfst, H. Huizing, P. Steeneken, and J. Schmitz, “Characterization of dielectric charging in RF MEMS capacitive switches,” in *2006 IEEE International Conference on Microelectronic Test Structures*. IEEE, 2006, pp. 133–136. [Online]. Available: <http://ieeexplore.ieee.org/lpdocs/epic03/wrapper.htm?arnumber=1614290>
- [63] R. Herfst, P. Steeneken, and J. Schmitz, “Time and voltage dependence of dielectric charging in RF MEMS capacitive switches,” in *2007 IEEE International Reliability Physics Symposium Proceedings. 45th Annual*, vol. 5. IEEE, Apr. 2007, pp. 417–421. [Online]. Available: <http://ieeexplore.ieee.org/lpdocs/epic03/wrapper.htm?arnumber=4227667>
- [64] J. McBride, “Electrical contact bounce in medium-duty contacts,” *IEEE Transactions on Components, Hybrids, and Manufacturing Technology*, vol. 12, no. 1, pp. 82–90, Mar. 1989. [Online]. Available: <http://ieeexplore.ieee.org/lpdocs/epic03/wrapper.htm?arnumber=19016>
- [65] M. Cychowski, M. Lishchynska, and K. Delaney, “Dual-pulse control to eliminate bouncing of ohmic RF MEMS switch,” in *IET Irish Signals and Systems Conference (ISSC 2010)*. IET, 2010, pp. 36–41. [Online]. Available: <http://link.aip.org/link/IEECPS/v2010/iCP566/p36/s1&Agg=doi>
- [66] J. Blecke, D. Epp, H. Sumali, and G. Parker, “A Simple Learning Control to Eliminate RF-MEMS Switch Bounce,” *Journal of Microelectromechanical Systems*, vol. 18, no. 2, pp. 458–465, Apr. 2009. [Online]. Available: <http://ieeexplore.ieee.org/lpdocs/epic03/wrapper.htm?arnumber=4796321>
- [67] A. Tazzoli, M. Barbato, F. Mattiuzzo, V. Ritrovato, and G. Meneghesso, “Study of the actuation speed, bounces occurrences, and contact reliability of ohmic RF-MEMS switches,” *Microelectronics Reliability*, vol. 50, no. 9-11, pp. 1604–1608, Sep. 2010. [Online]. Available: <http://linkinghub.elsevier.com/retrieve/pii/S0026271410003070>

- [68] R. P. LaRose and K. D. Murphy, "Impact dynamics of MEMS switches," *Nonlinear Dynamics*, vol. 60, no. 3, pp. 327–339, Nov. 2009. [Online]. Available: <http://link.springer.com/10.1007/s11071-009-9598-5>
- [69] P. Decuzzi, G. P. Demelio, G. Pascazio, and V. Zaza, "Bouncing dynamics of resistive microswitches with an adhesive tip," *Journal of Applied Physics*, vol. 100, no. 2, p. 024313, 2006. [Online]. Available: <http://scitation.aip.org/content/aip/journal/jap/100/2/10.1063/1.2214348>
- [70] K. L. Johnson, K. Kendall, and a. D. Roberts, "Surface Energy and the Contact of Elastic Solids," *Proceedings of the Royal Society A: Mathematical, Physical and Engineering Sciences*, vol. 324, no. 1558, pp. 301–313, Sep. 1971. [Online]. Available: <http://rspa.royalsocietypublishing.org/cgi/doi/10.1098/rspa.1971.0141>
- [71] V. Le Houerou, C. Gauthier, and R. Schirrer, "Mécanique des surfaces polymères : rôles conjugués de la taille des objets, de la souplesse des matériaux et de l'énergie de surface," June 2010, journées GDR Robotique/mecano, Paris. [Online]. Available: http://www.gdr-robotique.org/rapports/download.php?t=GT3&d=15_06_10&f=1278498193_VLH_GDR_Mecano.pdf
- [72] M. Pashley and D. Tabor, "Adhesion and deformation properties of clean and characterized metal micro-contacts," *Vacuum*, vol. 31, no. 10-12, pp. 619–623, Oct. 1981. [Online]. Available: <http://www.sciencedirect.com/science/article/pii/0042207X81900798><http://linkinghub.elsevier.com/retrieve/pii/0042207X81900798>
- [73] A. Fortini, M. I. Mendelev, S. Buldyrev, and D. Srolovitz, "Asperity contacts at the nanoscale: Comparison of Ru and Au," *Journal of Applied Physics*, vol. 104, no. 7, p. 074320, Jul. 2008. [Online]. Available: http://ieeexplore.ieee.org/xpls/abs_all.jsp?arnumber=4916413

Qualité et Fiabilité des Commutateurs MEMS-RF pour les Applications Spatiales

Résumé : Ce manuscrit traite de la fiabilité de micro-composants électro-mécaniques que l'on appelle des MEMS (Acronyme anglais signifiant Micro-Electro-Mechanical Systems). Les MEMS sont utilisés dans un grand nombre de domaines et le domaine qui nous concerne est celui des télécommunications. Plus précisément, notre domaine de travail se situe autour des radio-fréquences où les MEMS vont principalement réaliser des fonctions de commutation. On appellera ainsi nos composants des MEMS-RF, RF signifiant Radio-Fréquence. Dans ce domaine, les MEMS sont des candidats à fort potentiel grâce à une faible consommation de puissance, leur performance dans le domaine RF, leur encombrement et leur poids. De plus, en utilisant un procédé de fabrication dérivé de celui des semi-conducteurs, leur coût de production reste relativement faible. Dans ce manuscrit, on s'intéresse à la fiabilité de ces composants car c'est le dernier verrou avant une éventuelle industrialisation. Les principaux mécanismes de défaillance sont abordés dans une première partie, puis ce manuscrit se concentre sur l'étude du fluage mécanique et des facteurs d'accélération de modes de défaillance. On verra notamment l'influence de la température et des conditions de fonctionnement sur la durée de vie des commutateurs.

Mots clés : Fiabilité, MEMS-RF, commutateurs, fluage, Weibull, banc de mesure.

Quality and Reliability of RF-MEMS Switches for Space Applications

Abstract: The thesis deals with reliability of tiny electro-mechanical components called MEMS. MEMS stands for Micro-Electro-Mechanical Systems. These components, designed for switching applications, are suitable candidates for telecommunications due to their low power consumption, Radio-Frequencies (RF) performances, compactness and lightness. A MEMS is fabricated using processes of integrated circuit manufacturing that makes its cost relatively low. Few of these components are commercially available and more are expected to be in the market as soon as reliability issues will be solved. Reliability issues studied in the thesis regard mechanical creep and acceleration factors. The mechanical creep occurs in our suspended structures whilst enduring a constant force, it results in deformation of structures and shift of parameters. Two innovative test benches are developed to assess mechanical creep in RF-MEMS switches. The acceleration factors are keys to conduct accelerated testings and predict lifetime of RF-MEMS switches. Parameters such as bias voltage, input-to-output voltage, temperature are varied to assess lifetime of switches and extract these acceleration factors.

Keywords: Reliability, RF-MEMS, switch, creep, Weibull, assessment, test bench.

Xlim - UMR CNRS n° 7252

123, avenue Albert Thomas - 87060 LIMOGES CEDEX